INFORMATION TO USERS

This was produced from a copy of a document sent to us for microfilming. While the most advanced technological means to photograph and reproduce this document have been used, the quality is heavily dependent upon the quality of the material submitted.

The following explanation of techniques is provided to help you understand markings or notations which may appear on this reproduction.

1. The sign or "target" for pages apparently lacking from the document photographed is "Missing Page(s)". If it was possible to obtain the missing page(s) or section, they are spliced into the film along with adjacent pages. This may have necessitated cutting through an image and duplicating adjacent pages to assure you of complete continuity.

2. When an image on the film is obliterated with a round black mark it is an indication that the film inspector noticed either blurred copy because of movement during exposure, or duplicate copy. Unless we meant to delete copyrighted materials that should not have been filmed, you will find a good image of the page in the adjacent frame.

3. When a map, drawing or chart, etc., is part of the material being photographed the photographer has followed a definite method in "sectioning" the material. It is customary to begin filming at the upper left hand corner of a large sheet and to continue from left to right in equal sections with small overlaps. If necessary, sectioning is continued again—beginning below the first row and continuing on until complete.

4. For any illustrations that cannot be reproduced satisfactorily by xerography, photographic prints can be purchased at additional cost and tipped into your xerographic copy. Requests can be made to our Dissertations Customer Services Department.

5. Some pages in any document may have indistinct print. In all cases we have filmed the best available copy.

University
Microfilms
International

300 N. ZEEB ROAD, ANN ARBOR, MI 48106
18 BEDFORD ROW, LONDON WC1R 4EJ, ENGLAND

PALASZEWSKI, STEPHEN JOHN

AN AIR-VAPOR-DROPLET LOCAL INTERACTION MODEL FOR SPRAY UNITS

City University of New York PH.D. 1980

AN AIR-VAPOR-DROPLET LOCAL INTERACTION MODEL FOR SPRAY UNITS

by

STEPHEN J. PALASZEWSKI

A dissertation submitted to the Graduate Faculty in Engineering in partial fulfillment of the requirements for the degree of Doctor of Philosophy, The City University of New York

1980

This manuscript has been read and accepted for the Graduate Faculty in Engineering in satisfaction of the dissertation requirement for the degree of Doctor of Philosophy.

4/18/1980
date

Latif M. Jiji
Chairman of Examining Committee

4/18/1980
date

Frederick E. Nam
Executive Officer

Prof. Latif M. Jiji, Chairman

Prof. Rishi Raj

Prof. Reuel Shinnar

Prof. Sheldon Weinbaum

Prof. Herbert Weinstein
Supervisory Committee

The City University of New York

Abstract

AN AIR-VAPOR-DROPLET LOCAL INTERACTION MODEL

FOR SPRAY UNITS

by

Stephen J. Palaszewski

Advisor: Professor Latif M. Jiji

Co-Advisor: Professor Sheldon Weinbaum

A new three-dimensional model for predicting the flow and thermal characteristics of spray units is presented. The new model eliminates many of the more serious shortcomings of current theoretical approaches. In a marked departure from present theories, which are based in the large on the behavior of an average droplet in some uniform average environment, the new model examines the local variation in properties of both the air and the droplets throughout the flow field encompassing the spray umbrella. The model allows the air streamlines and droplet trajectories to follow substantially different paths and is able to determine the local change in the environment of the droplets throughout their motion. The conservation equations to determine the local absolute humidity, velocity and dry-bulb temperature of the air-vapor phase are written in Lagrangian form where the droplets are treated as spatially varying sources of mass, momentum and energy. Source strength is determined by the inter-

action between the air-vapor and droplet phases. The analysis takes into consideration stable and unstable meteorological conditions, turbulent mixing in the atmospheric surface layer and non-uniform upwind and local air-velocity profiles.

To illustrate its general applicability, model predictions of droplet return temperature along the spray perimeter were compared with data for two substantially different sprays used for power plant cooling. Predictions of downwind wet-bulb temperature were compared with available data. Good agreement was observed.

A parametric study was carried out to determine an optimum spray unit design. It was found that substantial improvements in the cooling obtained for a given spray power input can be achieved over currently used floating spray modules. It was shown that, for summer design conditions, the cooling obtained from a single spray of the Powered Spray Module can be realized by an alternate spray unit design requiring only one-half the power input.

The new model for spray units can be extended to predict the cooling performance of a pass of sprays aligned in the wind direction. The performance of an entire spray canal can be obtained by incorporating the model for a pass of sprays into a system model.

ACKNOWLEDGEMENTS

The author wishes to thank Professor Latif M. Jiji and Professor Sheldon Weinbaum for their guidance and encouragement during the course of this research. Appreciation is also extended to The City University of New York Computer Center for the use of their facilities. A very special thanks goes to Ms. B. Kay Johnson for her never-ending emotional support and her "man-size drop".

This research was sponsored by the National Science Foundation under Grant No. ENG. 78-20709. Their support is gratefully acknowledged.

TABLE OF CONTENTS

Page

ABSTRACT iii

ACKNOWLEDGEMENTS v

LIST OF TABLES ix

LIST OF FIGURES x

CHAPTER

I. INTRODUCTION

1.1. Spray Cooling Systems 1

1.2. Review of the Literature 4

1.2.1. Models of Spray Units 4

1.2.1a. The Number of Transfer Units (NTU) Model 4

1.2.1b. The Cellular Model 7

1.2.1c. The Particle-Source-in-Cell (PSI-Cell) Model 9

1.2.1d. Soo's Model 11

1.2.1e. Spray Energy Release (SER) Model 12

1.2.1f. The Berger and Taylor Model 13

1.2.2. Use of Spray Unit Models for Spray System Analysis 14

1.2.3. Evaluation of Current Models... 20

1.3. Research Objectives 25

II. AN AIR-VAPOR-DROPLET LOCAL INTERACTION MODEL FOR SPRAY UNITS

2.1. Introduction 26

2.2. Meteorological Considerations 30

Page

2.3. Assumptions 34

2.4. Conservation Equations 36

2.4.1. Conservation of Mass for a Droplet 36

2.4.2. Conservation of Droplet Momentum 39

2.4.3. Conservation of Energy for a Droplet 40

2.4.4. Water Vapor Continuity Equation 41

2.4.5. Conservation of Air Momentum ... 44

2.4.6. Air Continuity Equation 45

2.4.7. Air Energy Equation 51

III. SOLUTION OF MODEL EQUATIONS

3.1. Iterative Solution Technique 52

3.2. Solution of Droplet Equations 55

3.2.1. Droplet Momentum Equation 55

3.2.2. Conservation of Energy for a Droplet 61

3.2.3. Conservation of Mass for a Droplet 63

3.3. Solution of Air-Vapor Phase Equations 64

3.3.1. Conservation of Air Momentum ... 64

3.3.2. Air Continuity Equation 67

3.3.3. Air Energy Equation 67

3.3.4. Water Vapor Continuity Equation 69

Page

IV. SPRAY CHARACTERISTICS AND MODEL VERIFICATION

4.1. Spray Characteristics 70

4.2. Comparison of Model Predictions with Experimental Data 75

4.2.1. The Powered Spray Module (PSM) 75

4.2.2. The Spraco 1751 Nozzle 89

V. PARAMETRIC AND OPTIMIZATION STUDIES: DESIGN AND PERFORMANCE CHARTS

5.1. The Governing Parameters 115

5.2. Parametric Studies 119

5.3. Performance Charts 132

VI. SUMMARY AND CONCLUSIONS 136

APPENDIX..... 141

NOMENCLATURE..... 145

REFERENCES 151

LIST OF TABLES

TABLE		Page
1	PSM EXPERIMENTAL CONDITIONS	86
2	COMPARISON OF THEORY AND EXPERIMENT FOR DROPLET COOLING RANGE OF PSM.....	87
3	COMPARISON OF THEORY AND EXPERIMENT FOR PSM DOWNWIND WET-BULB TEMPERATURE AND AIR-VELOCITY	88
4	DROPLET SIZE DISTRIBUTION FOR SPRACO 1751 NOZZLE USED AS MODEL INPUT	92
5	GOVERNING PARAMETERS FOR LIQUID SPRAYS	116

LIST OF FIGURES

Figure		Page
1	Spray System and Spray Unit	2
2	Schematic of Spray System Model	17
3	Trajectory of a Fluid Element as it Crosses the Spray Field	27
4	Change in Streamtube Cross-Sectional Area Along a Streamline	48
5	Flow Chart for Spray Unit Analysis	53
6	Coordinate System for Spray Unit Analysis. Origin is at the Water Surface Directly Below the Nozzle	57
7	Spray Nozzle Showing Droplet Discharge Sites	58
8	Air-Vapor Streamlines Near Centerline of PSM for Low Wind (Elevation View) ...	76
9	Air-Vapor Streamlines Initially at a 2m Height Upwind of PSM (Plan View), Low Wind	77
10	Air-Vapor Velocity Profiles Near Centerline of PSM for Low Wind	78
11	Absolute Humidity Profiles Near Centerline of PSM for Low Wind	79
12	Air-Vapor Streamlines Near Centerline of PSM for High Wind (Elevation View)	80
13	Air-Vapor Streamlines Initially at a 2m Height Upwind of PSM (Plan View), High Wind	81
14	Air-Vapor Velocity Profiles Near Centerline of PSM for High Wind	82
15	Absolute Humidity Profiles Near Centerline of PSM for High Wind.....	83

Figure		Page
16	Centerline Droplet Return Temperature for Spraco 1751 ($U_{2m\infty}$=0.76m/s)	97
17	Centerline Droplet Return Temperature for Spraco 1751 ($U_{2m\infty}$=0.85m/s)	98
18	Centerline Droplet Return Temperature for Spraco 1751 ($U_{2m\infty}$=1.00m/s)	99
19	Centerline Droplet Return Temperature for Spraco 1751 ($U_{2m\infty}$=1.13m/s)	100
20	Centerline Droplet Return Temperature for Spraco 1751 ($U_{2m\infty}$=1.16m/s)	101
21	Centerline Droplet Return Temperature for Spraco 1751 ($U_{2m\infty}$=1.28m/s)	102
22	Centerline Droplet Return Temperature for Spraco 1751 ($U_{2m\infty}$=1.46m/s)	103
23	Centerline Droplet Return Temperature for Spraco 1751 ($U_{2m\infty}$=1.50m/s)	104
24	Centerline Droplet Return Temperature for Spraco 1751 ($U_{2m\infty}$=1.50m/s)	105
25	Centerline Droplet Return Temperature for Spraco 1751 ($U_{2m\infty}$=1.54m/s)	106
26	Centerline Droplet Return Temperature for Spraco 1751 ($U_{2m\infty}$=1.67m/s)	107
27	Centerline Droplet Return Temperature for Spraco 1751 ($U_{2m\infty}$=1.92m/s)	108
28	Centerline Droplet Return Temperature for Spraco 1751 ($U_{2m\infty}$=1.92m/s)	109
29	Centerline Droplet Return Temperature for Spraco 1751 ($U_{2m\infty}$=2.00m/s)	110
30	Centerline Droplet Return Temperature for Spraco 1751 ($U_{2m\infty}$=2.25m/s)	111
31	Centerline Droplet Return Temperature for Spraco 1751 ($U_{2m\infty}$=2.67m/s)	112
32	Centerline Droplet Return Temperature for Spraco 1751 ($U_{2m\infty}$=2.67m/s)	113

Figure		Page
33	Centerline Droplet Return Temperature for Spraco 1751 ($U_{2m\infty}$=2.88m/s)	114
34	Cooling Efficiency for a Single Spray. Design Chart	127
35	Total Heat Transfer for a Single Spray. Design Chart	128
36	Evaporation as a Percentage of Spray Flow Rate for a Single Spray	129
37	Cooling Effectiveness for a Single Spray. Design Chart	130
38	Effect of Discharge Angle and Wind Speed on PSM Single Spray Performance in Unstable Air	131
39	Performance Chart for PSM Single Spray in Unstable Air	134
40	Evaporation as a Percentage of Spray Flow Rate for PSM Single Spray in Unstable Air	135

CHAPTER I

INTRODUCTION

1. 1. Spray Cooling Systems

During the past decade considerable interest has been generated in waste heat dissipation from power generation. Public pressure and concern have precipitated stringent state and federal laws regulating traditional once-through open-cycle cooling. Aside from these regulations, the difficulty of waste heat management is compounded by increasing needs for power and accelerating demands on water resources.

Recognizing these developments and trends, the power industry has intensified its activity in exploring alternate methods for waste heat dissipation. A closed-cycle approach which has received favorable attention is spray canal cooling. Although spray cooling has been in use for many years, the type of spray system employed has changed since its introduction. The system used today consists of floating modules (as opposed to the previously used fixed sprays) each spraying a small percentage of the condenser discharge water into the air. Typically, a number of four-spray modules are aligned parallel tc the edge of the canal, which can be up to several miles long. Such an arrangement is illustrated schematically in Figure 1.

Spray cooling systems have a number of advantages over cooling towers. These include the ability to control the rate of heat dissipation by selectively shutting off or turning on any number of spray modules, economy of construction

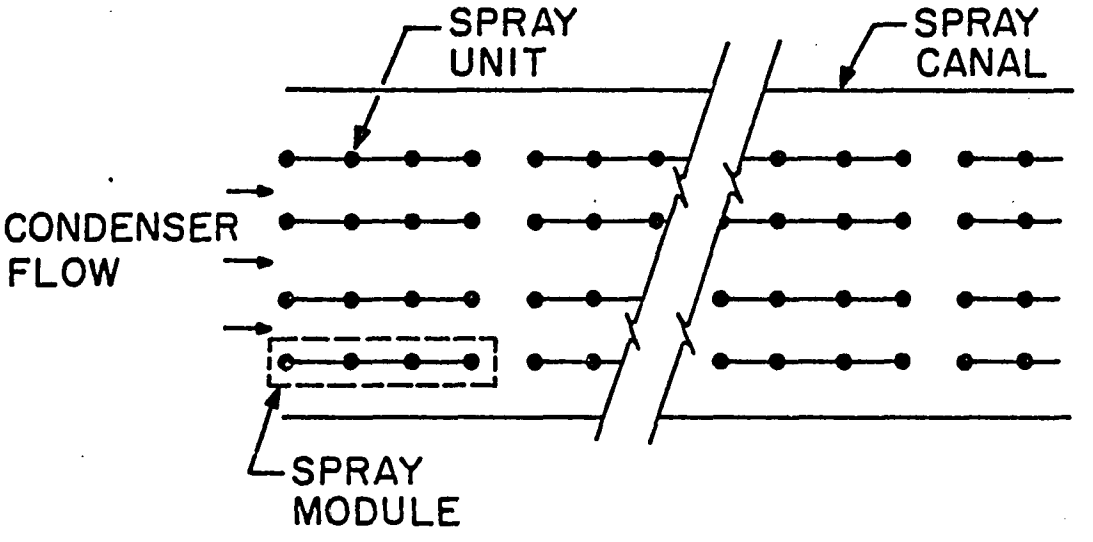

(a) SYSTEM

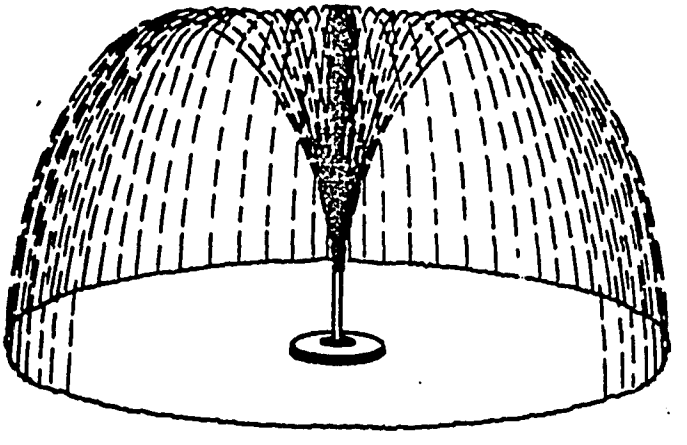

(b) UNIT

Figure 1. Spray System and Spray Unit.

and ease of maintenance. In spite of these desirable features, the adoption of spray cooling systems for waste heat dissipation has been very limited. The reluctance to use these systems is partially due to the lack of reliable theory and experiments to accurately predict their performance. In a 1976 review of theoretical models for spray cooling, Ryan and Myers [1] underscore the uncertainty in current theories by an example calculation where the number of required spray units for a given design criteria varies by a factor of 2.5 depending on the theoretical model used. A magnitude of uncertainty of this order is intolerable in view of the substantial operating costs of each spray module.

The difficulty in accurately predicting the performance of spray systems is traced to the complexity of the spray cooling process which involves a two-phase air-vapor-droplet energy and mass interaction in an unbounded region subject to varying meteorological conditions. It is not surprising, therefore, that the majority of present theories rely on design-specific empirical factors which limit their accuracy and applicability. This dependency of current models on design-specific factors precludes their use in optimization studies of spray units or spray systems. Furthermore, present models cannot be used to examine the performance of new designs or explore the effects of novel configurations. Another serious shortcoming of present theories is the lack of a systematic study to identify all the parameters which govern the performance of spray units and systems.

1. 2. Review of the Literature

Because sprays are commonly used in a wide range of engineering applications, there is an extensive theoretical and experimental literature on the subject drawn from several different areas of engineering research. Attention will be focused here on recent studies which have been motivated by interest in the use of sprays for heat dissipation from power plants.

Six basic models have been developed to predict the thermal performance of spray units. These models are 1) Number of Transfer Units (NTU), 2) Cellular, 3) Particle-Source in Cell (PSI-Cell), 4) Soo's, 5) Spray Energy Release (SER) and 6) Berger and Taylor's.

1. 2. 1. Models of Spray Units

1. 2. 1a. The Number of Transfer Units (NTU) Model

One method for describing the thermal performance of a spray unit is through a dimensionless index called the number of transfer units (NTU). This concept is also used in heat exchangers and wet cooling towers. The NTU approach is based on the Merkel Equation which is derived from conservation of energy for a droplet exchanging heat and mass with the ambient air. Merkel's equation is given by:

$$\overline{\left(\frac{A_d h}{M C_s}\right)} t_f = \int_{T_c}^{T_H} \frac{C_{pd}\, dT_d}{h(T_d) - h(T_{wb})} , \qquad (1)$$

where

A_d = surface area of a representative droplet

C_{pd} = specific heat of water

C_s = specific heat of air-vapor mixture

$h(T_d)$ = total enthalpy of saturated air-vapor mixture at local droplet temperature T_d

$h(T_{wb})$ = total enthalpy of air-vapor mixture at the local wet bulb temperature T_{wb}

h = droplet heat transfer coefficient

M = droplet mass

T_H = droplet initial temperature

T_c = droplet final temperature

t_f = droplet flight time

The term on the left hand side of equation (1) is called the number of transfer units, NTU, and is characteristic of the water droplet. In theory the NTU can be determined analytically. However, in practice the NTU for a given nozzle design is experimentally established.

The integral in Merkel's equation involves the total heat transfer to the ambient air along the entire trajectory of the droplet. To perform the integration, the wet bulb temperature of the ambient air as well as the local droplet temperature must be known. Since heating and humidification of the air takes place along virtually the entire trajectory, neither $h(T_d)$ nor $h(T_{wb})$ is constant. However, in all NTU models both are assumed constant.

Using the NTU approach, Hoffman [2] collected field data and calculated NTU values for different wind speeds.

Curves for average $\overline{NTU}$ vs. wind speed were then generated for different spray nozzles. By assuming an average value for $h(T_d)$ and letting $h(T_{wb})$ be given by upwind ambient conditions, the integral in equation (1) is evaluated and set equal to the experimentally determined $\overline{NTU}$. The result is given by:

$$NTU = \frac{C_{Pd}\,(T_H - T_c)}{\frac{1}{2}\left[h(T_H) + h(T_c)\right] - h(T_{wb\infty})}\,, \qquad (2)$$

where $T_{wb\infty}$ is the upwind wet bulb temperature. Hoffman's empirical $\overline{NTU}$ curves together with equation (2) are used to determine the cold water temperature T_c from a spray.

The NTU approach was also followed by Porter and Chen [3]. To determine the NTU values Porter and Chen used experimental data on existing spray systems of fixed design. Values of NTU were assigned such that the computed canal discharge temperatures matched those observed in the field within $0.05^{\circ}F$. A curve fit of the values thus obtained gave the required NTU vs. wind speed plot.

In another study Porter, Yang and Yanik [4] used a modified NTU approach to develop an analytic model for spray units and spray systems. They assumed that the total enthalpy of the air-vapor mixture is proportional to the local droplet temperature and integrated the Merkel equation to obtain

$$\frac{T_H - T_c}{T_c - \overline{T}_{wb}} = 1 - \exp\left(-\frac{NTU\ b_f}{C_{Pd}}\right), \qquad (3)$$

where

$\bar{T}_{wb}$ = The average of the upwind and downwind wet bulb temperature

b_f = $dh/dT_d = b(T_f)$ = constant

T_f = film temperature = $(T_H + \bar{T}_{wb})/2$

The NTU in this model must still be determined experimentally for each spray design. Measurements of local average wet bulb temperature and cold and hot water temperatures together with equation (3) yield the NTU value of a given spray. However, since direct sampling of sprays is difficult, Porter, Yang and Yanik recommend the use of spray system data with their corresponding analytic system model for the determination of NTU.

Arndt and Barry [5] presented a new NTU model for spray units and spray systems. Their unit model is similar to that used by Hoffman. It is based on an empirically determined NTU which can be approximated by a linear function of wind speed.

1. 2. 1b. The Cellular Model

This model is based on the assumption that the spray consists of identical droplets each surrounded by a unique cell of air. The temperature history of a droplet is examined from nozzle discharge to canal surface impact. The analysis is thus reduced to the treatment of a single droplet. This approach was used by Elgawhary [6] to formulate an analytical method for predicting the spray cold water temperature T_c. The major assumptions involved in his cellular model are:

(1) The air in each cell travels with the droplet throughout the droplet's trajectory.

(2) No mass or energy transfer takes place between cells.

(3) The water vapor concentration at the edge of each cell is quasi-constant and equal to the average concentration in the cell at time t.

(4) Evaporation stops when the air in the cell is saturated with water vapor.

(5) The ratio of cell radius to droplet radius is assumed constant, independent of wind speed and location in spray.

(6) The droplet velocity is neglected in the determination of the droplet Reynolds number, which is based solely on the wind velocity.

Based on these assumptions, Elgawhary applied the conservation principles to the droplet-cell system using empirical equations for the heat and mass transfer coefficients. The conservation equations were formulated in terms of an average cell to droplet radius ratio. The cold water temperature can be calculated using an iterative procedure for a specified value of radius ratio. This ratio cannot be established theoretically. It is used as a matching parameter to obtain agreement between theory and experiment. A value of 18 was found to give the best agreement with experimental results for a wind speed of 5 mph.

Elgawhary's cellular model was refined by Frediani and Smith [7] by relaxing some of the assumptions made. They based the volume of the air cells on the rate of air flow through the spray. This makes the water-air flow ratio in the spray a function of wind speed and spray geometry. They also based the Reynolds number on the droplet velocity. Furthermore, the effect of heat transfer on raising the temperature of the air

in the cell was taken into account. This allows more evaporation to occur than in Elgawhary's model.

While Elgawhary used the cell to droplet radius ratio as a matching parameter, Frediani and Smith [7] used the initial droplet size as the matching element in their model. Performance data for a single spray and a row of single sprays was used to determine the effective initial droplet size. The drop diameter was varied until agreement of the model predictions of the downstream canal temperature with data was achieved. The model was then applied to the analysis of large spray systems to test its applicability. Good agreement was observed for small values of $(T_H - T_C)$. Agreement for very large systems was found to be within ± 20 percent in most cases. Ryan [8], [9] states that it was found necessary to introduce fresh air into the cell to prevent the downwind wet bulb temperature from rising too quickly. No mention of entrainment is made by Frediani and Smith [7] and no comparisons with downwind wet-bulb temperature are made by them.

1. 2. 1c. The Particle-Source-in-Cell (PSI-Cell) Model

The PSI-Cell model represents a more rational treatment of gas-droplet flows which, in contrast to the cellular model, does not need to assume that the air and droplet phases follow the same trajectory. It has been introduced to deal with drying and combustion systems. Its application to the more complex problem of unbounded external power plant spray systems has not yet been attempted. Applications have been limited to one and two-dimensional internal flow systems of fixed gas flow rate and well defined boundaries.

The PSI-Cell model attempts to account for the mass, momentum and thermal coupling between a gas and a cloud of droplets within the gas. It is based on the concept of a droplet as a source of mass, momentum and energy to the gaseous phase. The basic features of the model will be outlined here since the treatment of the droplet phase is similar to that presented herein for open systems.

The flow field in the PSI-Cell model is sub-divided into a series of small, but not infinitesimal control volumes called cells. As droplets move through a cell they act as sources or sinks of mass, momentum and energy. The source concept of the droplet was first set forth by Migdal and Agosta [10]. They derived a system of differential equations from the conservation laws for two-phase flow through a control volume. The terms in the equations resulting from the presence of particles were defined as source terms. The formulation of these terms was outlined as a guide for specific applications.

The field equations for conservation of mass, momentum and energy are written in finite-difference form for each cell. The trajectories, sizes and temperature histories of the droplets are obtained by finite differencing the equation of motion and the equation for the conservation of energy for an individual droplet. Empirical expressions are used for the droplet heat and mass transfer rates.

The determination of the gas-droplet flow field is accomplished by first solving for the gas flow and temperature fields neglecting buoyancy, including turbulent diffusion and assuming no drops are present. This solution is used to

calculate droplet properties along their trajectories, giving an initial guess of the source terms for each cell. The gas flow and temperature fields are solved again, now incorporating the source terms but neglecting the effect of droplets on turbulence. The procedure is repeated until successive solutions closely match.

This model has been applied by Crowe [11] to analyze the two-phase velocity (but not temperature) field in the vicinity of a fuel nozzle in a gas turbine combustor. An isothermal flow field was assumed. Calculations showed that the model predicts greater penetration of the spray into the combustor than is found when gas-droplet interaction is neglected.

Other attempts at using the source approach have been limited to one and two-dimensional models. Kliegel [12] and Hultberg and Soo [13] have developed models for gas-particle flow in de Laval nozzles. These one-dimensional models have shown a significant influence of particles on the gas flow field. Crowe, et. al. [14] extended the application of this model to the analysis of two-dimensional spray cooling for gas flow through a duct. Sharma and Crowe [15], [16] applied this method to flow metering of gas-particle suspensions by a Venturi, and gas-particle flow through an orifice.

1. 2. 1d. Soo's Model

Soo's [17] analysis is based on the integration of the conservation of energy equation for a droplet along its trajectory. Correlation equations for the heat and mass transfer coefficients are used to carry out this integration numerically.

Soo assumes that the dry and and wet bulb temperature of the air-vapor phase remain constant along the trajectory and that only the droplet temperature changes. He also neglects the buoyancy and drag induced velocity field of the air-vapor mixture.

Unlike all NTU models, Soo's model determines the NTU theoretically using the above simplifications for the air-vapor phase. This unique feature eliminates one of the empirical factors required by the NTU models. Furthermore, Soo's model lends itself to optimization studies of droplet size, spray height and radius.

1. 2. 1e. Spray Energy Release (SER) Model

Chen and Trezek [18] developed a new approach which attempts to account for the change in ambient conditions as the air moves through the spray. They introduced a new factor, the Spray Energy Release (SER), which represents the actual quantity of energy released by the spray per unit total driving potential. The SER is defined as:

$$SER = \frac{C_{Pd}\left(T_H - T_c\right)}{h\left(\frac{T_H + T_c}{2}\right) - h\left(\frac{T_{wb\infty} + T_{wbf}}{2}\right)}, \qquad (4a)$$

where T_{wb_f} is the downwind wet bulb temperature.

As can be observed from equation (2) and (4a) the $\overline{NTU}$ and SER differ in the evaluation of the air total energy. The total heats for the saturated air-vapor mixture at the droplet surface and at the local wet bulb temperature are both calcu-

lated in terms of average values which are the mean of the initial and final conditions. The SER approach also requires the experimental determination of SER as a function of wind speed for a given spray unit using measured values for T_{wbf} and T_c. To predict the performance of spray units using this model, an additional empirical factor, SER_{min}, is required. SER_{min} is defined as:

$$SER_{min} = \frac{C_{pd}(T_H - T_c)}{h\left(\frac{T_H + T_c}{2}\right) - h(T_{wb\infty})} \quad . \qquad (4b)$$

Measurements of T_c and $T_{wb\infty}$ determine the variation of SER_{min} with wind speed.

1. 2. 1f. The Berger and Taylor Model

This model [19] is the first attempt at a totally theoretical treatment of spray cooling. The model is based on the solution of an integral form of the Bernoulli equation which includes the effects of pressure, buoyancy and average droplet drag force. The equation is solved by assuming that the local conditions in the spray field are uniform and identical to the exit conditions of the air-vapor mixture. For the condition of zero wind, the exit air is assumed saturated and is a function of exit air-vapor density, which is calculated from the model. The exit air velocity, which has only a vertical component, is obtained from a thermal energy balance on a control volume enclosing the spray, and is proportional to the total heat transfer from the spray. For a high cross wind, the solution of the Bernoulli equation, neglecting buoyancy and vertical drag, yields the exit air

velocity, which is horizontal. Exit-air saturated enthalpy is determined from another energy balance. For both zero wind and high wind regimes, the spray heat transfer is obtained by integrating the energy equation over the average flight time of a droplet, assuming the local air to be saturated. Continuity is satisfied for the zero wind condition by assuring that the air entrained horizontally through all vertical sides of a control volume enclosing the spray, exits the control volume vertically. For the high wind regime, the air flow rate is given by the product of the wind speed and the spray cross-sectional area facing the wind, as in Frediani and Smith's model [7] . Comparison of model predictions with data on cold water temperature for the Rancho Seco spray system showed good agreement.

1. 2. 2. Use of Spray Unit Models for Spray System Analysis

The problem of predicting the thermal performance of a system of sprays in cross wind is considerably more complicated than that of a single spray unit. To adequately analyze a spray system it is essential to accurately predict the air-vapor phase properties downwind of each spray unit. The modeling of this problem in previous studies will be examined.

Hoffman [2] assumes a uniform dry bulb temperature throughout the system. The downwind wet bulb temperature is arbitrarily set by adding one degree to the upwind value.

Porter and Chen [3] also assume a uniform dry bulb temperature. However, they use experimental data from existing spray systems to obtain correlations for the wet bulb temperature corrections. They introduced a correction factor f

defined as:

$$f = \left(T_{wbf} - T_{wb\infty}\right) / \left(T_H - T_{wb\infty}\right) . \qquad (5)$$

This form of the correction factor is suggested by the fact that the air wet bulb temperature is driven toward the local canal temperature. Using experimental data, they plotted f against distance downwind on the centerline of the first spray and obtained a reasonable correlation for f. The tests were carried out at a single ambient wet bulb temperature and a single condenser discharge temperature of an arrangement of one spray per pass, and the results were extrapolated for systems involving more than one spray per pass. This was accomplished by superposition, i.e., the wet bulb temperature is determined by the combined effects of the two upwind sprays. Measurements obtained from systems consisting of two sprays per pass showed good agreement with the correlation for f provided the distance normal to the rows of sprays is used independent of the wind angle to the canal. Porter and Chen's results on the wet bulb temperature corrections yield the following empirical relations:

$$T_{wbf} = T_{wb\infty} + 0.18\left[\left(T_H\right)_{ij} - T_{wb\infty}\right], \qquad (6)$$

for the air downwind of sprays in the first row, and

$$T_{wbf} = T_{wb\infty} + 0.26\left[\left(T_H\right)_{ij} - T_{wb\infty}\right], \qquad (7)$$

for the air downwind of sprays in each succeeding row, where i is the pass number and j is the row number (see Fig. 2).

To obtain an analytic solution for system performance Porter [20] utilizes an average correction factor $\bar{f}$ for a system of m rows. Assuming complete mixing of water across the canal, equation (3) is integrated to yield a closed form solution for system performance:

$$\frac{T_H - T_{wb\infty}}{T_{H_i} - T_{wb\infty}} = \exp\left\{-mpr(1-\bar{f})\left[1-\exp\left(-NTU\,\frac{bf}{c_{pd}}\right)\right]\right\}, \quad (8)$$

where

m = number of canal rows

p = number of passes

r = ratio of spray unit flow rate to initial canal flow rate

T_{H_i} = initial canal temperature

Arndt and Barry [5] introduced the concept of a virtual point source of sensible heat and vapor. Both are assumed to spread as a Gaussian distribution. Diffusion coefficients as a function of downwind distance are obtained from published data on atmospheric dispersion. A critical factor in modeling for the dry bulb temperature and relative humidity distribution is the choice of the origin of the source which is arbitrarily established.

In the cellular model, Elgawhary [6] side steps the problem of wet bulb temperature variation by adjusting the cell-to-droplet diameter ratio to obtain agreement between theory and experiment. On the other hand, Frediani and Smith [7] adjust the initial droplet diameter and air entrainment

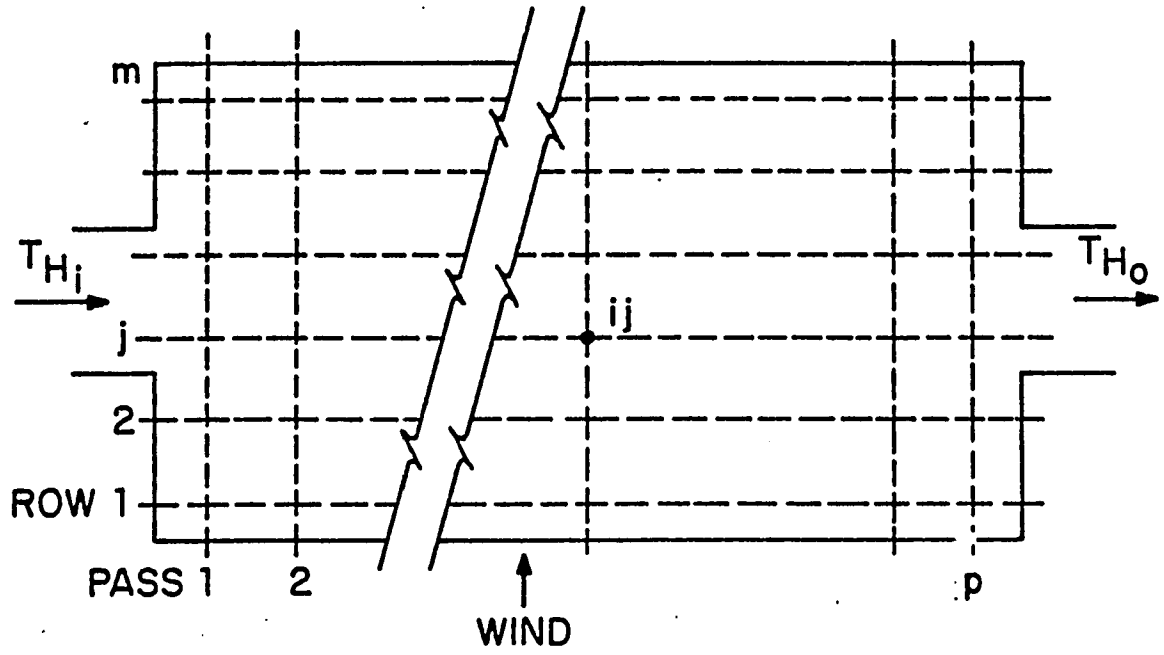

Figure 2. Schematic of Spray System Model.

until model prediction of the downwind wet bulb temperature and downstream canal temperature agree with experimental data.

The PSI-Cell model which has been developed and applied to one and two-dimensional internal flow systems should in theory predict the air-vapor properties downwind of a spray. Its extention to external three-dimensional spray systems has not been attempted.

Soo [17] assumes a uniform dry bulb temperature and specifies the minimum wind speed needed for uniform relative humidity throughout. Thus, the application of this model to a spray system is limited to either a canal with a single row of sprays or a multi-row canal under high enough wind speeds to justify the assumption of uniform relative humidity.

In developing a spray system model based on the SER concept, Chen and Trezek [18] introduce a drop size distribution function to determine the average horizontal air velocity leaving a spray. This is accomplished through the application of conservation of momentum of the air passing through a spray. The empirically obtained SER versus wind speed curve is used in an energy balance consideration to determine the air flow rate and the downwind dry and wet bulb temperatures.

Using an experimental open-air spray pond containing a column of three units to obtain spray performance data, Chen and Trezek [18] found that cold water termperatures were predicted to within 2% for the first two units and 14% for the third unit. Poor agreement for the third unit was explained by local fresh air entrainment.

To examine the effect of downwind spacings of spray units in a module on the performance, Chen and Trezek [18] use a mixing parameter σ which is a dimensionless form of the turbulent viscosity, conductivity and diffusivity. This parameter is obtained from measurements of the upwind psychrometric conditions and those downwind of the first spray unit along with the solution to the two-dimensional boundary layer equations. Average values of air velocity, total heat and specific humidity can be obtained downwind of each spray unit by integrating the boundary layer solutions over the spray height. Using the SER versus wind speed curve, the SER for each downwind spray unit can be determined. This boundary layer model was used to optimize spacings of spray units across a canal.

More recently, Chaturvedi and Porter [21] developed turbulence models for predicting local wet-bulb temperature proceeding windward through the spray field. They solved two-dimensional continuity and momentum equations, including the effect of droplet drag as a momentum source term. The wet-bulb temperature is obtained by integrating the convective-diffusion equations. Sensible and evaporative heat transfer from the droplets are accounted for by a source term incorporating the empirical factor NTU. Solutions of these boundary layer equations give the interference factor f as a function of distance into the spray field. The interference factor is either constant at a given station or exhibits a vertical profile, depending on the comprehensiveness of the model. Chaturvedi and Porter use four approximate models: 1)no

wind attenuation or turbulent diffusion, 2) diffusion only, 3) attenuation only, and 4) attenuation and diffusion. Theoretical values of the interference factor downwind through the spray field are plotted against data for Richards of Rockford and Ceramic Cooling Tower Company modules and data from the Rancho Seco Nuclear Station (California) spray ponds using No. 1751 Spray Engineering Company (Spraco) nozzles. In general, f is predicted low for the first row of sprays and reasonably well for succeeding rows.

1. 2. 3. Evaluation of Current Models

Examination of the NTU and cellular models show that they require two design-specific constants. All NTU models use experimentally determined NTU values. Furthermore, except for the model proposed by Arndt and Barry [5], NTU models require empirical wet bulb correction factors. While Arndt and Barry theoretically predict wet bulb variation, they introduce the source origin as an unknown factor in the solution. This factor is arbitrarily established.

The cellular model of Elgawhary [6] uses the cell to droplet diameter ratio as the matching parameter and does not deal with wet bulb temperature corrections. On the other hand, in the Frediani and Smith [7] cellular model, the initial droplet diameter and the air entrainment rate are the design-specific factors.

The cellular model is based on the concept that all of the air flowing through the cross-sectional area of the spray is entrained by the droplet and that the drop stays in the same cell throughout its trajectory. Both assumptions are unreal-

istic for the following reasons:

(1) The particle trajectories and the air streamlines are substantially different.

(2) The wet bulb temperature tends to rise faster than is observed experimentally. This suggests that, if one assumes total air entrainment, the cell volumes are smaller than the theory requires.

(3) If indeed all the air flowing through the first spray is entrained, in effect the downwind sprays experience zero wind velocity.

The dependence of the NTU and cellular models on empirical factors which depend on spray unit design and system configuration preclude their utilization in optimization studies. Furthermore, they cannot be used to predict the performance of new designs or to aid in the development of more efficient units and systems.

The PSI-Cell model does not depend upon the use of design-specific factors. It is best suited to analyze internal flows with known air flow rates and well defined boundaries. For external or unbounded flow systems the boundary conditions for the air-vapor phases are much more difficult to treat and the air flow rate is unknown. Therefore, application of this model to sprays may require the introduction of design-specific factors.

Soo's [17] model, despite its distinctive features, is based on uniform dry bulb temperature and relative humidity throughout the spray system. This restriction precludes its use for the determination of system performance as a function

of wind speed or for system configuration studies. His model does, however, lend itself to optimization of droplet size, spray height and diameter for maximum cooling.

The SER model requires two empirically determined functions for the prediction of system performance. In addition, the model for examining spray spacings requires the experimental determination of another design-dependent coefficient. This parameter must be increased by a factor of 135 over the classical turbulent viscosity to fit the experimental data [21] .

The model of Berger and Taylor requires no design-specific constants to predict spray performance. However, their assumption of saturated air in the entire spray domain would only hold true for zero or very low wind conditions, and for the last spray in a long pass of sprays for higher wind, where air has been progressively humidified by upwind sprays in the pass. The model is not valid for intermediate wind speeds and is physically inconsistent with known spray performance variations with wind speed. For a given set of ambient conditions, the model predicts better performance at zero wind speed than for moderate winds. Performance better than at zero wind speed is seen for higher winds. Applying this model to the study of optimizing the thermal performance of sprays is problematical due to several simplifying assumptions. The spray domain is not characterized by saturated air, except under conditions of highly humid ambient air and calm winds. This is the case for both a single spray and a spray system. The model cannot account for interaction

between sprays in a system since all sprays see saturated air under all wind and ambient conditions, which in effect, is specifying the wet-bulb interference factor in advance. The model also ignores detailed spray-air interaction by virtue of its bulk flow assumption.

Recognizing the importance of atmospheric turbulence and boundary layer characteristics in the performance of sprays, researchers have attempted to address this aspect of spray cooling. Arndt and Barry [5] utilize published turbulent diffusion coefficients that are functions of distance downwind from a virtual source to determine the variation of dry bulb temperature and humidity. Empiricism is introduced by the arbitrary determination of the source origin, although the position of the source can be varied with changes in wind direction.

Chen and Trezek [18] solve the two dimensional turbulent boundary layer equations for the mixing of parallel free shear layers using uniform upwind profiles of wind speed, temperature and humidity. A turbulent mixing parameter, which appears in the equations, is measured for a pass of three sprays that are spaced by a distance equal to the diameter of a spray umbrella. The mixing parameter is assumed constant for all spacings and ambient air conditions. This parameter essentially replaces the wet bulb correction factor as an empirical factor.

Although not used in their system model, Weinstein, et. al. [22] consider the effect of turbulence on the downstream dispersion of heat and humidity from a uniformly distributed

two-dimensional spray system of finite dimensions. These authors solve the two dimensional boundary layer equations using ambient turbulent diffusivity and wind profiles which depend on atmospheric stability and surface roughness. The simplified source term employed provides a reasonable description of the far field dispersion of heat and humidity and of fog formation far downwind of the spray canal where the effects of spray induced turbulent diffusivity and the detailed near field interaction between the wind and the sprays are neglected. The authors state that the good agreement with field data is somewhat fortuitous in view of their neglect of buoyancy effects in the model.

Chaturvedi and Porter [21] use wind and turbulent viscosity profiles of the equilibrium atmospheric surface layer obtained from Haltiner and Martin [23] in their model to predict local wet bulb temperature. While reasonable agreement with field data is obtained, the model relies on the empirical factor NTU to formulate the energy source term. Hence, the model is not suited for optimization studies on systems incorporating theoretically designed spray units.

Chen and Trezek [18] , Chaturvedi and Porter [21] and Weinstein, et. al. [22] do not use the latest information on the wind profiles and the related turbulent diffusivities in the atmospheric surface layer. Weinstein, et. al. use an empirical formula for the velocity profile from Sutton [24] which has since been substantially modified [25] .

In summary, current theories rely on design dependent empirical factors, lack design and performance optimization

capabilities and fail to adequately account for turbulence and atmospheric surface layer effects.

1. 3. Research Objectives

The present study will analyze the detailed local mass, momentum and energy interaction between the air-vapor phase and the droplets. The objectives of this comprehensive treatment of spray cooling phenomena are:

(1) Elimination of the need for design dependent empirical data such as NTU, SER, cell-droplet diameter ratio and air entrainment rate.

(2) Rigorous treatment of meteorological conditions such as the atmospheric boundary layer, turbulence and Reynolds stress.

(3) Formulation of a general (as opposed to design-specific) theory for spray units in terms of the governing parameters, with capabilities for design optimization.

(4) Prediction of the spatial distribution of the air-vapor velocity, dry bulb temperature and absolute humidity as well as the velocity, size and temperature of the droplets for an arbitrary wind profile.

The model can be extended to examine the interaction between neighboring downwind spray units in a system of sprays and to predict the performance of spray units in such a system.

CHAPTER II

AN AIR-VAPOR-DROPLET LOCAL INTERACTION MODEL FOR SPRAY UNITS

2. 1. Introduction

The present model for a spray unit is based on a dual Lagrangian description for both the air-vapor phase and the droplet phase. This model examines the detailed mass, momentum and energy interaction between droplet and air-vapor element having widely different time histories. An air-vapor element is a finite volume of the gas phase that travels through the spray field within a streamtube. The number of droplets contained within an air-vapor element varies according to the number of trajectories passing through the element and the number of droplets located along the portions of the trajectories lying within the element. Figure 3 depicts a finite element traversing the spray domain.

The droplet trajectory and the variation of droplet velocity, size and temperature along the trajectory are determined relative to the local conditions of the air velocity, dry-bulb temperature and wet-bulb temperature. Both droplet trajectories and air-vapor element streamlines are determined taking into account a detailed consideration of atmospheric phenomena including turbulent mixing, atmospheric stability and surface roughness. Droplet trajectories are found for an arbitrary initial discharge angle and size distribution using a particle momentum

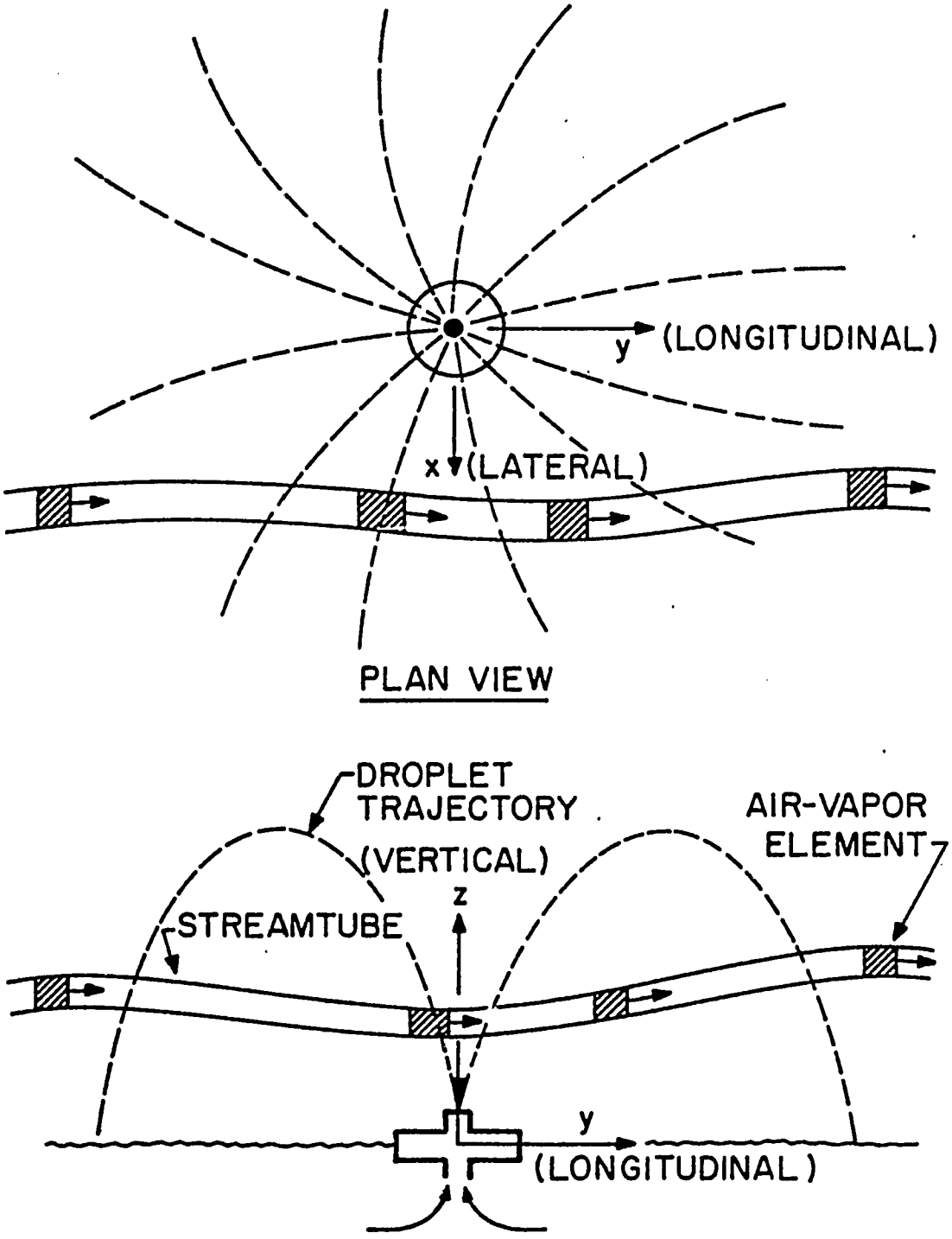

Figure 3. Trajectory of a Fluid Element as it Crosses the Spray Field.

equation in which the drag is based on the local velocity difference between the air-vapor and droplet phases. The droplet heat transfer and evaporation rate are similarly based on the local dry bulb temperature and absolute humidity in contrast to previous analyses which have been based on ambient or some constant average conditions.

The air-vapor streamlines are found for an arbitrary initial turbulent wind profile by integrating the equations of motion for an air-vapor element considering the local buoyancy force, droplet drag and turbulent diffusion along each air-vapor streamline. In this Lagrangian formulation for the air-vapor elements, the equations for conservation of species and energy are integrated along the streamlines of the air-vapor phase to determine the local variation in the dry bulb temperature and absolute humidity. In the species conservation equation, the local droplet evaporation rate along an air-vapor streamline is treated as a source term. Similarly, the convective and evaporative droplet energy transfer along an air-vapor streamline serve as source terms in the conservation of energy equation for the air-vapor element.

Turbulent diffusion of momentum, water-vapor and energy arising from mechanical shearing stresses and atmospheric instability is accounted for in the momentum, species and energy conservation equations for the air-vapor phase.

A complete description of the air-vapor field can thus be obtained by integrating these equations along selected streamlines across the spray umbrella. Since the

local properties of the air-vapor continuum and the droplet temperature and mass are all unknown initially, an iterative solution scheme must be developed as described in Chapter III.

The model uses no design-dependent empirical factors such as NTU, SER, effective initial droplet diameter and wet-bulb correction coefficients, which are obtained from experiments on sprays. The above mentioned empirical factors attempt to account for air-vapor-droplet interaction in an average sense. The present model involves the solution of the conservation equations that govern the local interaction between the air-vapor elements and the droplets. Hence, it obviates the need for design-specific empirical constants which are found necessary in previous models that do not attempt to satisfy all of the conservation laws for the two-phase spray field.

Empiricism is introduced in the present model to account for the heat and mass transfer from the droplets and turbulent mixing in the atmospheric surface layer. Correlation equations obtained from experiments on individual droplets falling in air are used to evaluate the droplet heat and mass transfer coefficients. Empirical turbulent mixing parameters (e.g. eddy viscosity, conductivity and diffusivity) are used to account for diffusion of momentum, heat and water vapor to or from the air-vapor elements in the atmospheric boundary layer.

2. 2. Meterological Considerations

Turbulence in the atmospheric surface layer (0-150m.) affects the shape of the ambient wind, temperature and humidity profiles. In particular, the diffusion of momentum, heat and water vapor from sprays is determined by the degree of turbulence in surface winds. While absolute humidity and dry-bulb temperature vary within the atmospheric surface layer, their variation is small over heights typical of sprays (5m.). Consequently, this temperature and humidity change with height can be neglected in the initial upwind profiles. However, turbulent mixing of these quantities within the spray itself is important. The initial upwind velocity variation over the spray height affects all subsequent transport processes occurring in the spray. The velocity profile in the turbulent surface layer takes on different forms depending on atmospheric stability. The stability of the atmosphere is characterized by the adiabatic lapse rate $\Gamma_{ad} = 9.8^{o}$ C/km:

$$\text{Neutral conditions:} \quad dT_{db}/dZ = -\Gamma_{ad}$$
$$\text{Unstable conditions:} \quad dT_{db}/dZ < -\Gamma_{ad}$$
$$\text{Stable conditions:} \quad dT_{db}/dZ > -\Gamma_{ad}$$

where Z is the height above the surface of the earth and T_{db} is the dry bulb temperature.

This wind velocity profile is given [25] as:

$$\bar{U}_\infty^*(z^*) = \alpha_s \left[\ln\left(\frac{z^*}{z_o^*} + 1\right) + \psi(z^*) \right], \quad (12)$$

where

$$\bar{U}_\infty^* \equiv \bar{U}_\infty / U_{\infty 2m}$$

$$z^* \equiv z / L_{mo}$$

$$z_o^* \equiv z_o / L_{mo}$$

$$\alpha_s \equiv u_* / k' U_{\infty 2m}$$

and

$\bar{U}_\infty$ = wind velocity

$\bar{U}_{\infty 2m}$ = wind velocity at Z = 2m

z_o = surface roughness height

u_* = friction velocity

k' = von Karman constant

L_{mo} = Monin-Obukhov length scale

$$= \frac{-\rho_a C_{pa} T_{db} u_*^3}{k' g H_o}$$

g = gravitational acceleration

C_{pa} = specific heat of dry air

H_o = vertical heat flux

The ℓn term in equation (12) is mechanical shear-produced turbulence whereas the second term is due to natural convection instabilities arising from thermal stratification.

The function $\psi(z^*)$ in the velocity profile takes on different forms depending on the stability condition of the atmosphere. For neutral air:

$$\psi(z^*) = 0 \quad . \tag{13}$$

For unstable air:

$$\psi(z^*) = -2\ell n\left[\tfrac{1}{2}\left(1+1/\phi_m\right)\right] - \ell n\left[\tfrac{1}{2}\left(1+1/\phi_m^2\right)\right] + 2\tan^{-1}\left(1/\phi_m\right) - \pi/2 \quad , \tag{14}$$

where

$$\phi_m = \left(1 - 15\,z^*\right)^{-1/4} \tag{15}$$

For stable air:

$$\psi\left(z^*\right) = 5\,z^* \tag{16}$$

Prediction of the turbulent diffusion of momentum, energy and water vapor in the air passing through a spray requires a knowledge of the turbulent mixing coefficients in the air. For neutral air the ratio of turbulent thermal conductivity to turbulent viscosity K_h/K_m is approximately equal to unity [25] :

$$\frac{K_h}{K_m} = \frac{K_{wv}}{K_m} \simeq 1 \tag{17a}$$

where K_{wv} is the turbulent diffusivity of water vapor in air. The turbulent air viscosity K_m is given by

$$K_m = u_*^2 \Big/ du/dz \,, \tag{17b}$$

where u is the longitudinal (in the wind direction) velocity component of air-vapor mixture within the spray.

For unstable air [25]

$$\frac{K_h}{K_m} = \frac{K_{wv}}{K_m} = \left(1 - 15 z^*\right)^{1/4} . \tag{17c}$$

For stable air the behavior of turbulent thermal conductivity K_h is uncertain [25] .

The atmospheric turbulent boundary layer can differ markedly from the familiar mechanical turbulent boundary layer profile when the Monin-Obukhov length is either negative or positive and of the order of the spray height or smaller. The wind profile has a profound effect on air-vapor-droplet interaction, controlling, along with the droplet drag and buoyancy, the process of momentum exchange.

The effect of the turbulent conductivity and diffusivity on the spray is to enhance (or retard, depending on atmospheric stability) the interchange of heat and water vapor among air-vapor elements and promote the mixing of ambient air with that undergoing energy exchange with the sprays. The inclusion of turbulent entrainment in the model enables one to examine the effect of the spacing of sprays in a spray module. The mixing of the heated and humidified

air downwind of a spray unit with ambient air is a function of spray spacing. Consideration of turbulent diffusion enables the model to predict the amount of wet-bulb depression as a function of such spacing, eliminating empirical mixing factors which are design specific.

2. 3. Assumptions

The major assumptions inherent in the theoretical analysis to follow are:

(1) Droplet mass is assumed constant in the total derivative terms of both the air and droplet momentum and energy equations. This is a reasonable approximation since the change in mass is less than 1% over the entire trajectory.

(2) Saffman, buoyancy, Basset and virtual mass forces are neglected in the droplet momentum equation. This can be justified by order of magnitude dimensional analysis (see Appendix).

(3) Droplets are always at a uniform temperature. This is true if the internal thermal relaxation time of the droplet is small compared to the flight time of the droplet. The thermal relaxation time depends on the intensity of fluid circulation within the droplet. Winnekow and Chao [26] observed experimentally that the amount of circulation within a droplet depends upon the value of:

$$b = \frac{2 + 3\,\frac{\mu_d}{\mu_a}}{1 + \sqrt{\frac{\rho_d}{\rho_a}\,\frac{\mu_d}{\mu_a}}}$$

where

μ_d = viscosity of fluid in droplet

μ_a = viscosity of ambient fluid

ρ_d = density of fluid in droplet

ρ_a = density of ambient fluid

For $b < 2.4$, vigorous internal circulation was observed in the droplet. For the air-water system considered here, the value of b is approximately 0.57. Hence, one can assume fully developed internal circulation.

The magnitude of the fluid velocity inside the droplet can be bracketed by calculating both the circulation velocities obtained from the inviscid flow solution (Hill's spherical vortex) and the Hadamard-Rybczynski velocity field for creeping flow. Both solutions are given in [27]. The inviscid flow solution gives a velocity at the center and surface of the droplet of $\frac{3}{2}|\bar{v} - \bar{u}|$, where $\bar{V}$ = droplet velocity in the ambient fluid and $\bar{U}$ = velocity of ambient fluid. In the creeping flow regime, the circulation velocity is given by $|\bar{v} - \bar{u}| / [2(1 + \mu_d/\mu_a)]$. For a water droplet whose diameter is 0.6 inches (1.524 cm) moving at 11.6 meters per second in air, the time required for the fluid in the droplet to complete one circulation is of the order of 10^{-3} seconds in the inviscid flow regime, and 0.25 seconds in the creeping flow regime. Since the time of flight of a droplet is approximately 2 seconds, and the internal flow field of the droplet is expected to approach

the inviscid flow solution (high Reynolds number), sufficient internal mixing exists to justify the assumption of an instantaneous uniform droplet temperature.

(4) Conduction in the air energy equation is neglected in comparison to convection, evaporation and turbulent thermal diffusion.

(5) The air pressure field is hydrostatic.

(6) The mass of water vapor in the air is small (typically less than 5%) and is neglected in the air continuity equation.

(7) Droplets can be treated as volumetric sources of mass, momentum and energy.

2. 4. Conservation Equations

2. 4. 1. Conservation of Mass for a Droplet

To determine the amount of evaporation that a droplet experiences during its time of flight, one relates the time rate of change of droplet mass to the evaporative flux across the concentration boundary layer of the droplet:

$$\frac{dM}{dt} = -\rho_a h_D \pi d^2 \left[\omega_s (T_d) - \omega\right]. \qquad (18a)$$

Equation (18a) can be written in the following dimensionless form:

$$\frac{d(d^*)}{dt^*} = \left(\frac{2\,Fr_o\,\tilde{\rho}\,\tilde{C}_p}{Sc_o\,Re_o\,Sf_o\,B_o}\right)\left(\frac{Sh\,D^*}{d^*}\right)\left[\omega_s^*(T_d^*) - \omega^*\right], \quad (18b)$$

where the superscript * denotes a dimensionless quantity and the subscript o denotes an initial value at the spray discharge.

B_o = Bowen ratio = $C_{pa}(T_{do} - T_{wb\infty}) \Big/ \left[L_{io}(\omega_s(T_{do}) - \omega_\infty)\right]$

C_{pa} = specific heat of air

C_{pd} = specific heat of water

$\tilde{C}_p = C_{pa}/C_{pd}$

D = mass diffusivity of water vapor in air

$D^* = D/D_o$

d_o = initial mean droplet diameter

$d^* = d/d_o$

Fr_o = Froude number = $V_o^2/g d_o$

g = acceleration due to gravity

h_D = mass transfer coefficient

L_{io} = latent heat of vaporization of water at T_{do}

$Re_o = \rho_a V_o d_o/\mu_a$

$Sc_o = \mu_a/\rho_a D_o$

Sf_o = Stefan number = $L_{io}/C_{pd}(T_{do} - T_{wb\infty})$

Sh = Sherwood number = $h_o d/D$

t^* = dimensionless time = gt/V_o

T_d = droplet temperature

$T_d^* = (T_d - T_{wb\infty})/(T_{do} - T_{wb\infty})$

T_{wb_∞} = wet-bulb temperature of the ambient air

v_o = initial speed of the mean size drop

μ_a = air viscosity

ρ_a = air density

ρ_d = droplet (water) density

$\tilde{\rho} = \rho_a / \rho_d$

ω = local absolute humidity of air

$\omega^* = (\omega - \omega_\infty) / (\omega_s(T_{d_o}) - \omega_\infty)$

$\omega_s(T_d)$ = absolute humidity of saturated air at T_d

$\omega_s^* = (\omega_s(T_d) - \omega_\infty) / (\omega_s(T_{d_o}) - \omega_\infty)$

ω_∞ = ambient absolute humidity

The Sherwood number Sh is determined by empirical correlations given by Ranz and Marshall [28] :

$$Sh = 2 + 0.6 (Re)^{1/2} (Sc)^{1/3} , \qquad (19a)$$

where

Re = Reynolds number = $\rho_a d |\bar{v} - \bar{u}| / \mu_a$

$\bar{u}$ = air velocity

Sc = Schmidt number = $\mu_a / \rho_a D$

The dimensionless mass diffusivity, D*, is given in [29] :

$$D^* = \left(\frac{T_d + 273.2}{T_{d_o} + 273.2} \right)^{1.75} ,$$

where T_d and T_{d_o} are in ^oC.

2. 4. 2. Conservation of Droplet Momentum

Droplet velocities are determined by applying Newton's law for a particle. Consideration is taken of gravitational forces and the drag induced by the local vector-velocity difference between the droplet and the air-vapor continuum. The resulting equation is:

$$M\frac{d\bar{v}}{dt} = M\bar{g} - \frac{C_D}{8}\rho_a \pi d^2 \left|\bar{v}-\bar{u}\right|\left(\bar{v}-\bar{u}\right) \qquad (20a)$$

In dimensionless form, equation (20a) becomes:

$$\frac{d\bar{v}^*}{dt^*} = \frac{-3}{4d^*}\tilde{\rho}\, C_{Do} F_{r_o} C_D^* \left|\bar{v}^* - \bar{u}^* V_e\right|\left(\bar{v}^* - \bar{u}^* V_e\right) - \bar{k} \;, \qquad (20b)$$

where

C_{Do} = drag coefficient for $Re > 1000$, $C_{Do} = 0.44$

$$C_D^* = \frac{C_D}{C_{Do}} = \frac{54.54}{Re}\left(1+0.15\,Re^{0.687}\right), \quad Re \le 1000 \quad [30]$$

$\bar{k}$ = unit vector in vertical direction

$\bar{u}$ = total air velocity $= \bar{U}_\infty + u'$, where $\bar{U}_\infty$ is the wind velocity and u' is the induced air velocity

$\bar{u}^* = \bar{u} / U_{\infty 2m}$

$U_{\infty 2m}$ = wind speed at a 2m. height

$\bar{v}^*$ = dimensionless droplet velocity $= \bar{v}/v_o$

V_e = velocity ratio $= U_{\infty 2m}/v_o$

A droplet trajectory is found from:

$$\frac{d\bar{s}_d^*}{dt^*} = \bar{v}^* \;, \qquad (21a)$$

where $\bar{S}_d^*$ is the displacement vector of the droplet:

$$\bar{S}_d^* = \frac{\bar{S}_d\, q}{V_o^2} \tag{21b}$$

2. 4. 3. Conservation of Energy for a Droplet

Taking into consideration surface convection and evaporation, and assuming that the droplet is at each instant at a uniform temperature, the energy balance gives:

$$-MC_{Pd}\frac{dT_d}{dt} = \tilde{\pi} d^2 h\left(T_d - T_{db}\right) + \tilde{\pi} d^2 \rho_a h_D \left(\omega_s(T_d) - \omega\right) L \tag{22a}$$

The terms on the right hand side are the energy given up by the droplet due to convection and evaporation, respectively. Non-dimensionalizing equation (22a) yields:

$$\frac{dT_d^*}{dt^*} = \frac{-6F_{ro}\tilde{\rho}\tilde{C}_P}{Re_o (d^*)^2}\left\{\frac{Nu}{Pr}\left(T_d^* - T_{db}^*\right) + \frac{Sh\, L^* D^*}{Sc_o\, B_o}\left[\omega_s^*(T_d^*) - \omega^*\right]\right\}, \tag{22b}$$

where

h = convective heat transfer coefficient

k_a = thermal conductivity of air

$L^* = L/L_o$

Nu = Nusselt number = hd/k_a

Pr = Prandtl number = $\mu_a C_{Pa}/k_a$

T_{db} = local dry bulb temperature of the air

$$T_{db}^{*} = \left(T_{db} - T_{wb_\infty}\right) \Big/ \left(T_{do} - T_{wb_\infty}\right)$$

The latent heat of vaporization of water, L, is given by Chow and Rowe [31] as:

$$L = 2326\left[1093.3258 - 0.57909483\left(1.8\,T_d + 32\right) + 2.28937\times10^{-4}\left(1.8\,T_d + 32\right)^2 - 1.113056\times10^{-6}\left(1.8\,T_d + 32\right)^3\right] \frac{J}{kg}$$

where T_d is in ^{o}C.

The Nusselt number Nu is obtained from empirical correlations for a droplet given by Ranz and Marshall [28] :

$$Nu = 2 + 0.6\,(Re)^{1/2}\,(P_r)^{1/3} \quad . \tag{23}$$

Equation (22b) when integrated along the droplet trajectory reduces to the Merkel equation (1) if one assumes a unit Lewis number, $h/h_D C_{ps} = 1$ and introduces the total heat function h(T) of the air.

2. 4. 4. Water Vapor Continuity Equation

To determine the variation of absolute humidity along any air-vapor streamline in the spray field, species conservation along a streamline is required. Conservation of mass for the water vapor in a fluid element gives:

$$\rho_a V \frac{dw}{dt} = \rho_a \pi d^2 n\, h_D \left[w_s(T_d) - w\right] + \rho_a V K_{wv} \frac{\partial^2 w}{\partial x^2} \tag{29}$$

where

$d\omega/dt$ is a Lagrangian derivative

V = volume of a finite air-vapor element

n = number of droplets in an air-vapor element

The first term on the right hand side of equation (29) is a source term giving the total amount of water vapor released by all droplets within the air-vapor element at any given time. The second term is the net efflux of water vapor across the boundaries of the element due to turbulent diffusion. It is seen that there is no net efflux of water vapor in the longitudinal and lateral directions, (for coordinate system, see Figure 3) as is also the case for turbulent transport of momentum and energy. This is true since there are no upwind gradients of wind velocity, absolute humidity and dry-bulb temperature in the longitudinal and lateral directions. It is these gradients that give rise to the turbulent viscosity, diffusivity and conductivity as can be seen, for example, from equation (17b). In the spray domain, lateral and longitudinal gradients will be produced by air-vapor-droplet interaction. It is assumed that these gradients are small compared to the vertical gradients.

If an element is considered to have the shape of a rectangular parallelpiped, the volume of an element can be characterized by an equivalent cube, whose side dimension is some multiple of the initial mean droplet diameter:

$$V = (c_o d_o)^3 \tag{30}$$

where

c_o = number indicative of the length scale of an element at any location in the spray field.

The element volume is determined by continuity considerations and is given by the streamtube cross-sectional area multiplied by a constant longitudinal dimension which is set arbitrarily. These considerations are explained in section 2.4.6.

Utilizing the above definition of element volume, equation (29) can be written in the following dimensionless form:

$$\frac{dw^*}{dt^*} = \frac{n\pi Fr_o Sh\, d^* D^*}{c_o^3 Sc_o Re_o}\left[w_s^*(T_d^*) - w^*\right] + \left[\frac{Tu_{wv\infty am} K_{wv}^*}{Re_o Fr_o}\right]\frac{\partial^2 w^*}{\partial z^{*2}} \tag{31}$$

where

$K_{wv}^* = K_{wv}/K_{wv\infty am}$

$K_{wv\infty am}$ = turbulent thermal diffusivity upwind of the spray at $z = 2$ m.

n = number of droplets in an element

$Tu_{wv\infty am}$ = diffusivity turbulent number = $K_{wv\infty am}/\nu_q$

z^* = dimensionless vertical coordinate = zg/v_o^2

Equation (31) is integrated along the gas-phase streamlines to determine ω^*. These streamlines are obtained from the momentum equation for the air-vapor element.

2. 4. 5. Conservation of Air Momentum

The velocity of an air-vapor element is found from a Lagrangian form of the momentum equation, as is done for the droplet velocity. Forces on the element are droplet drag, natural convection buoyancy and turbulent diffusion. The air momentum equation can be written as:

$$\rho_a V \frac{d\bar{u}}{dt} = \frac{1}{8} n \rho_a C_D \widetilde{\pi d^2} \left|\bar{v}-\bar{u}\right| \left(\bar{v}-\bar{u}\right) - \rho_a \beta_T V \bar{g} \left(T_{db}-T_{db_\infty}\right) + \rho_a V K_m \frac{\partial^2 u_y}{\partial z^2} \bar{\gamma} \qquad (32)$$

where

β_T = coefficient of thermal expansion of air

u_y = longitudinal (in the wind direction) air-vapor velocity

The dimensionless form of equation (32) is:

$$\frac{d\bar{u}^*}{dt^*} = \frac{n\widetilde{\pi} C_{D_0} Fr_0}{8 c_0^3 Ve} C_D^* d^{*2} \left|\bar{v}^* - Ve\,\bar{u}^*\right| \left(\bar{v}^* - Ve\,\bar{u}^*\right) + \frac{Gr\, Fr_0}{Ve\, Re_0^2} \left(T_{db}^* - T_{db_\infty}^*\right) \bar{k} + \left[\frac{Tu_{m_\infty am}\, K_m^*}{Re_0\, Fr_0\, Ve}\right] \frac{\partial^2 u_y^*}{\partial z^{*2}} \bar{\gamma} \qquad (33)$$

where

G_r = Grashof number = $c_o^3 \beta_T g d_o^3 (T_{do} - T_{wb\infty}) / \nu_a^2$

$K_m^* = K_m / K_{m\infty am}$

$K_{m\infty am}$ = turbulent viscosity of air upwind of spray at $z = 2m$.

$Tu_{m\infty am}$ = momentum turbulent number = $K_{m\infty am} / \nu_a$

ν_a = kinematic viscosity of air

2. 4. 6. Air Continuity Equation

The continuity equation for the air-vapor phase is formulated for a rectangular streamtube. The cross-sectional area of the streamtube upwind of the spray is given by the frontal area of an air-vapor element. The frontal area is the area of the face of the element perpendicular to the wind direction. This area changes as the element moves through the spray domain according to the following equation:

$$\rho_a v_y A = \rho_a U_\infty A_\infty \qquad (34)$$

where

A = cross-sectional area of a streamtube

A_∞ = cross-sectional area of a streamtube upwind of the spray

U_∞ = wind speed in the streamtube upwind of the spray

v_y = air-vapor velocity in the streamtube at any longitudinal distance y

If the cross-sectional area of a streamtube is given by:

$$A = \ell m \tag{35}$$

where

ℓ = lateral dimension of streamtube (dimension perpendicular to the wind direction and parallel to the X-axis)

m = vertical dimension of streamtube

equation (34) becomes:

$$\ell m = \frac{U_\infty}{v_y} \ell_\infty m_\infty \tag{36}$$

Defining

$$\ell^* = \frac{\ell}{v_o^2/g} \quad , \quad m^* = \frac{m}{v_o^2/g} \quad , \quad U_\infty^* = \frac{U_\infty}{U_{\infty am}} \quad ,$$

equation (36) can be written:

$$A^*(x^*, y^*, z^*) = \ell^* m^* = \frac{U_\infty^*}{v_y^*} \ell_\infty^* m_\infty^* \tag{37}$$

Equation (37) is solved for $A^*(x^*, y^*, z^*)$ along each streamtube.

Since the continuity equation (37) contains the two unknowns ℓ^* and m^*, one additional equation is necessary to solve for the streamtube dimensions. Such an equation can be derived from conservation of air momentum.

The streamtube dimensions ℓ^* and m^* depend upon the magnitude of the forces on the element in the lateral and vertical directions. By taking a ratio of the lateral and vertical components of the air momentum equation (33), one can formulate the additional equation needed to find ℓ^* and m^*.

Equation (37) requires the solution of only the longitudinal component of the air momentum equation (33), which is integrated stepwise in the wind direction. Hence, the ratio of the lateral and vertical components of equation (33) will be a function of longitudinal distance:

$$\frac{du_x^*/dt^*}{du_z^*/dt^*} = \frac{du_x^*}{du_z^*} = f^*(y^*) \tag{38}$$

where

$$f^*(y^*) = \left[\frac{n\hat{\pi} C_{D_o} Fr_o}{8 c_o^3 Ve} C_D^* d^{*2} \left|\bar{v}^* - Ve\,\bar{u}^*\right| \left(v_x^* - Ve\,u_x^*\right)\right] \Bigg/ \left[\frac{n\hat{\pi} C_{D_o} Fr_o}{8 c_o^3 Ve} C_D^* d^{*2} \left|\bar{v}^* - Ve\,\bar{u}^*\right| \left(v_z^* - Ve\,u_z^*\right) + \frac{Gr\,Fr_o}{Ve\,Re_o^2}\left(T_{db}^* - T_{db_\infty}^*\right)\right] \tag{38a}$$

Figure 4 depicts the change in streamtube dimensions as the air-vapor element moves through the spray field. As one proceeds from station 1 to station 2, ℓ^* and m^* change by the increments $d\ell^*$ and dm^*.

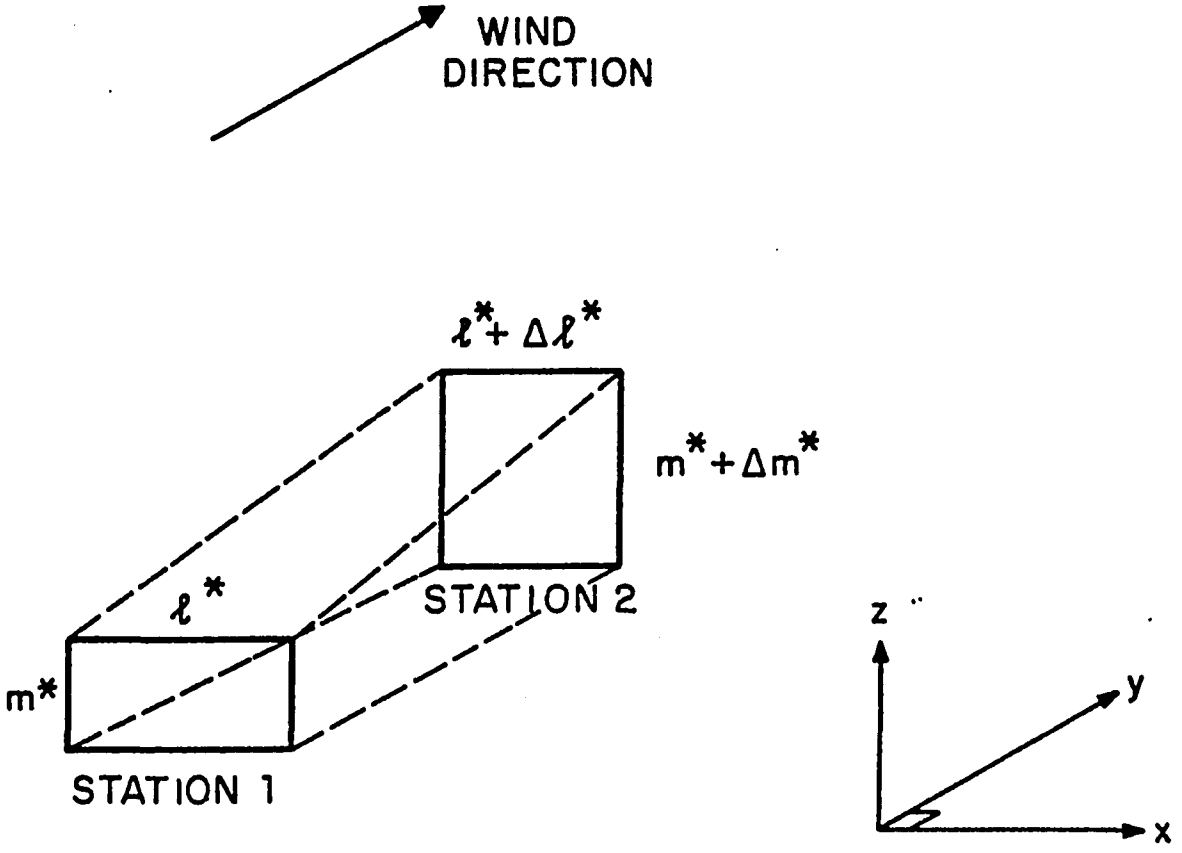

Figure 4. Change in Streamtube Cross-Sectional Area Along a Streamline.

Hence, one can write:

$$\frac{dl^*}{dt^*} = du_x^* \quad \text{and} \quad \frac{dm^*}{dt^*} = du_z^* \tag{39a,b}$$

Dividing (39a) by (39b) and using (38) one gets:

$$\frac{dl^*}{dm^*} = \frac{du_x^*}{du_z^*} = f^*(y^*) \tag{40}$$

Therefore, the ratio of the incremental changes of the lateral and vertical streamtube dimensions can be obtained from the ratio of the lateral and vertical components of the air momentum equation.

The change in streamtube area is given by:

$$\frac{dA^*}{dt^*} = \frac{d(l^* m^*)}{dt^*} = l^* \frac{dm^*}{dt^*} + m^* \frac{dl^*}{dt^*} \tag{41}$$

Multiplying through by dt*, one obtains:

$$dA^* = l^* dm^* + m^* dl^* \tag{42}$$

Solving equations (40) and (42) simultaneously gives:

$$dl^* = \frac{dA^* f^*(y^*)}{l^* + m^* f^*(y^*)} \tag{43a}$$

and

$$dm^* = \frac{dA^*}{\ell^* + m^* f^*(y^*)} \qquad (43b)$$

The incremental area dA* is obtained from the numerical solution of equation (37) along a streamline. $f^*(y^*)$, m^* and ℓ^* are known from the preceding streamline station. Having $d\ell^*$ and dm^* at the new station, the new streamtube dimensions are calculated from:

$$\ell^*_{i+1} = \ell^*_i + d\ell^* \qquad (44a)$$

and

$$m^*_{i+1} = m^*_i + dm^* \qquad (44b)$$

New vertical and lateral air-vapor velocities are given by:

$$U_x{}^*_{i+1} = U_x{}^*_i + dU_x{}^* \qquad (45a)$$

$$U_z{}^*_{i+1} = U_z{}^*_i + dU_z{}^* \qquad (45b)$$

where, $dU_x{}^*$ and $dU_z{}^*$ are obtained from equations (39a,b) and $U_x{}^*_i$, $U_z{}^*_i$ are known from the previous streamline station. The air-vapor streamline itself is found from:

$$\frac{d\bar{s}_a{}^*}{dt^*} = \bar{U}^* \qquad (46)$$

2. 4. 7. Air Energy Equation

Neglecting conduction in comparison with turbulent diffusion of heat, one can write for conservation of energy along an air-vapor streamline:

$$\rho_a C_{pa} V \frac{dT_{db}}{dt} = n\bar{\pi} d^2 h (T_d - T_{db}) + n\bar{\pi} d^2 L h_D \rho_a (\omega_s(T_d) - \omega) + \rho_a C_{pa} V K_h \frac{\partial^2 T_{db}}{\partial z^2} \quad (47)$$

Taking $K_h = K_{wv}$, one can write equation (47) in dimensionless form as:

$$\frac{dT_{db}^*}{dt^*} = \frac{n\bar{\pi} F_{ro}}{C_o^3 Pr Re_o} \left[\frac{Nu d^*}{Pr} (T_d^* - T_{db}^*) + \frac{Sh d^* L^* D^*}{Sc_o B_o} (\omega_s^*(T_d^*) - \omega^*) \right] + \left[\frac{T u_{wv\infty am} K_{wv}^*}{Re_o Fr_o} \right] \frac{\partial^2 T_{db}^*}{\partial z^{*2}} \quad (48)$$

The terms on the right hand side of equation (48) represent convective and evaporative heat transfer from the droplets and turbulent diffusion of heat in that order.

CHAPTER III

SOLUTION OF MODEL EQUATIONS

In this chapter, the detailed solution procedure for determining the droplet trajectories, sizes and temperatures, the air-vapor streamlines, and the dry-bulb temperature and absolute humidity in the spray domain and downwind of a single spray unit will be presented. The iterative solution technique used in solving the conservation equations for the air-vapor-droplet, two-phase system is described below.

3. 1. Iterative Solution Technique

Figure 5 depicts the general method utilized to solve for the two-phase flow, temperature and humidity fields of a spray. In obtaining the lowest order solution for the droplet velocities, locations, temperatures and sizes, one considers the local environment of the drops to be that of the ambient air-vapor phase. However, the first order solution for the air-vapor velocities, streamlines, temperatures and humidities yields a correction to the local environment of the drops. The corrected air-vapor phase solutions are utilized in the next iteration on the droplet phase as detailed below.

Droplet trajectories and air-vapor streamlines cross at many locations in the spray domain. The velocity, temperature and humidity of the air-vapor element as it crosses a given droplet trajectory is the local environment of the

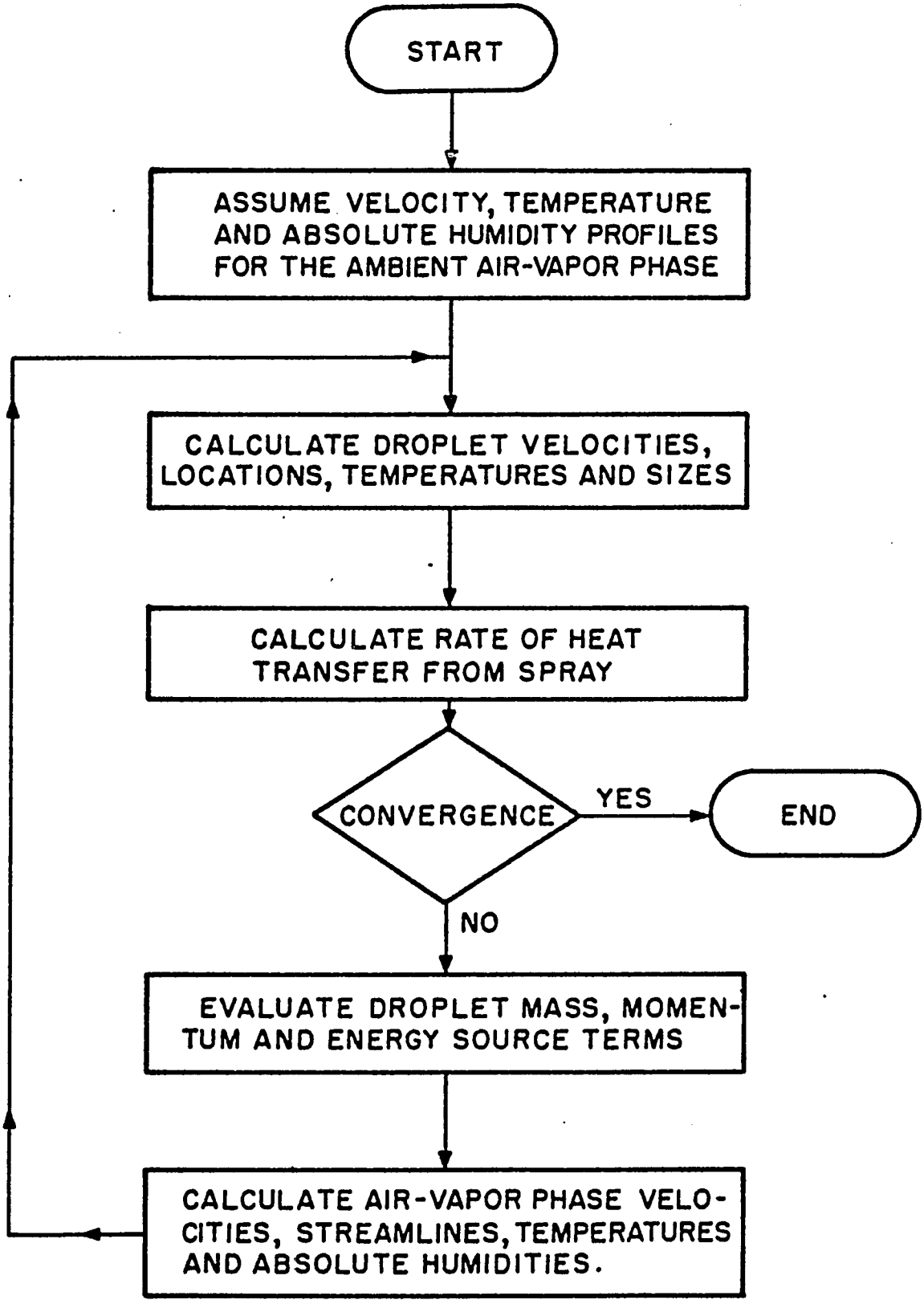

Figure 5. Flow Chart for Spray Unit Analysis.

droplets at this location. By assigning the new air-vapor properties to locations along each droplet trajectory where the trajectories and streamlines cross, one obtains the first order corrections to the air-vapor phase along each trajectory. One can now solve the droplet equations again, using the corrected local values of the air-vapor properties instead of the ambient values given by the upwind velocity, temperature and humidity profiles of the air-vapor continuum. The resulting solutions for droplet location, velocity, temperature and size are utilized in the evaluation of the mass, momentum and energy source terms appearing in the air-vapor phase equations. Hence, one can obtain the second order solution for the gas phase and again assign the air-vapor properties obtained to the droplet trajectories where they cross the gas-phase streamlines. This would complete the second order solution for the two-phase system.

The above iterative solution procedure is repeated until successive iterations on the droplet phase yield values of the rate of heat transfer from the spray that fulfill the following convergence criteria:

$$\frac{\dot{Q}_k - \dot{Q}_{k-1}}{\dot{Q}_{k-1}} \leq \epsilon \qquad (49)$$

where

$\dot{Q}_k$ = rate of heat transfer from the spray calculated for iteration k

ϵ = prescribed tolerance

The total heat transfer from the spray is given by:

$$\dot{Q}_k = \frac{\rho_d C_{pd} \pi}{6} \sum_{j=1}^{T} \dot{n}_{dj} \left[T_{do} d_j^3 - T_{cj} d_{cj}^3 \right] \qquad (50)$$

where, subscript c refers to the value of the variable when the droplet returns to the canal, and

T = total number of trajectories

$\dot{n}_{dj}$ = number of drops of size d_j ejected per unit time along a given trajectory

The following sections describe how the droplet and air-vapor phase conservation equations are solved for each iteration.

3. 2. Solution of the Droplet Equations

3. 2. 1. Droplet Momentum Equation

Since the model takes into consideration the local two-phase interaction between the drops and the air-vapor phase, the spatial distribution of the droplets throughout the flow field must be found. The droplet trajectories are determined by integrating equation (20b) for conservation of droplet momentum, and the distribution of droplets along the trajectories is found from the auxiliary equations derived below.

The water ejected from the nozzle is assumed to immediately break up into drops of either a single size or a discrete distribution of sizes.

Knowing the mass flow rate of water through the nozzle, $\dot{m}_o$, one can determine the number of drops ejected per unit time from:

$$\dot{N}_{di} = \frac{\gamma_i \dot{m}_o}{\rho_d \pi d_i^3/6} \tag{51}$$

where

$\dot{N}_{di}$ = number of drops of size d_i ejected from the nozzle per unit time

γ_i = fraction of nozzle flow rate discharged as drops of size d_i

d_i = diameter of droplet of the ith size

If it is assumed the drops are discharged at a finite number of sites around the circumference of the nozzle, the number of drops of size d_i ejected from each of these sites per unit time is

$$\dot{n}_{di} = \frac{\dot{N}_{di}}{\alpha} \tag{52}$$

where

α = number of discharge sites around the circumference of the nozzle (See Figure 7).

For the coordinate system shown in Figure 6, the initial velocity components of each drop are:

$$V_{xi}^* = \left(\frac{V_{oi}}{V_o}\right) \cos\varphi \cos\theta \tag{53a}$$

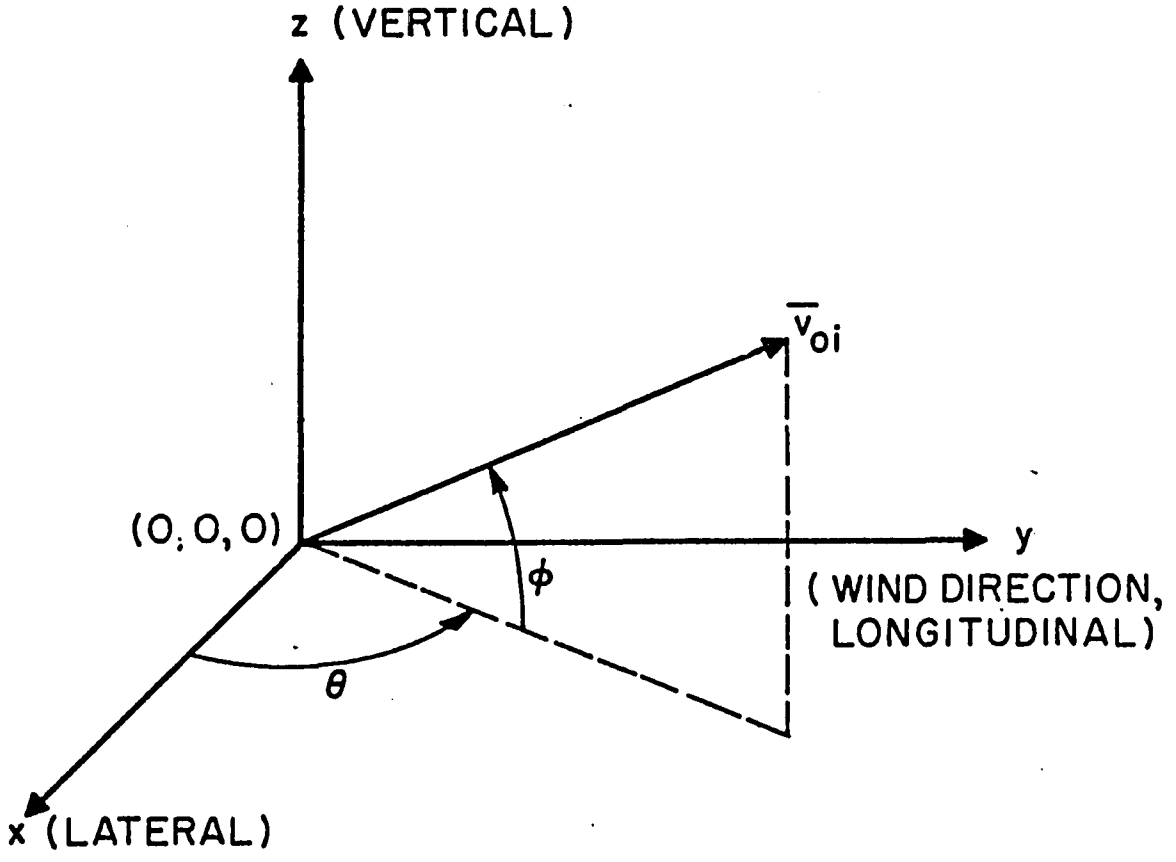

Figure 6. Coordinate System for Spray Unit Analysis. Origin is at the Water Surface Directly Below the Nozzle.

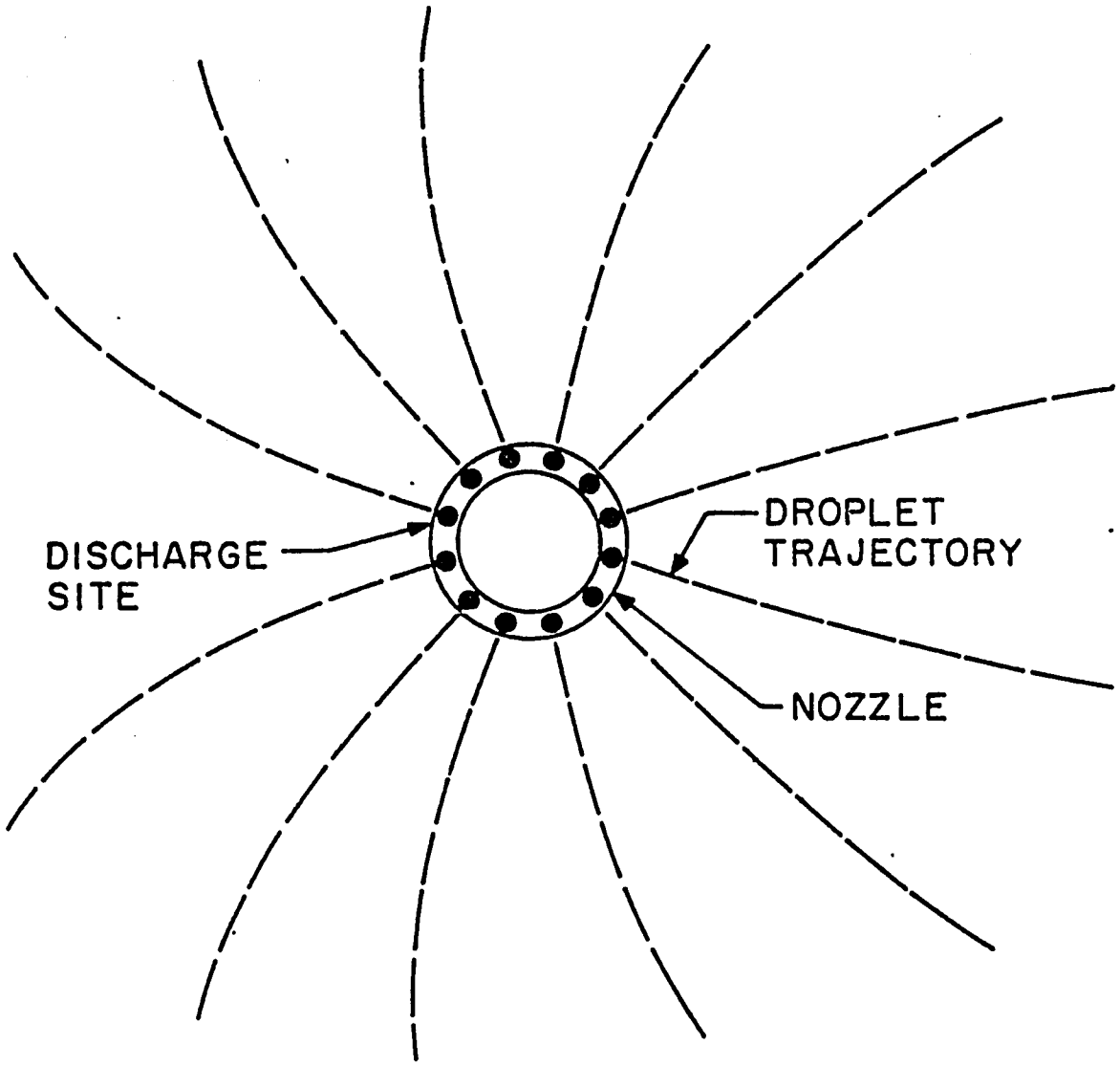

Figure 7. Spray Nozzle Showing Droplet Discharge Sites.

$$v_{yi}^{*} = \left(\frac{v_{oi}}{v_o}\right) \cos\varphi \sin\theta \qquad (53b)$$

$$v_{zi}^{*} = \left(\frac{v_{oi}}{v_o}\right) \sin\varphi \qquad (53c)$$

where

v_{oi} = initial speed of drops of size i.

The solution of the droplet momentum equation requires the specification of the turbulent wind profile. The wind velocity profile given earlier is

$$U_{\infty}^{*}(z^{*}) = \alpha_s \left[\ln\left(\frac{z^{*}}{z_o^{*}} + 1\right) + \psi(z^{*}) \right] \qquad (12)$$

The surface roughness height z_o, and the Monin-Obukov length scale L_{mo}, can be obtained from [32] for given surfaces and weather conditions. This gives the value of the dimensionless parameter $z_o^{*} = z_o / L_{mo}$. Equation (12) can then be solved for α_s by specifying the wind speed at a two-meter height and using the appropriate expression for $\psi(z^{*})$ depending on atmospheric stability (equations (13), (14), or (16)).

During the first iteration on the droplet phase, the velocity profile given by (12) is assumed to exist throughout the spray field. For subsequent iterations, the air-vapor velocity profiles used are those obtained by considering air-vapor-droplet momentum exchange.

Using boundary conditions (53, a, b, c), one integrates equation (20b) to determine the velocity as a function of time for each size droplet throughout its trajectory. For example, if one specifies 36 sites around the nozzle circumference where drops are ejected, and five different droplet sizes, then there will be five trajectories originating at each site, one for each size drop, for a total of 180 trajectories. The trajectory of the droplet is found from equation (21a) once the velocity history of the droplet is known.

The spatial distribution of the drops along a given particle trajectory is found by the method described below.

The numerical solution of equations (20b) and (21a) gives the time of flight for a droplet on any given trajectory. Multiplying the number of drops of size d_i ejected per site per second by the time of flight of the droplet gives the total number of droplets of size d_i in flight along a given trajectory. The droplet momentum equation is now solved again to locate each droplet. This is done by requiring that drops be positioned along the trajectory at equal time intervals Δt^*_{ij} in the solution of equations (20b) and (21a), where Δt^*_{ij}, the time interval between droplets, is given by:

$$\Delta t^*_{ij} = \frac{t_{fij} / (v_o/g)}{n_{dij}} \tag{54}$$

where

t_{fij} = time of flight of droplet d_i in flight along trajectory j

n_{dij} = total number of droplets of size d_i in flight along trajectory j = $\dot{n}_{dij} t_{fij}$

This procedure is repeated for each trajectory to obtain the complete description of the instantaneous positions of all droplets in the spray domain. At each particle location, one knows the droplet velocity components (from the solution of equation (20b)) needed to evaluate the momentum source term in the air-momentum equation.

3. 2. 2. Conservation of Energy for a Droplet

The numerical integration of equation (22b) along each particle trajectory gives the temperature of a droplet in flight along that trajectory. At each iteration, one assumes that the droplet trajectory is known from the procedure outlined in section 3. 2. 1. The convective and evaporative terms in equation (22b) require the evaluation of the local Reynolds number which appears in the empirical correlations for the Nusselt and Sherwood numbers. The Reynolds number is found from the known distribution of droplet velocities obtained in section 3. 2. 1., and the local values of air velocity obtained from the previous iteration on the air-vapor phase. The local dry-bulb temperature and absolute humidity used in evaluating the driving potential for convection and evaporation from the drops, are also obtained from the previous iteration on the air-vapor phase.

In the immediate vicinity (boundary layer) of the drops, the environment is one of air saturated with water vapor. The difference between the absolute humidity of this saturated air and the local absolute humidity of the air-vapor fluid element containing the drops is the driving force for evaporative heat transfer. The absolute humidity of an air-vapor mixture can be found from the Carrier Psychrometric Equation [33] :

$$\omega = 0.622\left[P_{wvs} - (P - P_{wvs})(T_{db} - T_{wb}) \times \left(1531.7 - 1.433\,T_{wb}\right)^{-1}\right] \frac{\text{kg water}}{\text{kg dry air}} \qquad (55a)$$

where

P_{wvs} = vapor pressure of saturated air (atm)

P = total air pressure (atm)

The vapor pressure of saturated air is found from:

$$P_{wvs} = \frac{P_{wvos}}{760}\left[1.000775 - 3.13 \times 10^{-4} T_{wb}\right] atm \qquad (55b)$$

where

$$P_{wvos} = 10^{\left[8.10765 - \frac{1750.286}{235 + T_{wb}}\right]} \; mm\ Hg \qquad (55c)$$

The dry-bulb and wet-bulb temperatures in equations (55a,b,c) are in degrees Centigrade. The air-vapor mixture in a thin boundary layer surrounding the droplet can be assumed satur-

ated at the temperature of the drop. Setting $T_{db} = T_{wb} = T_d$ in equations (55a, b, c) one obtains

$$\omega_s(T_d) = 8.184 \times 10^{-4} P_{wvos} \left[1.000775 - 3.13 \times 10^{-4} T_d \right] \frac{\text{kg water}}{\text{kg dry air}} \quad (56a)$$

$$P_{wvos} = 10^{\left[8.10765 - \frac{1750.286}{235 + T_d} \right]} \text{ mm Hg} \quad (56b)$$

All drops exiting from the nozzle are assumed to be at the same temperature, T_{do}. In dimensionless form ($T^*_{do}=1$) this temperature is used as the initial condition to solve the droplet energy equation along each trajectory.

3. 2. 3. Conservation of Mass for a Droplet

The change in droplet diameter during its flight is found from the integration of equation (18b). Drops of a given initial size which are ejected from the same site along the nozzle circumference, follow the same trajectory. Since droplets of one or more discrete initial sizes in the drop size distribution are ejected from each site, a different trajectory will be generated for each initial size. The initial droplet diameter, scaled to the diameter of the mean size drop, is used as the initial condition in solving equation (18b). This yields the diameter of each drop along its entire trajectory.

One now has the complete solution for the droplet phase for a given iteration.

3. 3. Solution of Air-Vapor Phase Equations

3. 3. 1. Conservation of Air Momentum

The air-vapor streamlines are obtained by solving equation (33). The initial velocity for each air-vapor streamline entering the spray is given by the turbulent wind profile upwind of the spray. The frontal area (area normal to the wind direction) of a three-dimensional air-vapor element is obtained by specifying the number of streamlines to be computed laterally and vertically. This technique is described below.

From the solution of the droplet trajectories, one can find the furthest lateral distance from the nozzle that a drop has traveled before striking the canal surface. In addition, one can find the maximum height of the spray umbrella. The product of these two dimensions gives the cross-sectional area for air-vapor flow through half the spray field. One only needs to determine trajectory and streamline solutions for half the spray domain due to symmetry considerations. If one wishes to calculate 20 streamlines vertically and ten streamlines laterally for half the flow field, the frontal area of each air-vapor element is 1/400th of the total frontal rectangular cross-sectional area for the entire flow. A streamline originates

from each corner of the rectangle forming the frontal area of an air-vapor element. The longitudinal dimension of the element is arbitrarily taken to be equal to about 1/100th of the longitudinal extent of the spray field.

As an air-vapor element enters the spray, it sees a non-uniform field of droplet velocities, temperatures, number densities and sizes. These droplets are the sources of mass, momentum and energy to the air-vapor phase. The momentum source term in equation (33) is evaluated as described below.

The solution of the droplet momentum and trajectory equations gives the velocity of each drop in flight and its location in the spray field. Hence, the identity of droplets within any air-vapor element as it traverses the spray is known. The drop velocity used in the momentum source term is taken to be a weighted average of all drop velocities in the moving control volume of the air-vapor element. The weighted average drop velocity components are found from:

$$V_x^* = \sum_{i=1}^{H} \frac{n_i}{n} V_{xi}^* \tag{57a}$$

$$V_y^* = \sum_{i=1}^{H} \frac{n_i}{n} V_{yi}^* \tag{57b}$$

$$V_z^* = \sum_{i=1}^{H} \frac{n_i}{n} V_{zi}^* \tag{57c}$$

where

I = total number of different droplet sizes in the air-vapor element

n_i = number of droplets of size d_i in the element

n = total number of droplets in the element

$V^*_{xc_i}, V^*_{yc_i}, V^*_{zc_i}$ = velocity components of drop size d_i in the element

The droplet size d* used in the momentum source term is a weighted average size obtained in the same manner as the velocity components.

The second term on the right hand side of equation (33) gives the buoyancy force on the air-vapor element arising from the elevation of the local dry-bulb temperature over ambient. The local dry-bulb temperature is obtained by solving the air energy equation simultaneously with the air momentum equation. The ambient dry-bulb temperature, $T_{db\infty}$, is given by its uniform profile upwind of the spray.

Turbulent diffusion of momentum from the air-vapor element is given by the last term in equation (33). The evaluation of this term requires a knowledge of the local air velocity profiles in the spray domain. As the air-vapor element enters the spray, this profile is given by the turbulent wind velocity profile. Local momentum interaction disturbs the upwind profile, creating local profiles with bumps and valleys. These profile irregularities tend to

be washed out due to the smoothing effect of turbulence. In solving the air momentum equation, the second derivative in the diffusion term is calculated from the local air velocity profile immediately upwind of the present position on the streamline. This forward marching technique allows equation (33) to be solved explicitly.

3. 3. 2. Air Continuity Equation

The method used for satisfying conservation of mass for the air-vapor phase was detailed in section 2. 4. 6. The determination of the local streamtube dimensions requires the solution of equation (33) for the longitudinal component of the air-velocity. This longitudinal component is used to determine the cross-sectional area of the streamtube through the use of equation (37). The new vertical and lateral streamtube dimensions are obtained from equations (44a, b) along with equations (43a, b). Whereas the longitudinal component of the air velocity is given by the solution of the air momentum equation, the lateral and vertical components are obtained from equations (45a) and (45b), respectively. Equations (45a, b) are solved with the help of equations (39a, b) and (43a, b), which require evaluation of the remaining two components of the air momentum equation, which were unused up to this point.

3. 3. 3. Air Energy Equation

The droplets act as sources of heat and water vapor to the air-vapor elements. The number of droplets of each

size that are contained within a given element at a given time is known from the spatial distribution of the droplets in the spray field. The weighted average temperature of the droplets within the air-vapor element is obtained from:

$$T_d^* = \sum_{i=1}^{I} \frac{n_i}{n} T_{d_i}^* \tag{58}$$

Knowing n and T_d^*, the convective and evaporative source terms in equation (48) can be evaluated.

The second derivative of the dry-bulb temperature with respect to height, which appears in the diffusion term of equation (48) is evaluated from the dry-bulb temperature profile immediately upwind of the current station. The turbulent diffusivity K_{wv}^*, is calculated from equations (17a,c). The dry-bulb temperature profiles are uniform upwind of the spray. As the air enters the spray, boundary conditions are imposed on the profiles. At the canal surface, the dry-bulb temperature is equal to the water temperature. At the top of the spray, the dry-bulb temperature is ambient. The thermal boundary layer grows with increasing longitudinal distance and the streamlines tend to rise. The uppermost streamline at the top of the spray is at the ambient dry-bulb temperature. The air energy equation is solved simultaneously with the air momentum equation and the water vapor continuity equation along each air-vapor streamline.

3. 3. 4. Water Vapor Continuity Equation

The evaporative source term in equation (31) is evaluated in the manner described in the preceding section. The second derivative of absolute humidity with respect to height, contained in the diffusion term, is evaluated from the local absolute humidity profile immediately upwind of the current streamline station. Boundary conditions are imposed on these profiles. The absolute humidity at the canal surface is given by the saturated absolute humidity evaluated at the canal temperature. The uppermost streamline is maintained at the ambient absolute humidity.

This completes the solution for the droplet and air-vapor phases for any given iteration.

CHAPTER IV

SPRAY CHARACTERISTICS AND MODEL VERIFICATION

The present model is capable of predicting the air-vapor velocity, absolute humidity and temperature fields of a spray unit, in addition to the droplet trajectories, velocities, temperatures and sizes. To demonstrate this ability, the characteristics of the spray field are shown for a selected spray unit design operating under typical summer environmental conditions. Verification of the predicted flow fields awaits more extensive experimental investigations.

The validity of the present model was tested by comparing model predictions of cold droplet temperatures, downwind air wet-bulb temperatures and downwind air velocities for a single spray unit. The data were obtained from the literature for two different types of sprays used for power plant cooling. These sprays are the Powered Spray Module (PSM) manufactured by the Ceramic Cooling Tower Company and the Spraco 1751 manufactured by the Spray Engineering Company.

4. 1. Spray Characteristics

The model was used to calculate the detailed two-phase flow field for a unit of the Powered Spray Module (PSM).

The PSM is composed of four individual nozzles spaced 12.2 m. apart and connected by a manifold. The

module is supported on the water surface by floats, one located at each spray nozzle, one between each set of two nozzles, and one supporting the pump at the center of the module. The module is aligned parallel to the canal edge (see Figure 1). The pump is powered by a 56kw electric motor directly coupled to the pump's impeller. Each nozzle sprays approximately 9470 liters of water per minute. The nozzles are located three feet (0.92 m) above the water surface. The maximum spray height is 6.1 meters and the radius of the spray pattern is 6.1 meters at the water surface in the absence of wind.

The initial droplet velocity ($V_o = 11.64$ m/s), and the spray discharge angle ($\varphi = 74°$), were obtained from Wilson [34]. In the model, droplets were discharged from 36 sites around the nozzle perimeter, producing a droplet trajectory every 10 degrees. The model was applied to only half the spray domain due to symmetry considerations, as explained in Chapter 3.

The spray was assumed to be monodisperse since no data are available on the droplet size distribution of the PSM. The value of the initial droplet size exiting the nozzle was obtained by varying the drop diameter until the single particle momentum equation (20b) yielded a trajectory of 6.1 m height above the canal surface, and 6.1 m from the nozzle in a horizontal plane, for the condition of zero wind.

Figures 8-15 show model predictions of the detailed air-vapor-droplet flow fields of a spray unit. All results

are for summer ambient design conditions. These conditions are given in section 5.2.

Figure 8 shows the trajectories of droplets ejected from the PSM at initial angles of $\Theta_o = -85^o$ and $\Theta_o = 85^o$ in the x-y plane for the condition of low wind (Ve=0.10). Also shown are a number of air-vapor streamlines traversing the spray domain near the centerline (y-axis) of the PSM. The effect of the upwind droplets in blocking the air-vapor flow is seen by the rising of the streamlines upwind of the nozzle. Continuity demands that the streamlines rise due to the reduced air-vapor velocity and the small lateral forces of the droplets on the air (the streamlines are not deflected very much laterally). Downwind of the nozzle, the droplets speed up the air and force the streamlines to descend.

Figure 8 also reveals the effect of buoyancy on the streamline pattern. Near y*=-0.39, the droplets following the upwind trajectory have a horizontal velocity component which is small compared to the vertical component, since the droplets are falling almost vertically. One would therefore expect little blockage of the air-vapor flow near the lowest streamline in Figure 8, and consequently, little rise of this streamline near y*=-0.39. These expectations are borne out in the figure. However, at y*=-0.39 the other streamlines, which have not as yet interacted with the spray, are seen to rise substantially.

This effect is due to the buoyancy force produced by the heated air near the lowest streamline which has undergone thermal interaction with the droplets near $y^*=-0.39$.

The streamlines at $y^*=0.0$ have not seen the downwind droplets. As stated above, the effect of the downwind droplets is to speed up the air and cause the streamlines to descend. However, one notices the streamlines descending before the air-vapor elements interact with the downwind droplets. This results from turbulent diffusion of heat from the hot air-vapor elements near the top of the spray to the cooler ambient free stream.

Figure 9 is a plan view of the PSM spray field at low wind. Droplet trajectories are plotted for half the spray domain. Air-vapor streamlines initially at a 2 meter height are also shown. One can readily see the small effect of drag on the droplets at low wind since the droplet trajectories lie essentially in vertical planes. The lateral entrainment of air by the spray is revealed by the compression of the streamlines downwind of the nozzle. This effect is also seen in Figure 10, where the air-vapor velocities are higher downwind of the spray than upwind. Vertical air entrainment can be seen from Figures 8 and 10. In these figures, the uppermost streamline is lower downwind of the spray than upwind, indicating the tendency of the spray to pull ambient air downward. Entrainment of ambient air is required to satisfy continuity. In Figure 9, the closer streamline spacing downwind of the spray is due

exclusively to momentum interaction between air-vapor and droplets. The higher air-vapor velocities downwind of the nozzle demand a smaller flow area to conserve mass. Since the flow area downwind of the nozzle is less than the spray cross-sectional area (which is also the initial area for air-vapor flow), ambient air is drawn from the surroundings to replace that which has been drawn closer to the centerline of the nozzle. For the case of vertical entrainment, cooling of the air-vapor flow due to turbulent diffusion of heat from the air-vapor elements, as well as the acceleration of the air-vapor flow by the downwind droplets can cause ambient air to enter the spray domain in satisfaction of continuity. The lateral and vertical entrainment by the spray at low wind indicates that more air participates in the local mass, momentum and energy interaction with the spray than initially enters the spray domain with the ambient wind. The ability of the model to predict this effect obviates the necessity of empirical entrainment coefficients used by other investigators.

Figure 11 shows typical absolute humidity profiles near the PSM centerline for low wind. Upwind of the spray, the absolute humidity profile is uniform. As air enters the spray, it is progressively humidified, and exhibits the developing profiles depicted in Figure 11. The lower boundary condition on the profiles is the saturated humidity at the temperature of the canal water. One notices that the humidity boundary layer that develops at low wind is substantially different from the momentum boundary layer

(Figure 10). Dry-bulb temperature profiles exhibit similar behavior to the absolute humidity profiles.

Figures 12-15 show PSM droplet trajectories, air-vapor streamlines, air-velocity profiles and absolute humidity profiles for high wind conditions. Figures 12 and 13 reveal the substantial distortion of the droplet trajectories at high wind, while the air-vapor streamlines are little affected by the droplets. Streamline spacing is wider downwind of the spray than upwind indicating that no significant entrainment has taken place. Rather, slightly less air interacts with the spray than initially enters the spray domain via the wind. The growth of the momentum and humidity boundary layers is depicted in Figures 14 and 15. The blockage effect of the spray is seen in Figure 14 where the air-velocities downwind of the spray are lower than the upwind ambient air-velocities. Comparing Figures 11 and 15, one notices that the humidity profiles develop more rapidly at low wind than at high wind. The greater air flow through the spray at high wind results in local conditions closer to ambient conditions and accounts for the smaller increase in local humidity.

4. 2. Comparison of Model Predictions with Experimental Data

4. 2. 1. The Powered Spray Module (PSM)

The present model for a single spray unit was compared with data [35] for one spray of the PSM. The data were obtained from field measurements at Dresden and Quad-Cities Nuclear Stations of the Commonwealth Edison Company. Data

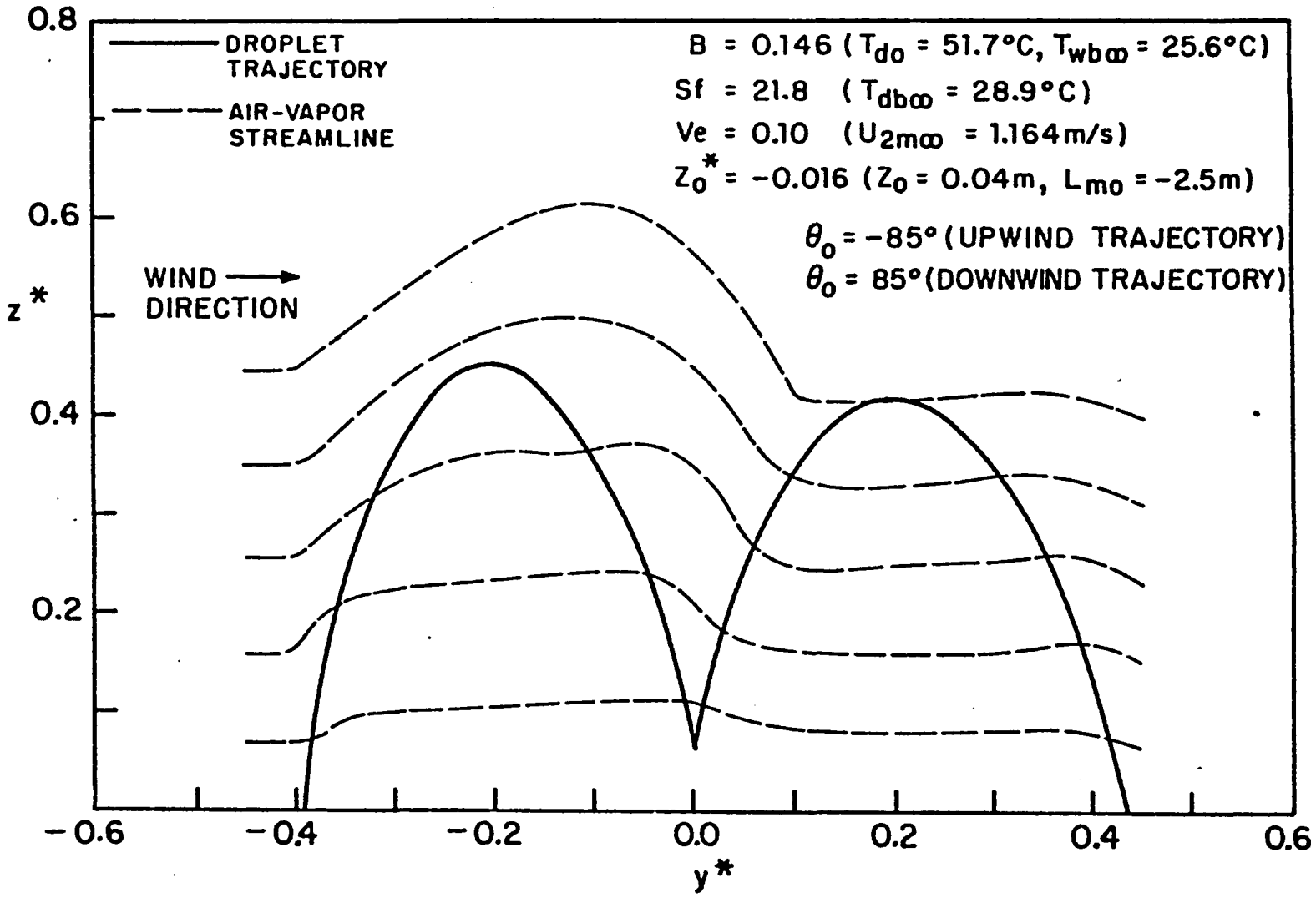

Figure 8. Air-Vapor Streamlines Near Centerline of PSM for Low Wind (Elevation View).

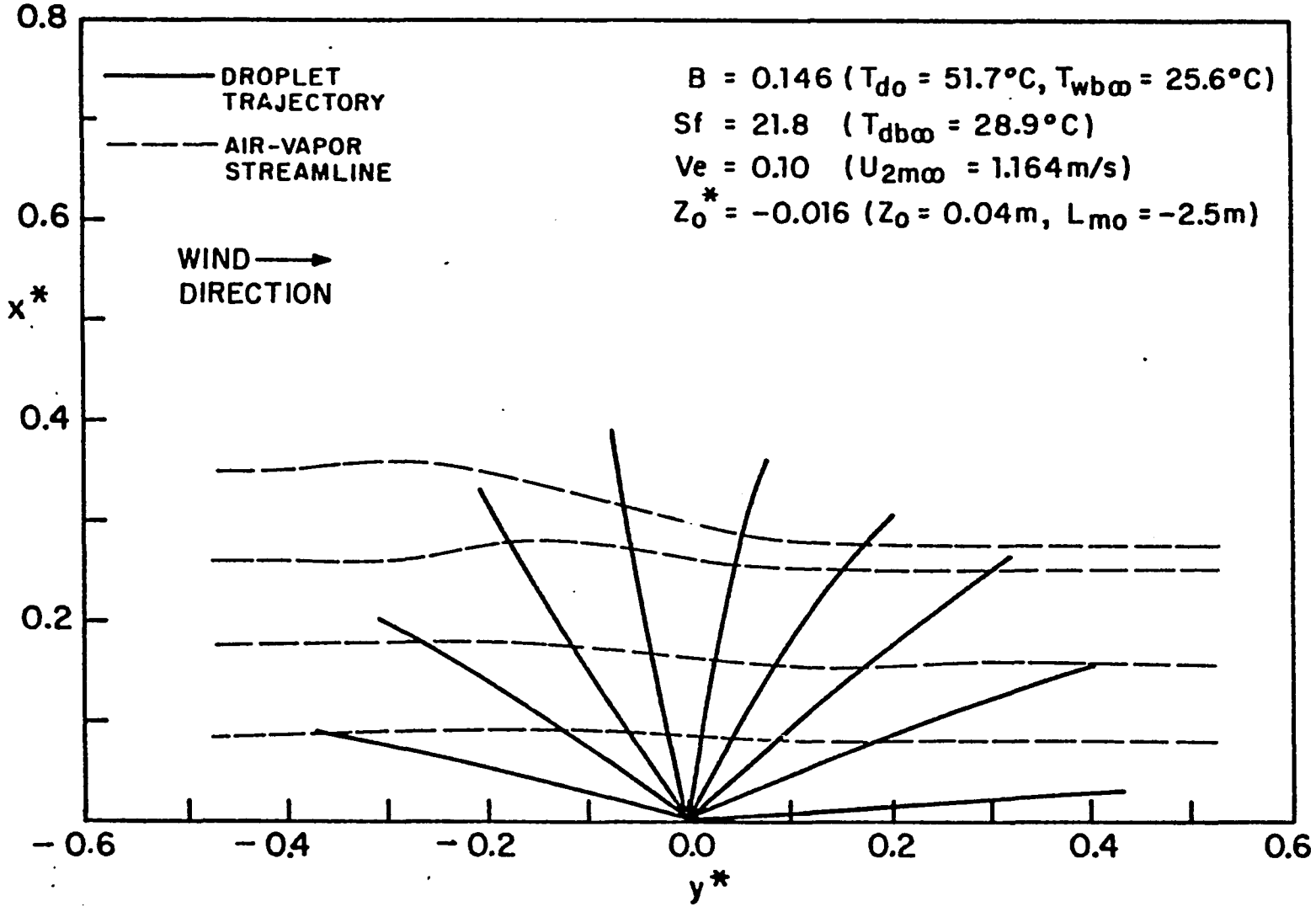

Figure 9. Air-Vapor Streamlines Initially at a 2m Height Upwind of PSM (Plan View). Low Wind.

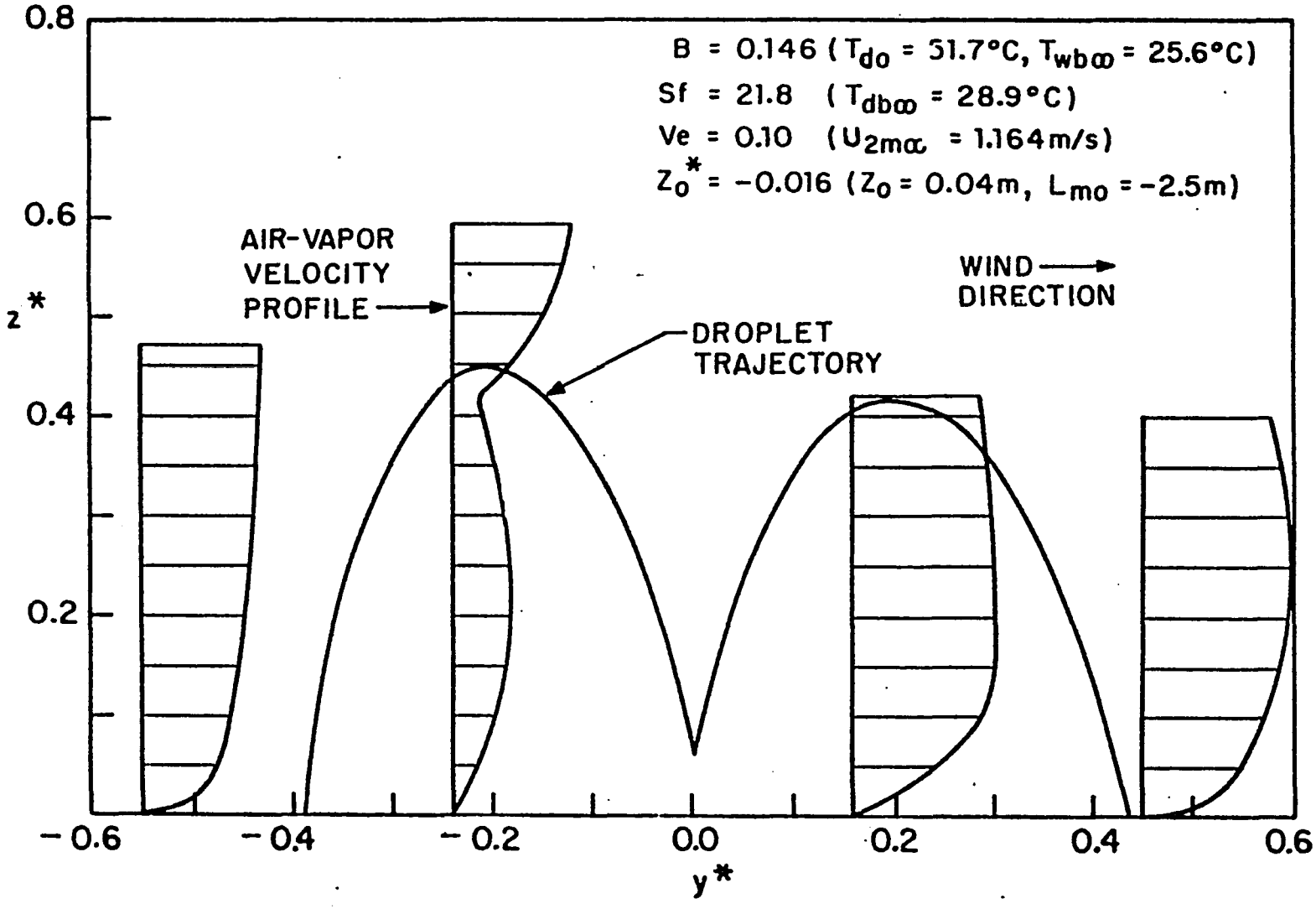

Figure 10. Air-Vapor Velocity Profiles Near Centerline of PSM for Low Wind.

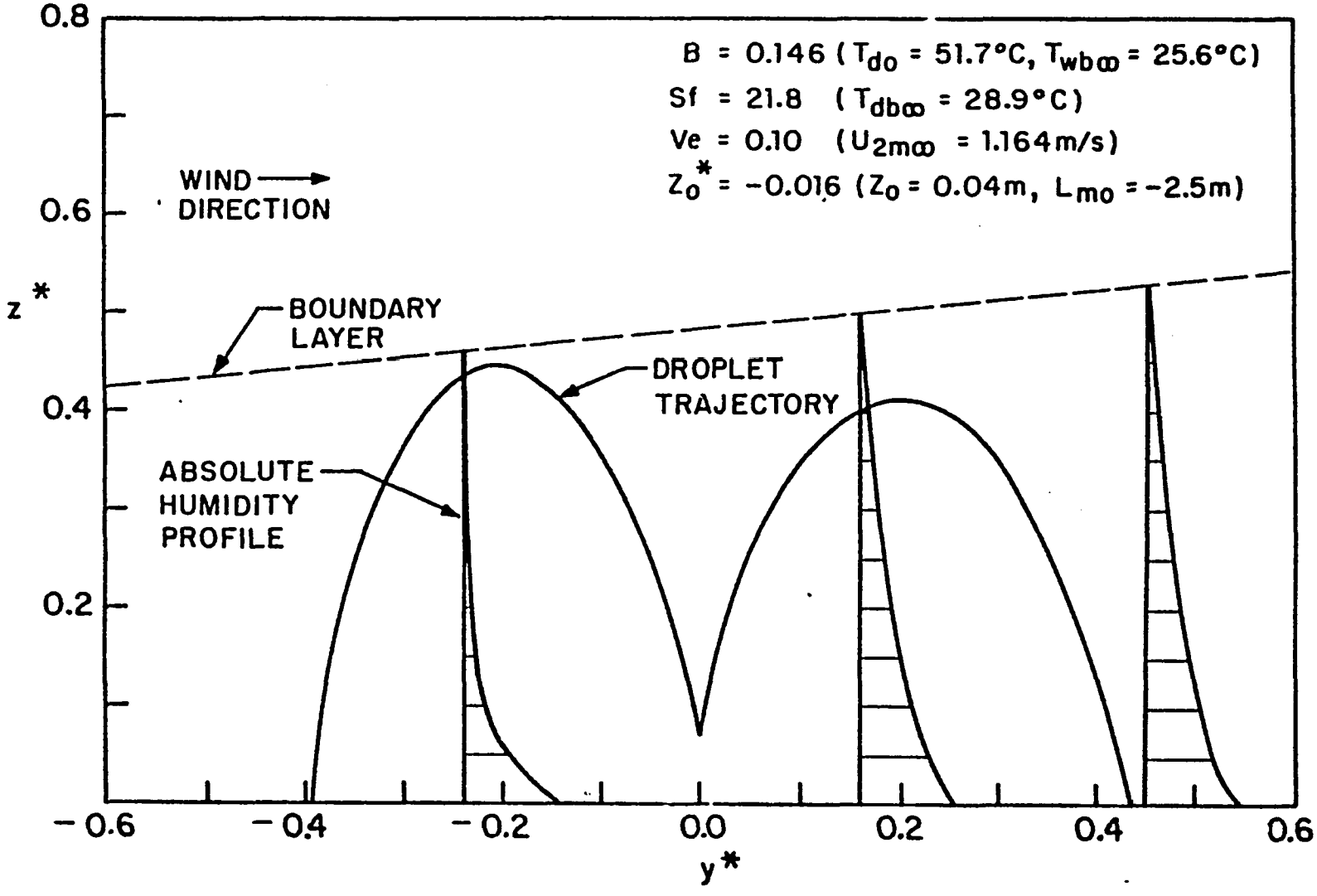

Figure 11. Absolute Humidity Profiles Near Centerline of PSM for Low Wind.

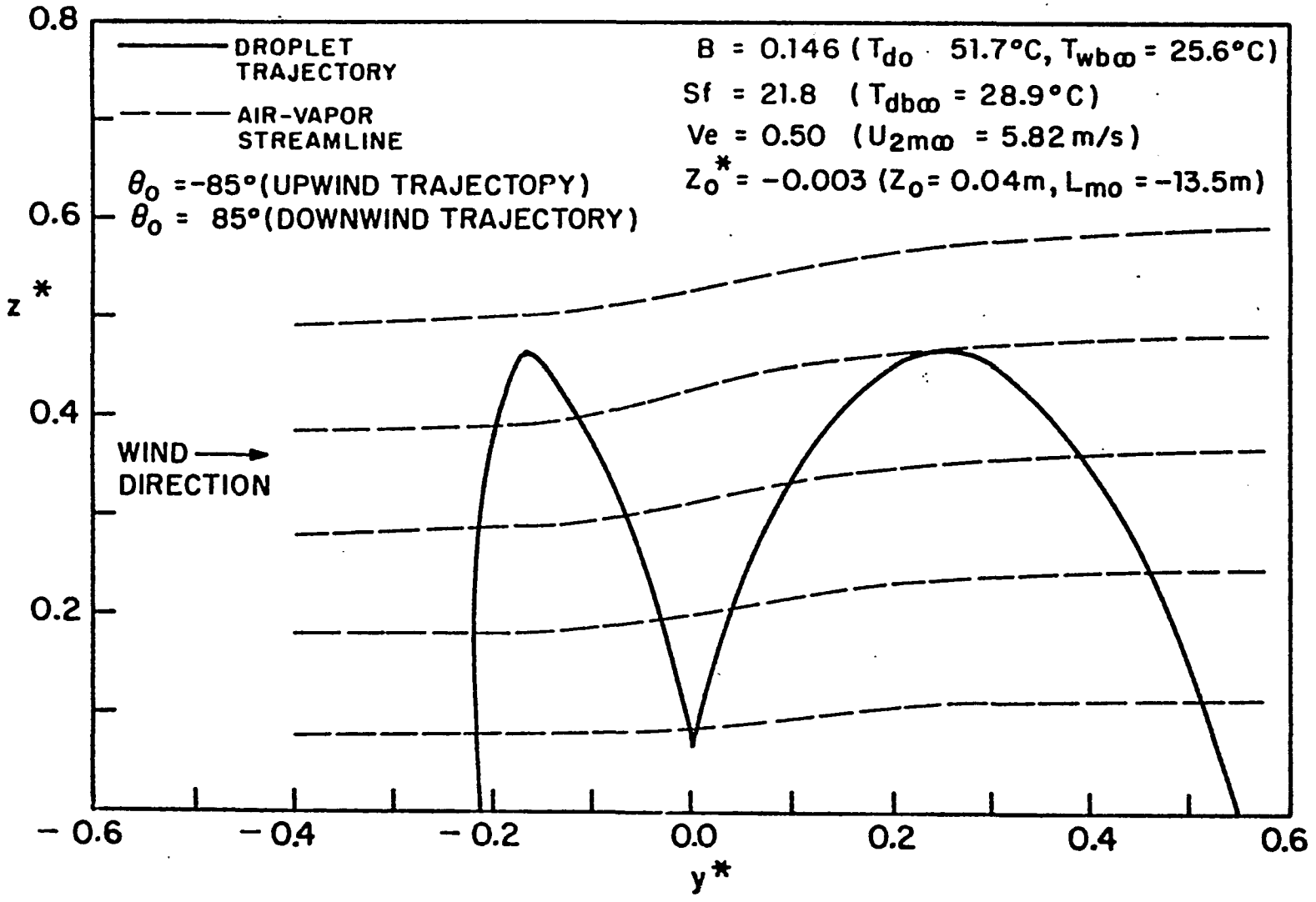

Figure 12. Air-Vapor Streamlines Near Centerline of PSM for High Wind (Elevation View)

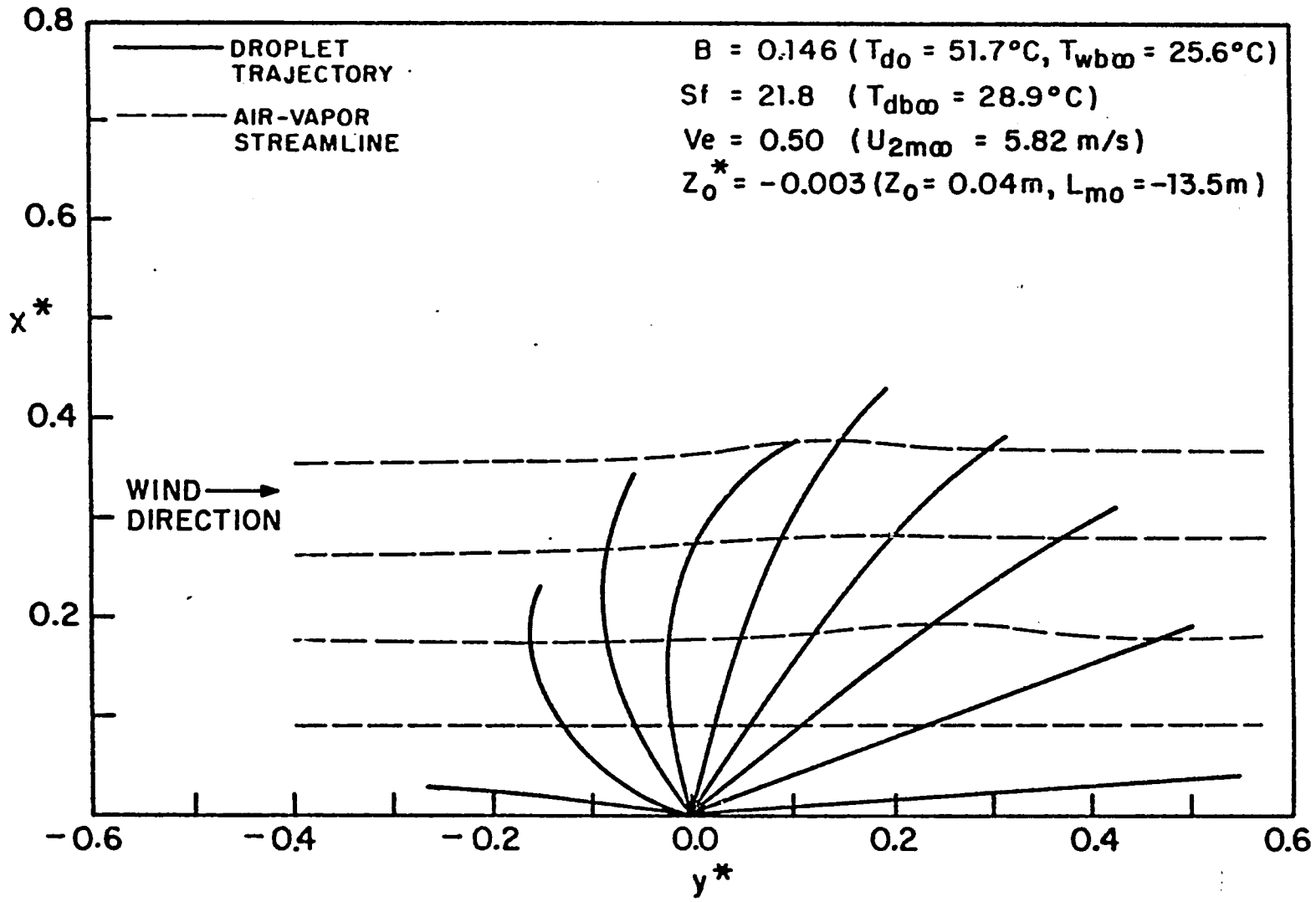

Figure 13. Air-Vapor Streamlines Initially at a 2m Height Upwind of PSM (Plan View). High Wind.

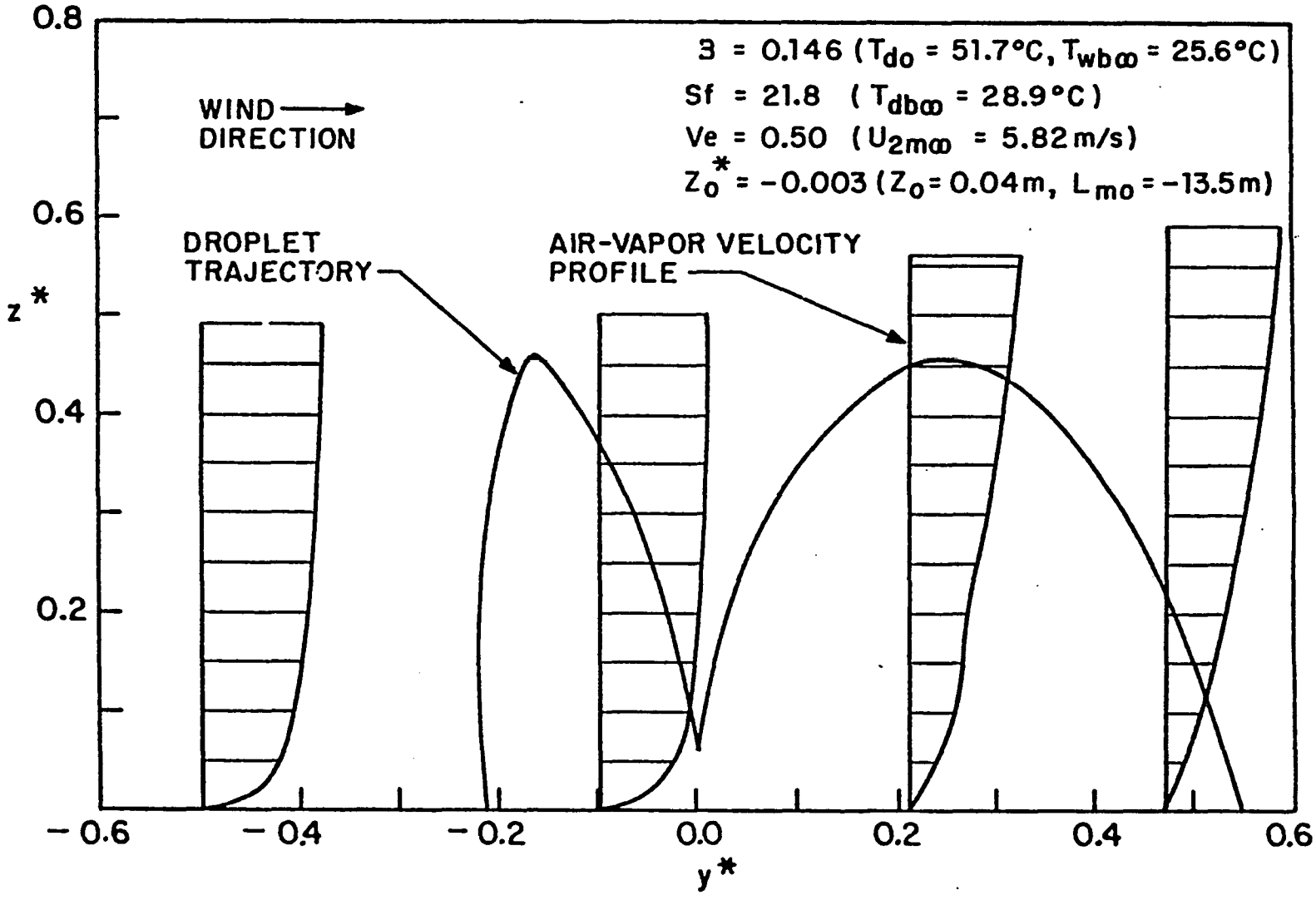

Figure 14. Air-Vapor Velocity Profiles Near Centerline of PSM for High Wind.

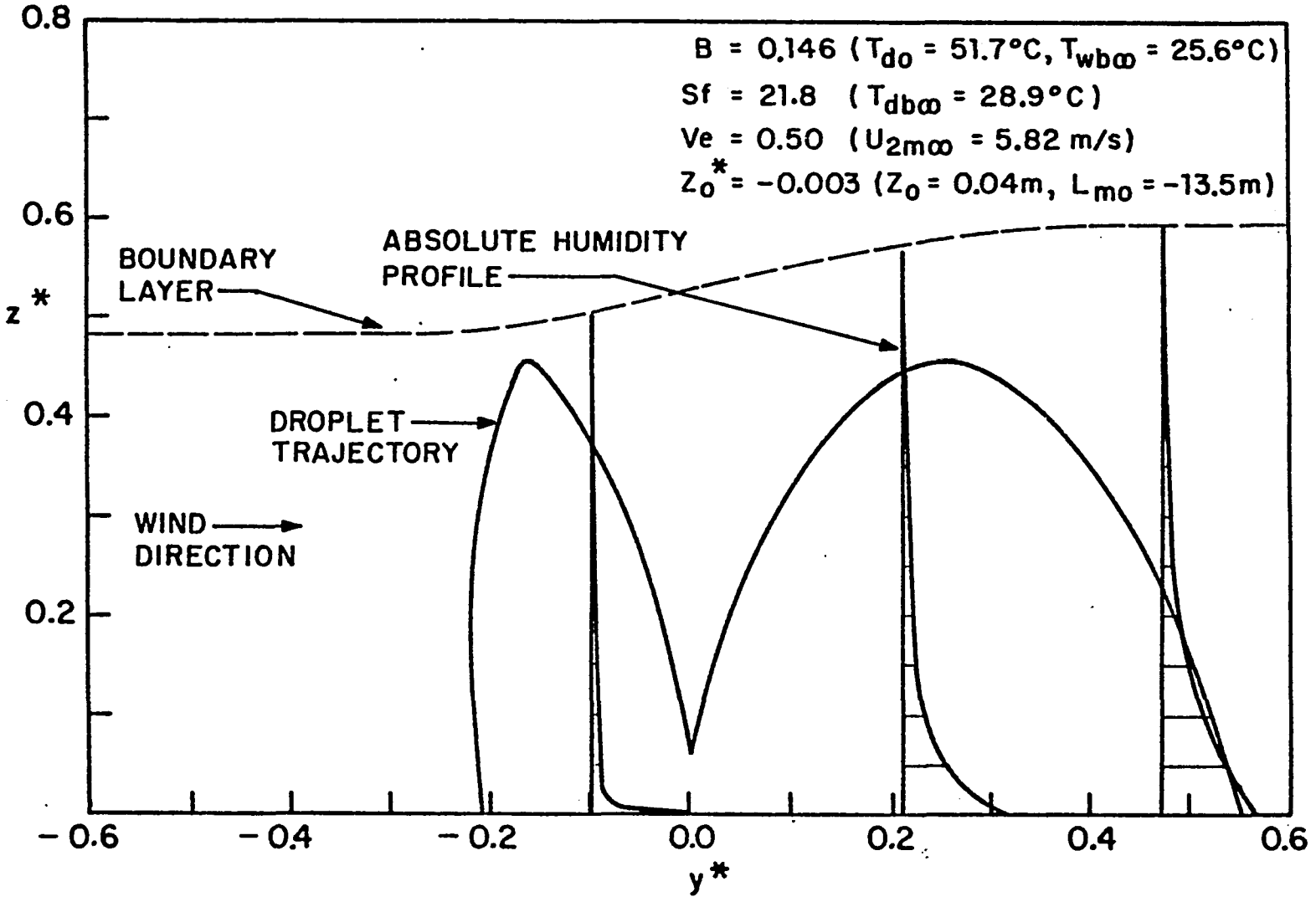

Figure 15. Absolute Humidity Profiles Near Centerline of PSM for High Wind.

on ambient wet-bulb and dry-bulb temperatures, wind speed, wind direction to the canal and initial droplet temperatures were used as input to the model to predict the following: (1) temperature of the droplet upon its return to the canal at any point along the spray perimeter; (2) the air wet-bulb temperature downwind of the spray unit and (3) the air velocity downwind of the spray unit.

The theory was compared with data only for the operating spray units nearest the canal upwind edge, since the most upwind sprays are the only ones that see ambient air. Sprays downwind of the first row see air that has been slowed, heated and humidified by the upwind units. The model for a single spray unit cannot be applied to these downwind sprays since no data are available on the air-velocity, absolute humidity and dry-bulb temperature profiles downwind of the first row of sprays. Measurements of air-velocity, wet-bulb and dry-bulb temperatures were taken only at one height (2m) between downwind sprays on their longitudinal centerline. This data is insufficient to predict performance of downwind sprays from the present model for a single spray. However, the extension of the model to the case of a pass of sprays will enable prediction of downwind-spray performance.

In the experiments, measurements were made of the droplet return (cold) temperature at four positions around the spray perimenter and of the horizontal air velocity and wet-bulb temperature two meters above the canal and 6.1

meters from the upwind spray nozzle along a line perpendicular to the canal edge. Table 1 lists the experimental conditions. Comparisons between theoretical predictions and the data are given in Tables 2 and 3. In Table 2, the square or circle underneath each experiment number along with the catch pan number, indicates where the droplet temperature measurement was made. The drawing in Table 2 indicates the location of the catch pans and the direction of the wind . Agreement between the theoretical and measured values of the droplet cooling range is generally within the reported experimental error of 0.2° C. Droplets ejected on the upwind side of the nozzle are expected to experience a greater amount of cooling than droplets ejected downwind of the nozzle. This is due to the progressive humidification and heating of the air flowing through the spray. Upwind droplets see air close to ambient conditions, while downwind droplets see air that has undergone substantial interaction with the spray. The data and theoretical predictions in Table 2 clearly indicate this trend. For experiments 2 and 3a, the upwind catch pans are #2 and #3 and the downwind catch pans are #1 and #4. For both of these experiments, the sprayed water collected by pans 2 and 3 show a greater cooling range than the water collected by pans 1 and 4. For experiments 5b, 5bES and 5bS, the upwind pans (1 and 2) also collected cooler water than the downwind pans (3 and 4).

Table 3 shows comparisons between predicted and measured values of the change in wet-bulb temperature at a two-meter height ($\Delta T_{wb\,2m\,\ell}$) of the air passing through the spray, and the air-velocity at a two meter height downwind of the spray. For most of the experiments the measured wet-bulb temperature rises faster than the prediction. The discrepancy results from the fact that the model assumes the spray unit to be isolated from any neighboring sprays. The experiments were carried out for a spray

TABLE 1

PSM EXPERIMENTAL CONDITIONS

Exp. #	L_{mo} (m)	T_{do} (°C)	$T_{db\infty}$ (°C)	$T_{wb\infty}$ (°C)	$U_{\infty 2m}$ (m/s)
2	-4.5	34.4	22.5	14.0	4.27
3a	-8.5	30.2	21.0	16.2	4.64
3b1	-4.5	31.3	22.3	15.5	2.30
3b2	-4.5	31.4	22.7	14.9	2.50
5a1	-4.5	25.7	15.5	11.9	1.28
5a2	-2.5	25.9	16.3	13.3	1.80
5b	-13.5	26.4	17.5	13.6	2.43
5bES	-4.5	26.0	17.5	13.8	2.02
5bS	-13.5	26.0	17.5	13.5	2.68

Note: z_o = 0.04 m for all experiments

Data from Reference [35]

TABLE 2

COMPARISON OF THEORY AND EXPERIMENT

FOR DROPLET COOLING RANGE OF PSM

Experiment No.	ξ^o		Droplet Cooling Range (°C) Catch Pan No. 1	2	3	4
2	10	experiment	1.5	1.8	2.7	2.2
□		theory	1.7	2.1	2.2	2.0
3a	19	experiment	0.9	1.2	1.5	1.2
□		theory	1.1	1.4	1.4	1.3
5bES	73	experiment	1.0	1.1	0.8	0.8
o		theory	1.0	1.0	0.8	0.8
5bS	79	experiment	1.2	1.2	1.0	1.0
o		theory	1.0	1.0	0.9	0.9
5b	83	experiment	1.0	0.9	0.7	1.0
o		theory	1.0	1.0	0.9	0.9

Note: Data from Reference [35]

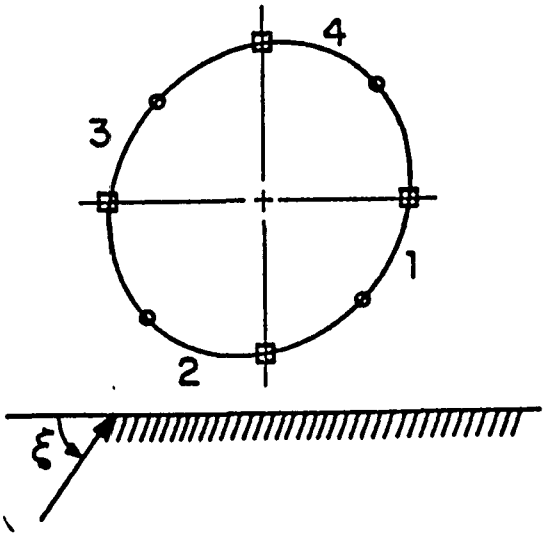

TABLE 3

COMPARISON OF THEORY AND EXPERIMENT FOR PSM

DOWNWIND WET-BULB TEMPERATURE AND AIR-VELOCITY

Exp. #	ξ^o	$\Delta T_{wb2m\ell}$ (°C)		$U_{2m\ell}$ (m/s)	
		experiment	theory	experiment	theory
3b2	14	3.8	3.2	1.50	1.68
3b1	27	3.1	2.8	1.40	1.57
5a1	29	2.7	4.0	1.26	0.80
5a2	62	3.9	3.6	1.20	1.15
5bES	73	3.3	2.8	1.75	1.25
5bS	79	3.0	4.8	2.41	1.40
5b	83	-	-	1.74	1.60

Note: Data from Reference [35]

in a module, where the measured spray is bordered by other sprays on both sides. Air entering the spray field at an angle less than 90° sees parts of the neighboring spray before seeing the measured spray. This results in a larger rise in wet-bulb temperature than for an isolated spray.

The predicted and measured values of local air velocity show good agreement for the experiments in which good results were obtained for the rise in wet-bulb temperature . This observation is consistent with expected behavior. If the predicted air velocity is lower than the data, the predicted local wet-bulb temperature is expected to be higher than shown by the data. The lower the local air velocity, the less ventilation the spray experiences and the greater the buildup of heat and water vapor in the spray domain. For experiments 5a1 and 5bS, predicted air velocities substantially lower than the data result in local wet-bulb temperatures substantially higher than the data.

4. 2. 2. The Spraco 1751 Nozzle

The present model was compared with data [36] obtained for the Spraco 1751 nozzle in an outdoor laboratory facility located at the Richmond Field Station, University of California, Berkeley. The nozzle was mounted five feet (1.52m) above the pond surface. The flow rate of water through the nozzle was 53 gallons per minute (200.6 liters/minute) at a nozzle pressure of 7.4 psig (0.51 bar). The height of the spray above the pond at

this nozzle pressure and zero wind speed is four meters, and the spray radius at the pond surface is about 4.9 meters. To collect the sprayed water, seven catch pans were placed on the pond surface along the nozzle centerline in the wind direction (y-axis). Cold spray temperatures were measured in the catch pans for different wind speeds, ambient psychrometric conditions and droplet discharge temperatures.

The droplet size distribution was measured for the nozzle. Five discrete droplet diameters from the size distribution, and the mass fraction of the total spray flow rate for each size, were used as input to the model. It was found [36] that droplets of different sizes were ejected from the nozzle at different angles . Photographic measurements of droplet discharge angle were attempted, but insurmountable difficulties were encountered in trying to take pictures at the nozzle exit. Instead, photographs of the descending droplets were taken at the pond surface for low wind to determine the drop trajectories. Chen [36] assumed values of the discharge angle for 14 different drop sizes in the range $0.05\ cm < d_o < 0.54\ cm$. He used a particle trajectory equation including drag to calculate where the drops hit the pond. He varied the discharge angle until the calculated and measured trajectories matched for each drop size. His results showed a range of discharge angles for each discrete size. For the present predictions, the average value of

the discharge angle φ was taken for the five sizes used as model input. For a given drop size, φ is different for drops ejected upwind and downwind from the nozzle. Table 4 lists the drop diameters, mass fractions of total spray flow rate and discharge angles used as model input.

In the model, droplets were discharged from ten sites around the nozzle perimeter. All five droplet sizes were discharged from each site. The discharge velocity V_{oi}, for each droplet size is given by:

$$V_{oi} = \frac{V_{oz}}{\sin \varphi_i} \tag{59}$$

where

V_{oz} = initial vertical component of droplet velocity.

The initial vertical velocity component of the droplets discharged by ramp-bottom swirl nozzles (e.g., Spraco 1751) is a constant for all droplet sizes at a given spray flow rate, and is found empirically. For the Spraco 1751 nozzle discharging 200.6 l/min, v_{oz}=8.093 m/s, as given by Chen [36]. Just as for the PSM, the model was applied to only half the spray domain due to symmetry.

For all model predictions, the atmosphere was assumed to be unstable under strong solar insolation. The surface roughness was set at z_o=0.04 meter (30 cm high weeds). These assumptions were made in the absence of any specification of atmospheric turbulence conditions in the data.

TABLE 4

DROPLET SIZE DISTRIBUTION FOR SPRACO 1751

NOZZLE USED AS MODEL INPUT

Drop Diameter d_o (cm)	Mass Fraction of Spray Flow Rate	Discharge Angle φ (degrees) Upwind	Downwind
0.102	0.140	80.0	80.0
0.178	0.220	73.5	64.5
0.254 (mean)	0.220	70.0	60.5
0.368	0.315	68.0	57.5
0.533 (maximum)	0.105	63.0	54.0

Note: Data from Reference [36]

The effect of using a value of z_o equal to 0.02 m. is to increase the upwind velocities by about 5% for heights below 2m., and to decrease the upwind velocities by about 5% for heights above 2 m. The reverse is true if one uses z_o=0.06 m. These observations indicate that the choice of a value for z_o other than 0.04 m. will not have a significant effect on model predictions.

Figures 16-33 compare predicted and measured values of dimensionless cold spray temperature $\left(T_c^* = (T_c - T_{wb_\infty}) / (T_{d_o} - T_{wb_\infty})\right)$ of the water collected by the catch pans versus dimensionless distance $\left(y^* = yg/v_o^2\right)$ along the nozzle centerline in the wind direction (y-axis). Also shown is the same data corrected for heat and mass transfer losses from the water in the catch pans. The corrections were necessary due to the design of the catch pans. The pans were one foot in diameter and four inches deep and were equipped with an overflow line. A thermistor was mounted at the mouth of the overflow line to record the water temperature in the pan. Chen [36] states that it appeared the thermistors measured the temperature of the collected spray water instead of the temperature of the droplets as they struck the pond. He developed expressions to account for the difference in temperatures and used them to calculate the droplet cold temperatures taking into account heat and mass losses from the collected spray water.

For wind speeds below 1.1 meters per second, Figures 16-18, both the local interaction and no-interaction cooling curves show apparent symmetry for the upwind and the downwind cold droplet temperatures. The no-interaction theory, depicted by the dashed curves, gives the maximum amount of cooling that can be experienced by the droplets under the given ambient air conditions and wind speed. That is , the environment of the drops during their entire time of flight is ambient-air absolute humidity, dry-bulb temperature and velocity profile. The no-interaction predictions were obtained from the first iteration on the droplet phase in the computer generated results.

In general, the local interaction theory shows good agreement with the corrected data, while the no-interaction theory underpredicts the measured data. Since the local air in the spray domain is progressively heated and humidified as it passes through the spray, it is expected that the droplets do not experience the amount of cooling predicted by the no-interaction theory. This is indicated by the data.

Equal size droplets ejected upwind and downwind from the nozzle at the same discharge angle will not be cooled by equal amounts. The droplet ejected upwind will experience a large relative velocity to the wind and see air close to ambient conditions. A large relative velocity translates into a large Reynolds number and greater convective and evaporative heat transfer from the

upwind droplet. Local air close to ambient conditions also results in greater heat transfer from the upwind droplet. The downwind droplet experiences a smaller relative velocity to the local wind and substantially heated and humidified local air. It therefore experiences less cooling. Table 4 shows that droplets of the same initial size were not discharged at identical angles upwind and downwind from the nozzle. Since the downwind droplets were discharged at a lower angle, one would expect even less cooling than for equal upwind and downwind discharge angles. This results from the shorter time of flight at small discharge angles. Figures 16-33 show the cooling experienced by a droplet of initial diameter equal to 0.254 cm. (mean size drop) by the up and down arrows. In each case, the downwind drop experienced less cooling (higher T_c^*) than the upwind drop. It may also be noticed that the points at which the droplets strike the pond surface are shifted to the right (against the wind) if one takes local interaction into account. This effect is due to the blockage of incoming air by the spray, slowing down the air due to momentum exchange with the droplets. The decreased drag on the drops resulting from the lower air velocity causes the drops to strike the pond further upwind.

The predictions of the local interaction theory show that the cooling curves have a steeper slope upwind

of the nozzle than downwind. This is due to air drag causing the droplets discharged upwind to land closer to the nozzle than the downwind drops. The windward component of the air velocity is in the same direction as the horizontal velocity component of the drops ejected downwind. Hence, the air drag "stretches out" the trajectories of these drops resulting in a flatter downwind cooling curve. This trend exhibited by the predicted cooling curves agrees with the experimental data.

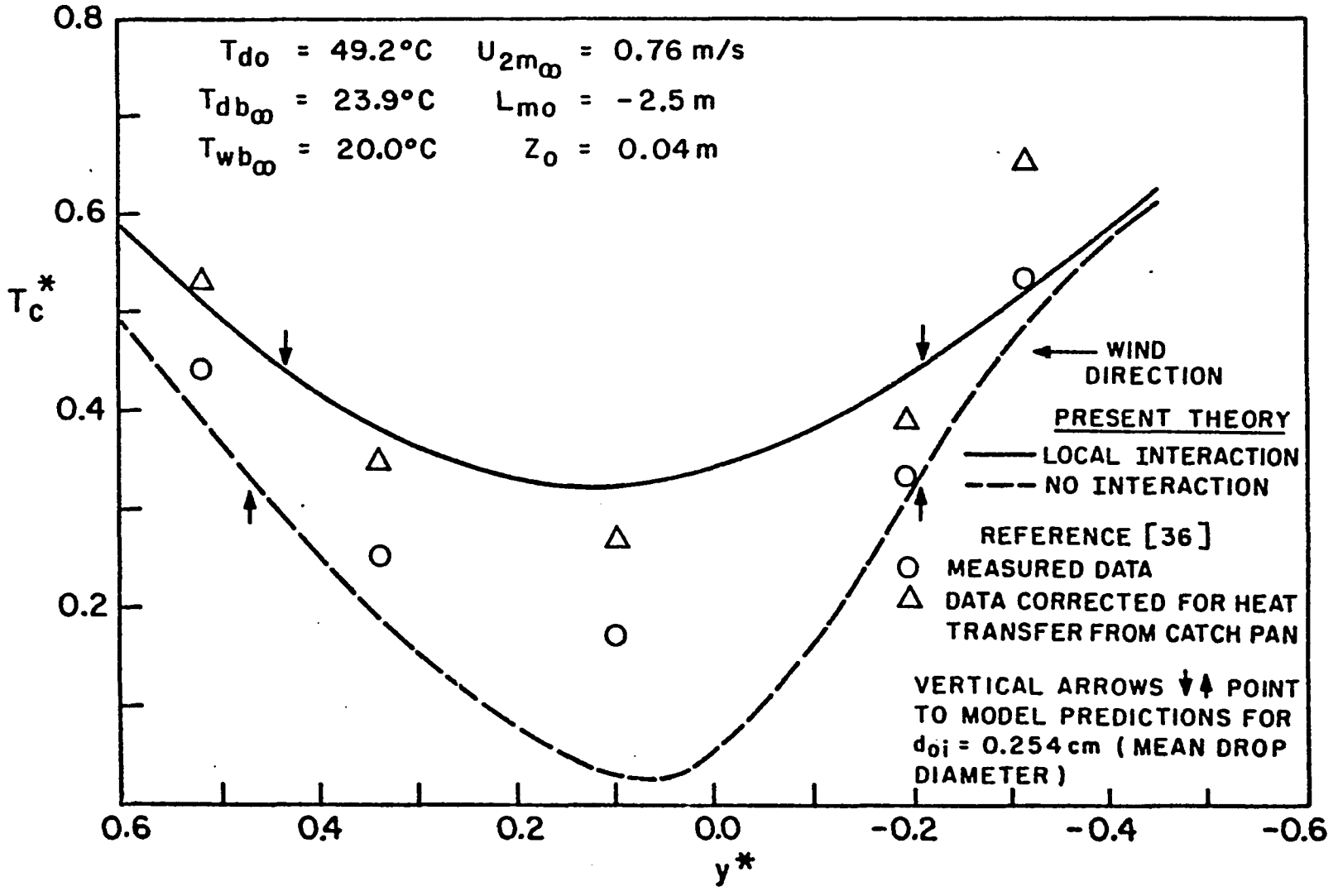

Figure 16. Centerline Droplet Return Temperature for Spraco 1751 (U_{2m_∞} =0.76m/s)

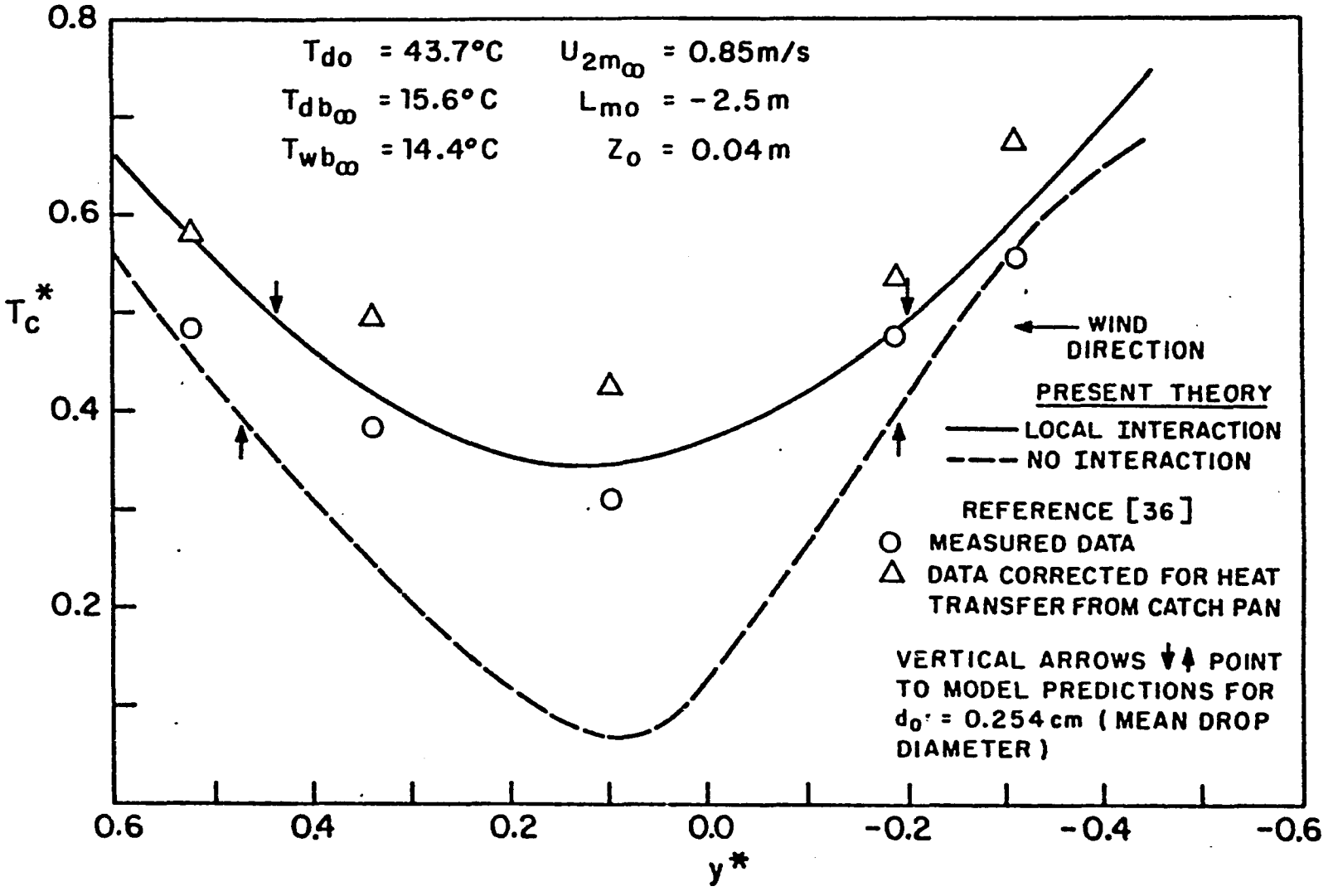

Figure 17. Centerline Droplet Return Temperature for Spraco 1751 (U_{2m_∞} =0.85m/s)

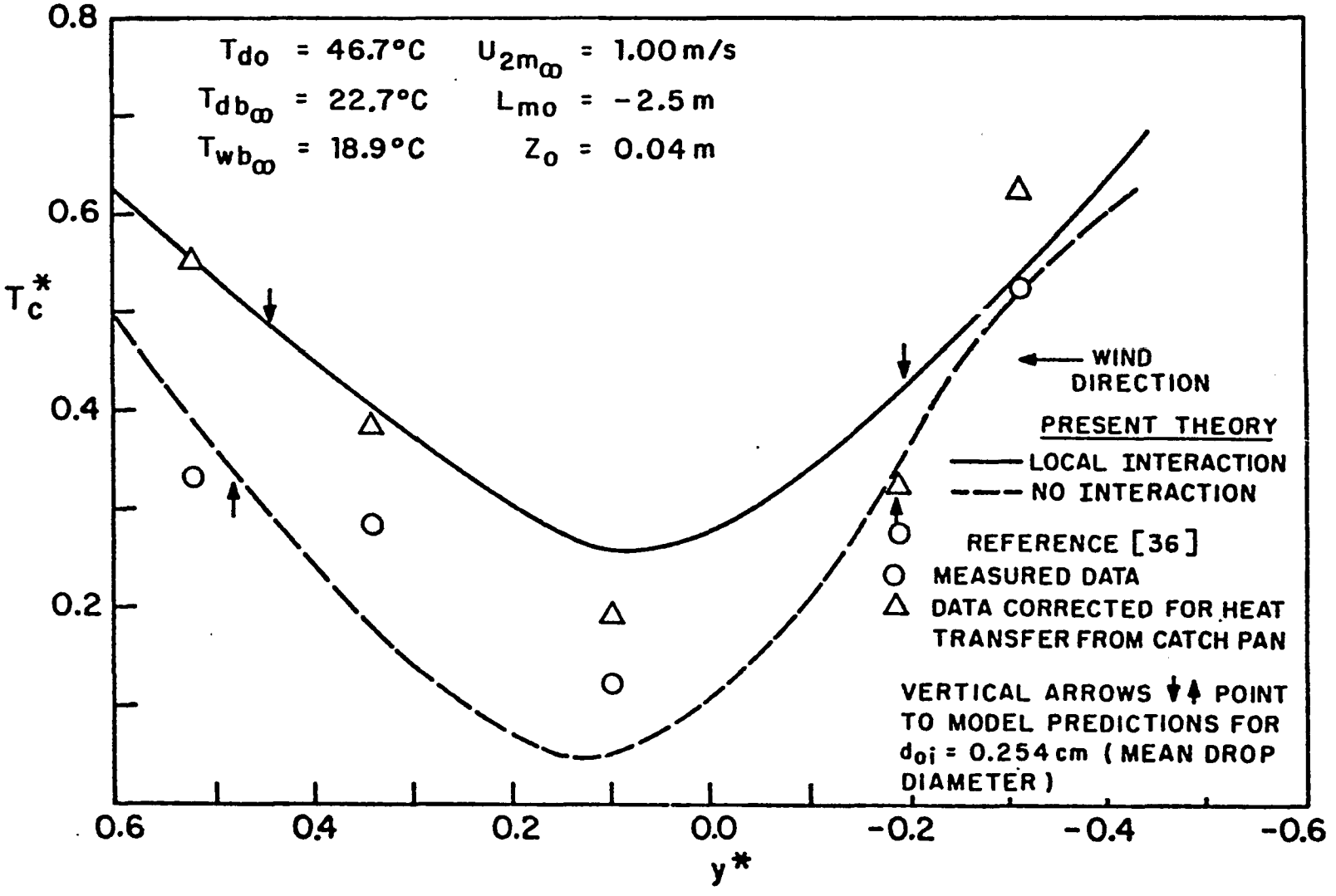

Figure 18. Centerline Droplet Return Temperature for Spraco 1751 (U_{2m_∞} =1.00m/s)

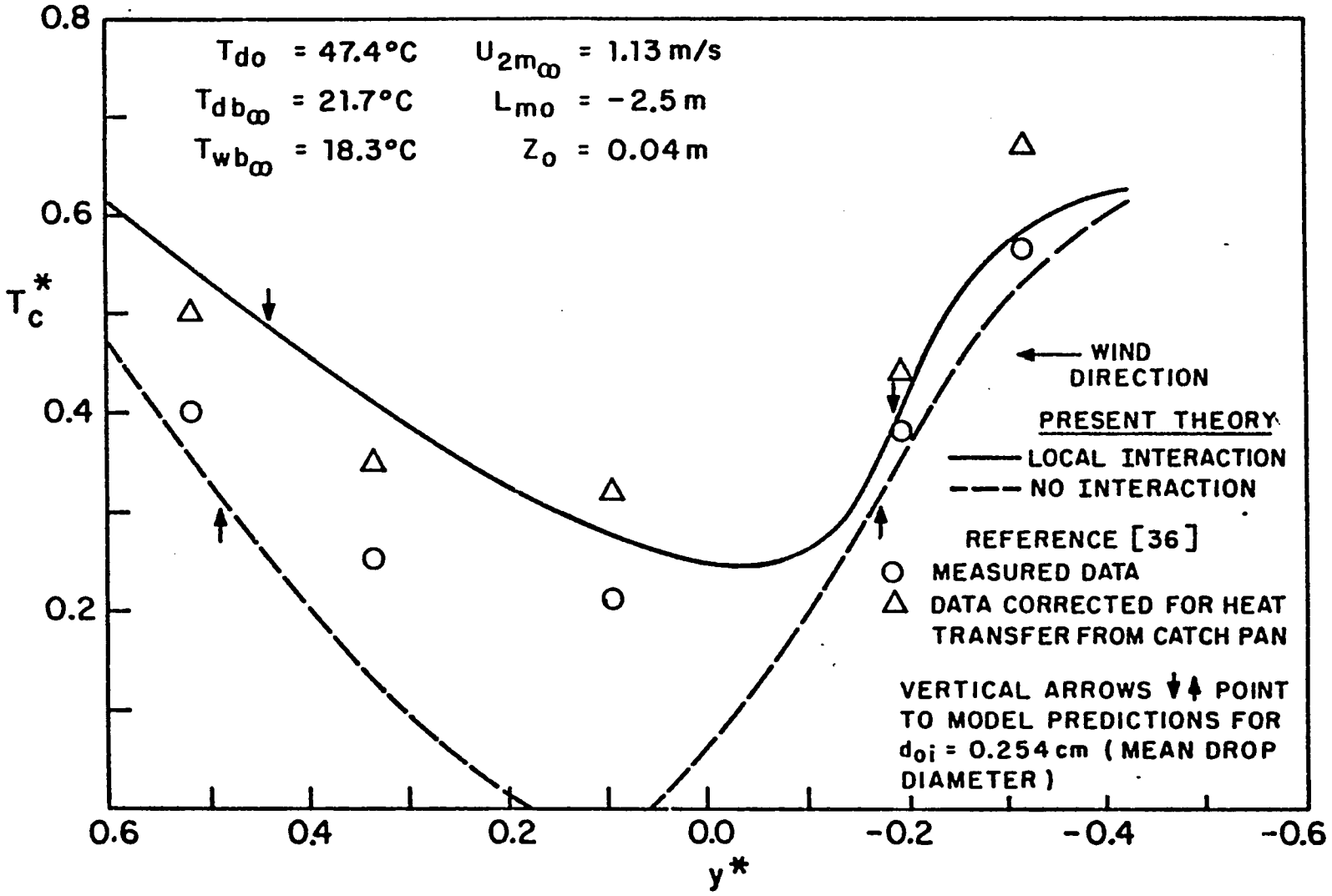

Figure 19. Centerline Droplet Return Temperature for Spraco 1751 (U_{2m_∞} =1.13m/s)

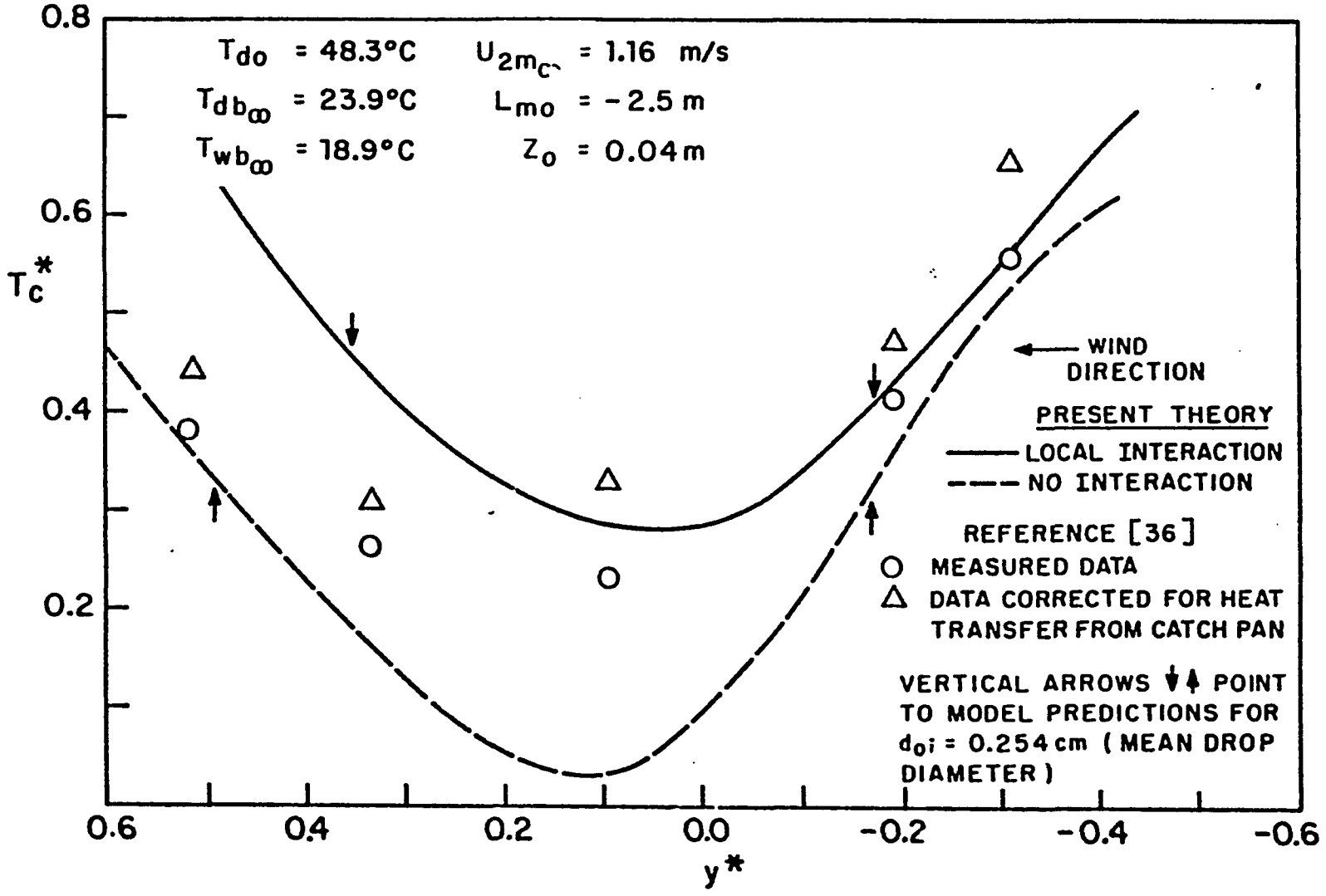

Figure 20. Centerline Droplet Return Temperature for Spraco 1751 ($U_{2m\infty}$ =1.16m/s)

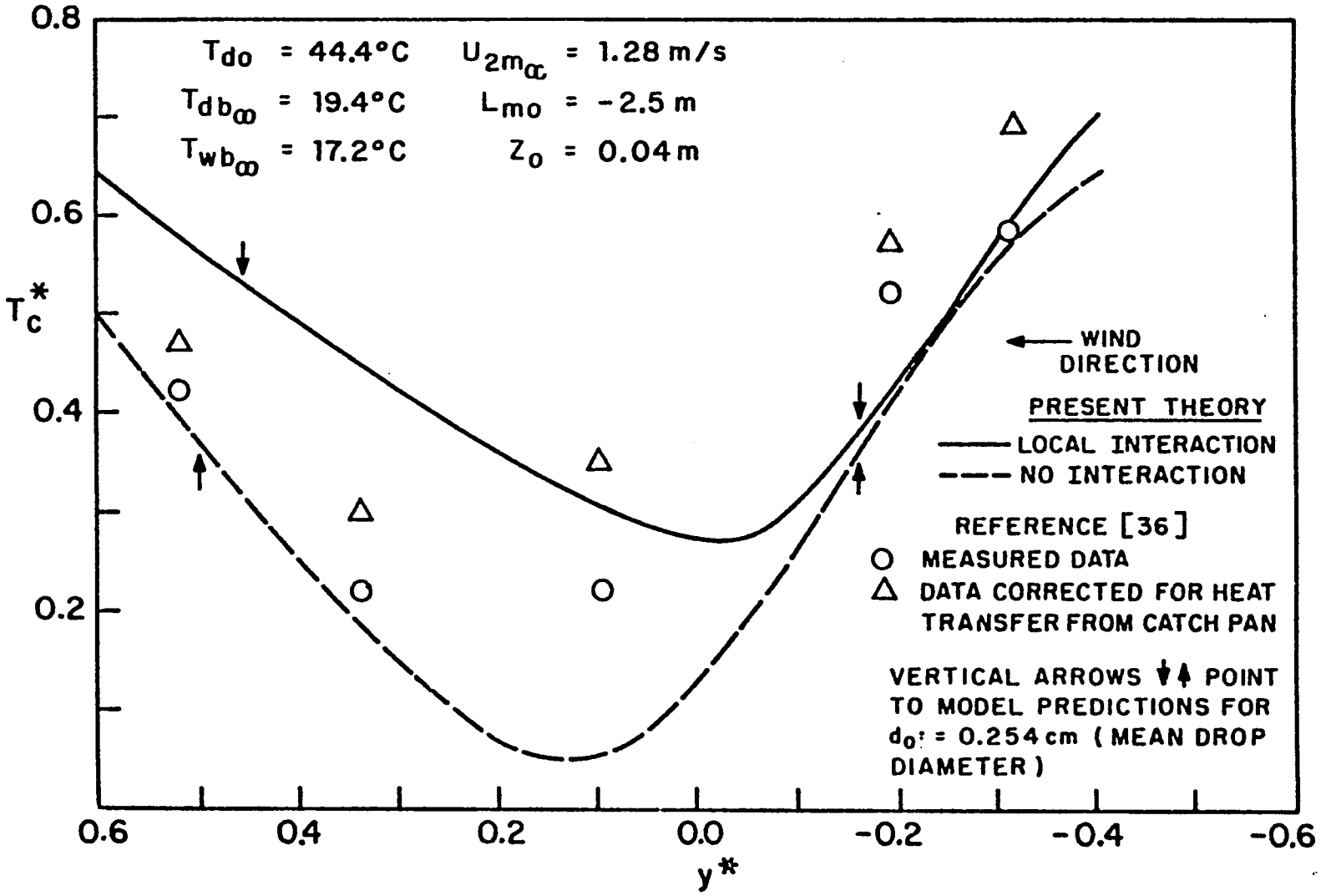

Figure 21. Centerline Droplet Return Temperature for Spraco 1751 (U_{2m_∞} =1.28m/s)

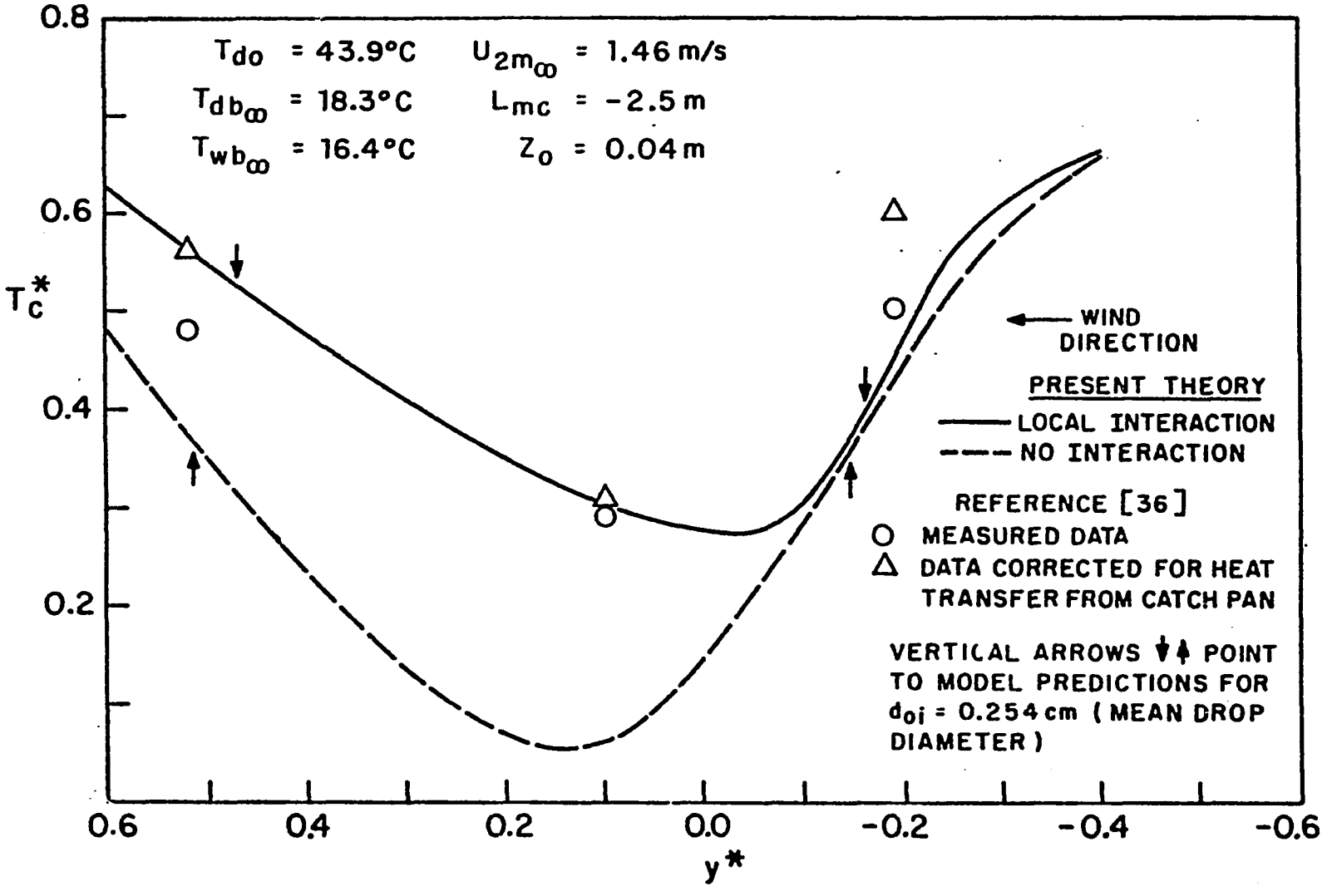

Figure 22. Centerline Droplet Return Temperature for Spraco 1751 (U_{2m_∞} =1.46m/s)

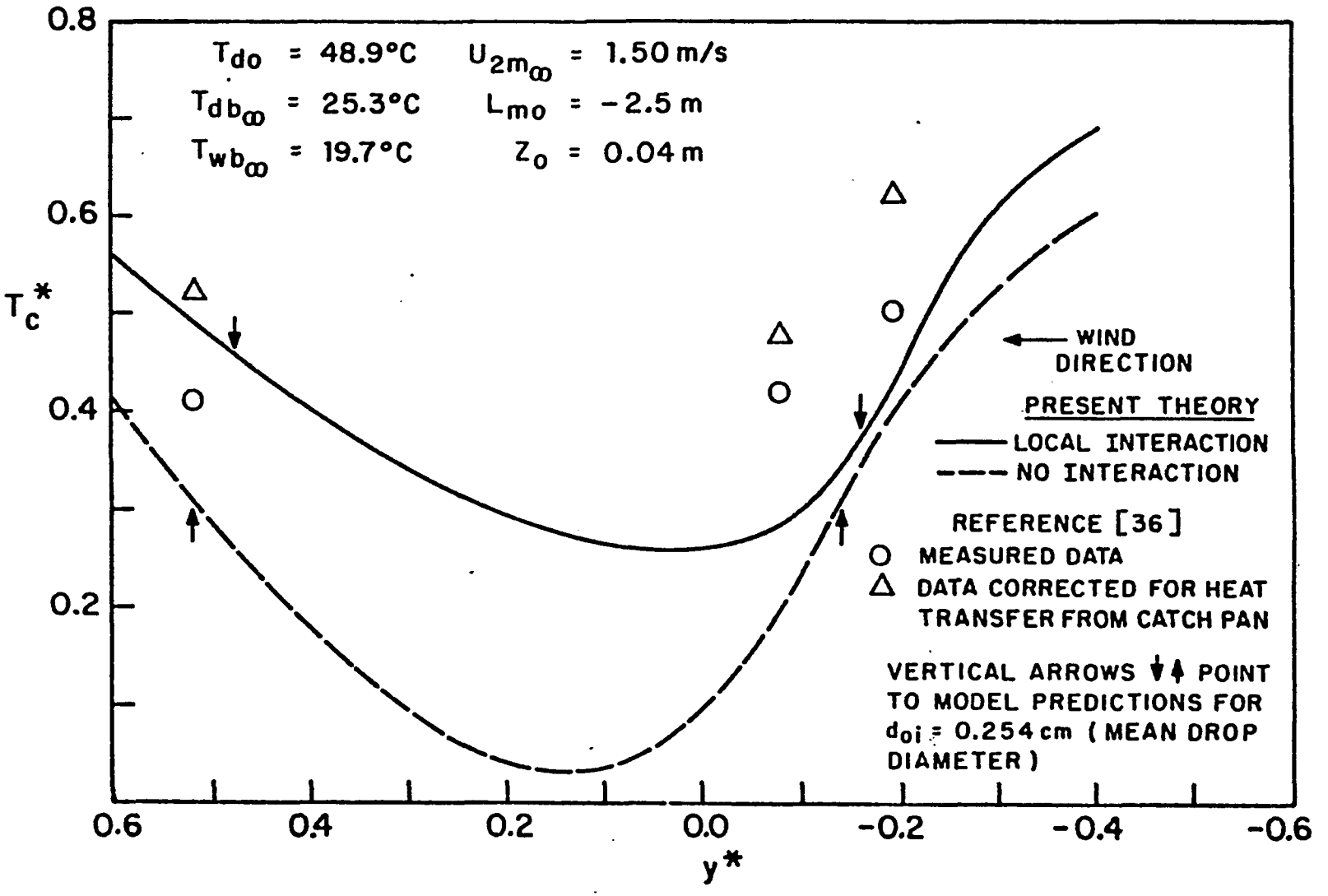

Figure 23. Centerline Droplet Return Temperature for Spraco 1751 ($U_{2m\infty}$ =1.50m/s)

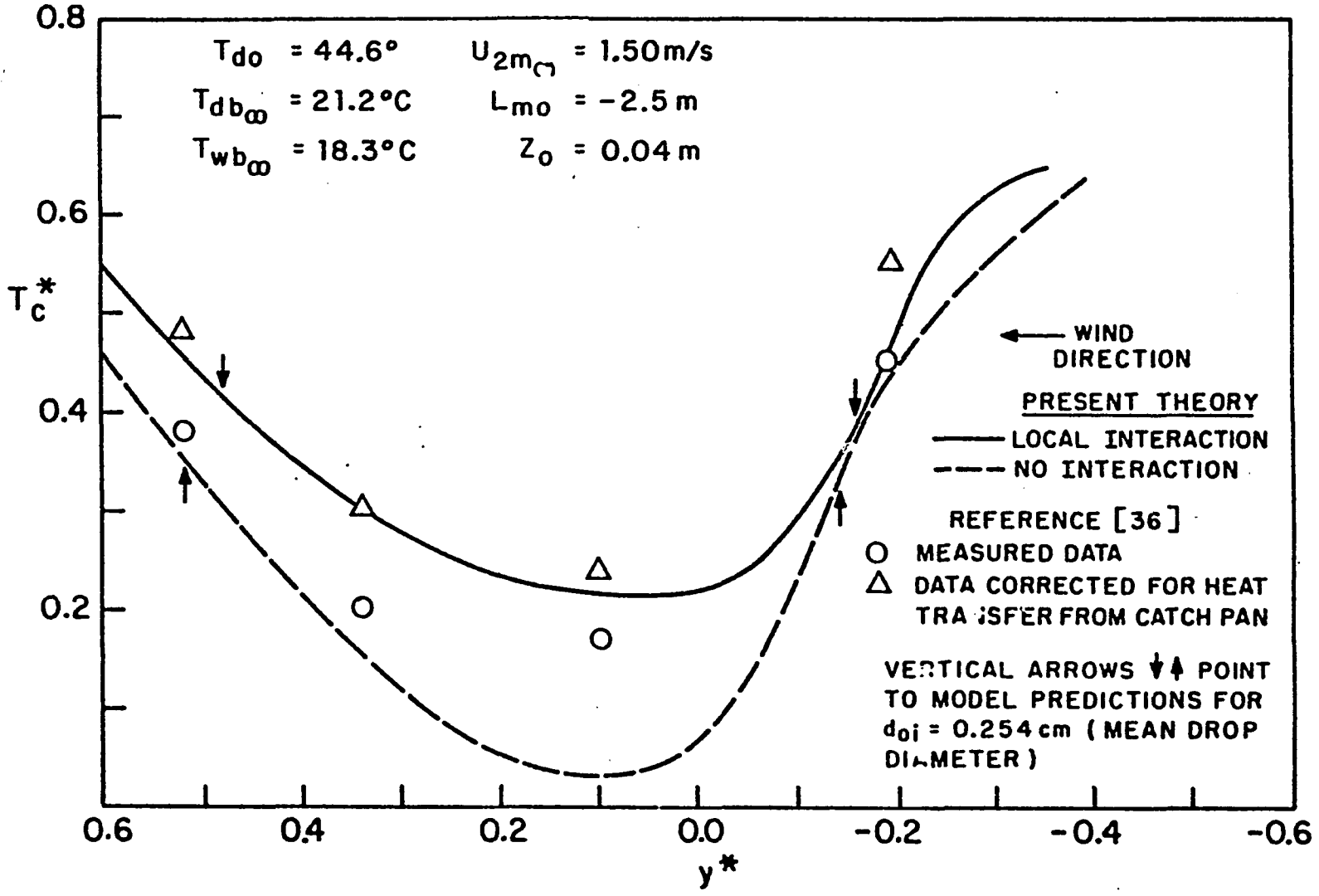

Figure 24. Centerline Droplet Return Temperature for Spraco 1751 ($U_{2m\infty}$ =1.50m/s)

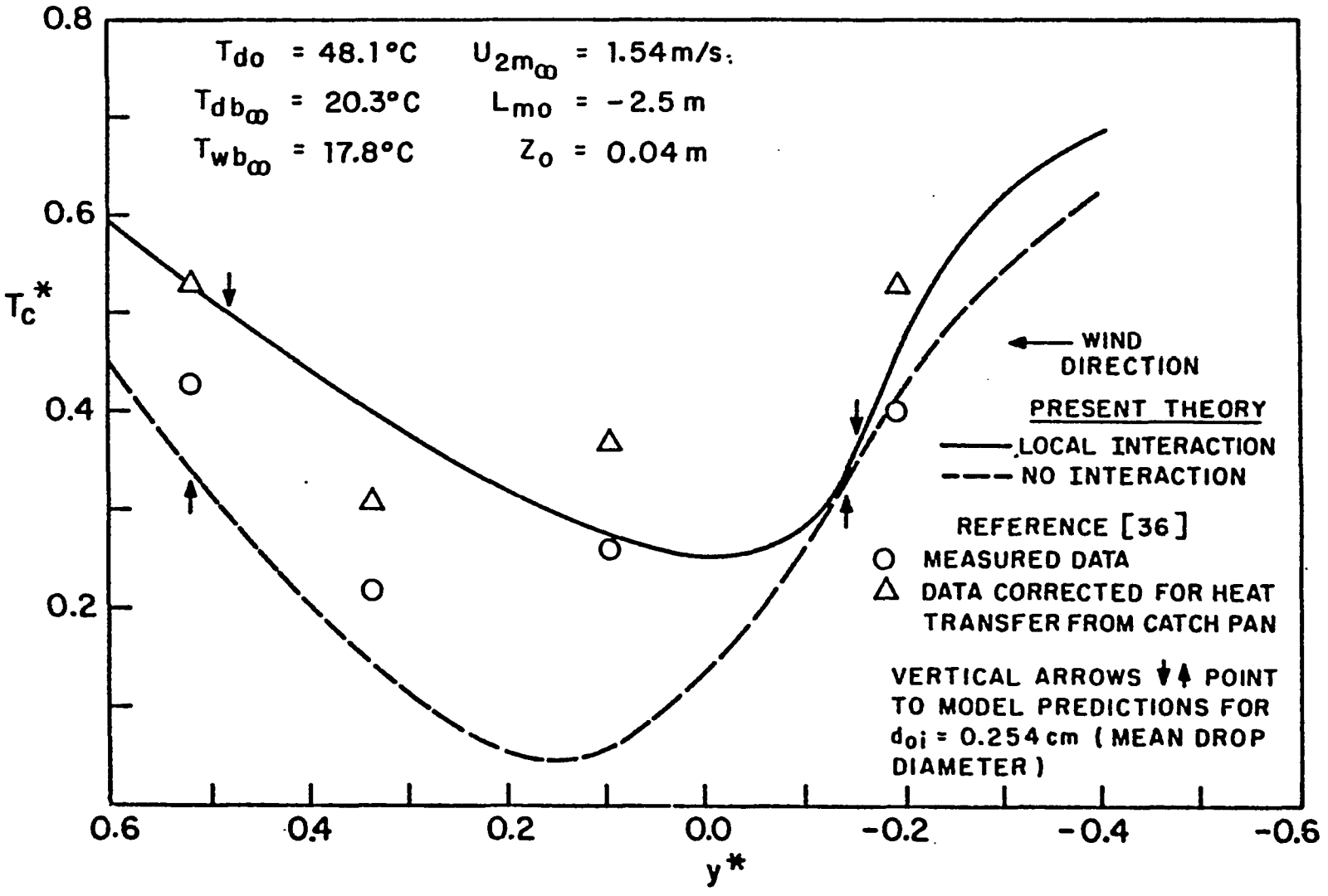

Figure 25. Centerline Droplet Return Temperature for Spraco 1751 ($U_{2m\infty}$ =1.54m/s)

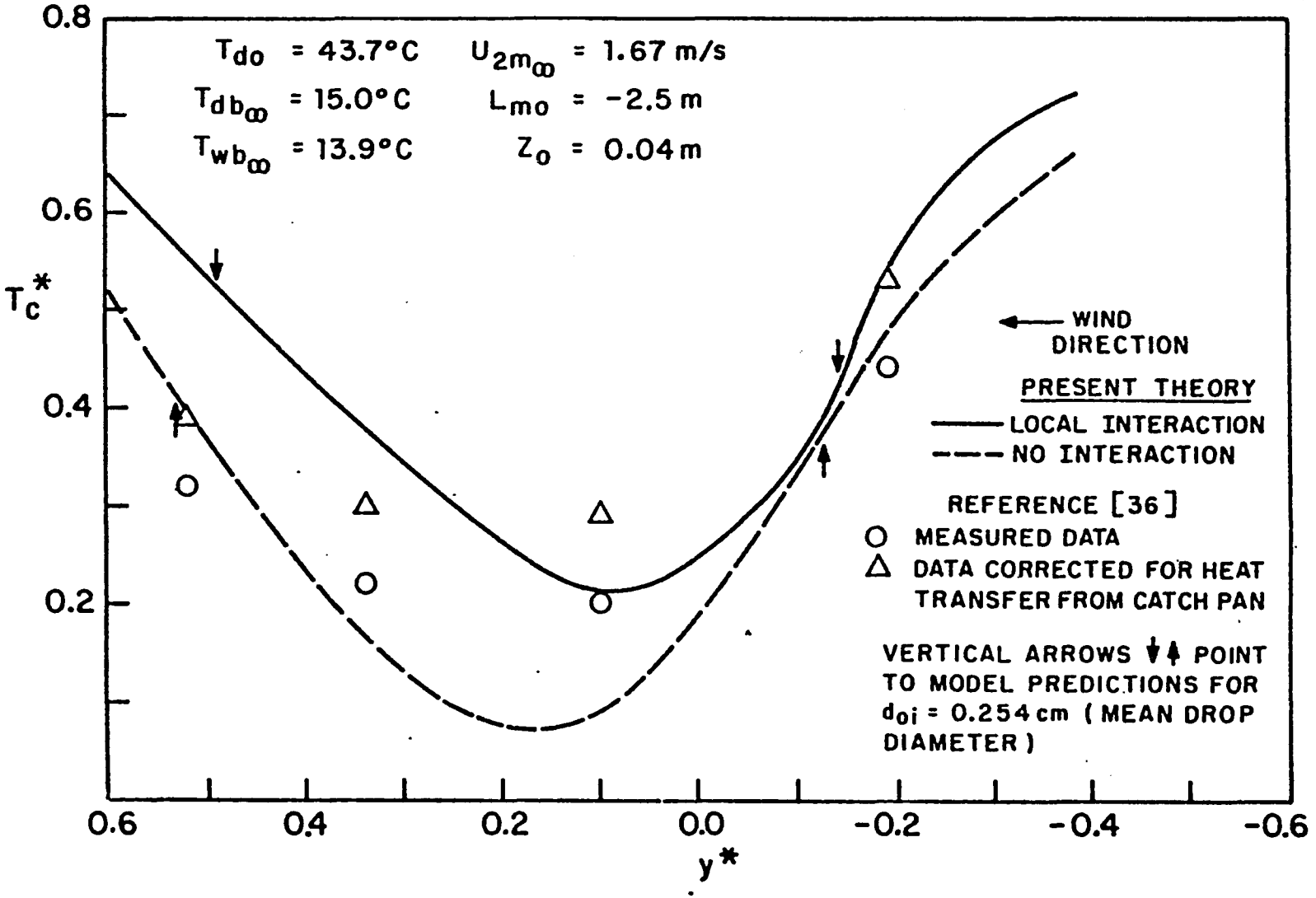

Figure 26. Centerline Droplet Return Temperature for Spraco 1751 ($U_{2m\infty}$ =1.67m/s)

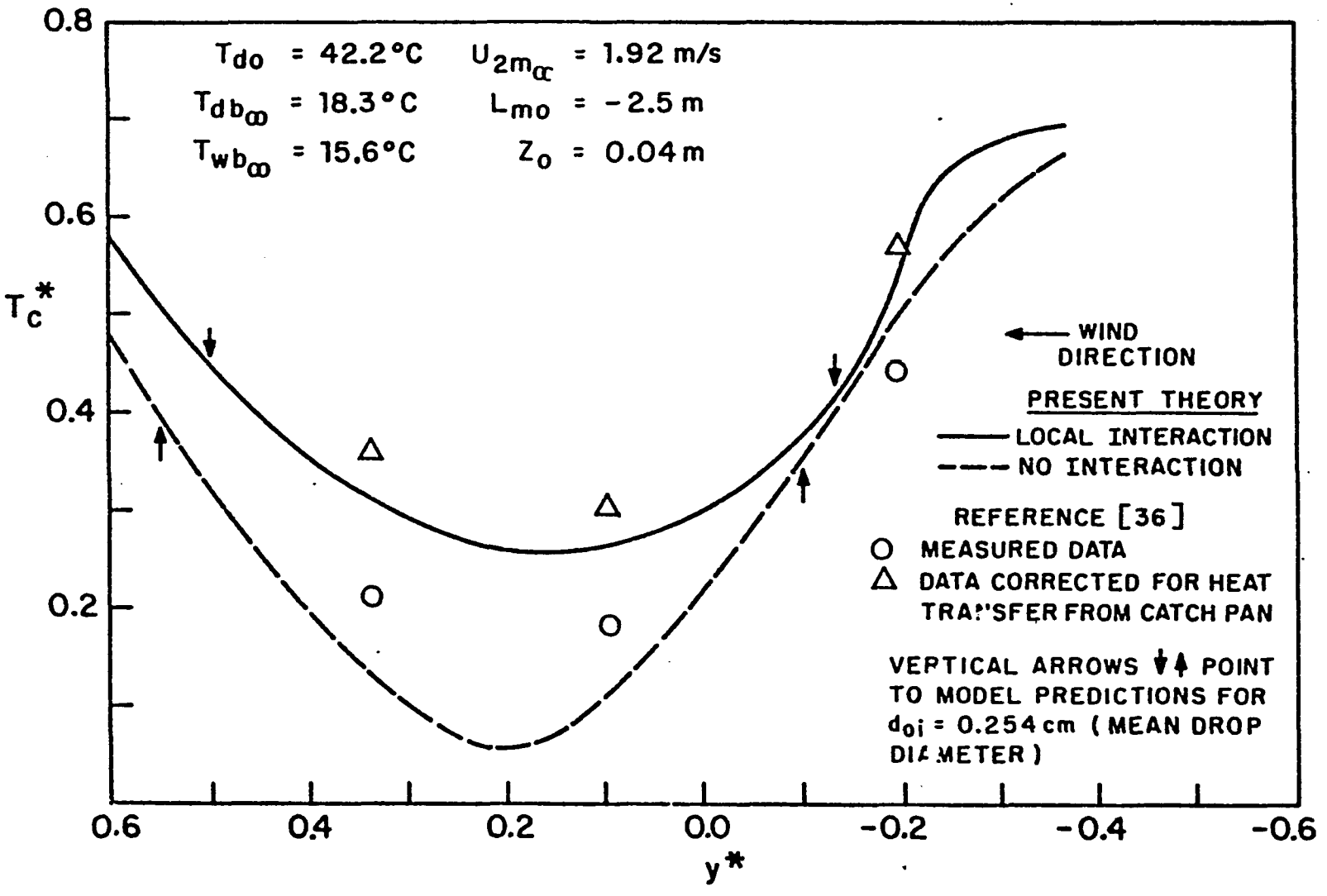

Figure 27. Centerline Droplet Return Temperature for Spraco 1751 ($U_{2m\infty}$ =1.92m/s)

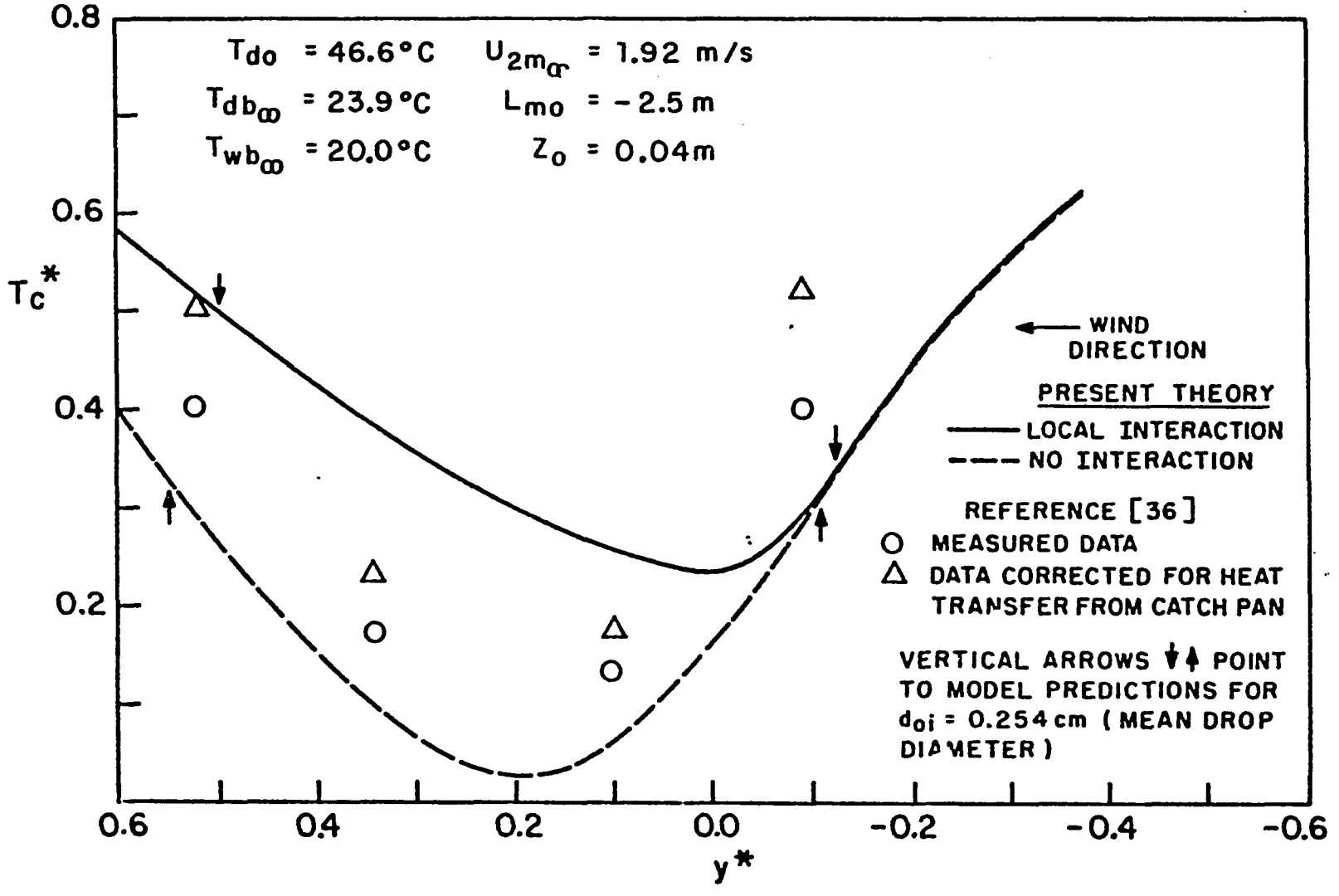

Figure 28. Centerline Droplet Return Temperature for Spraco 1751 ($U_{2m\infty}$ =1.92m/s)

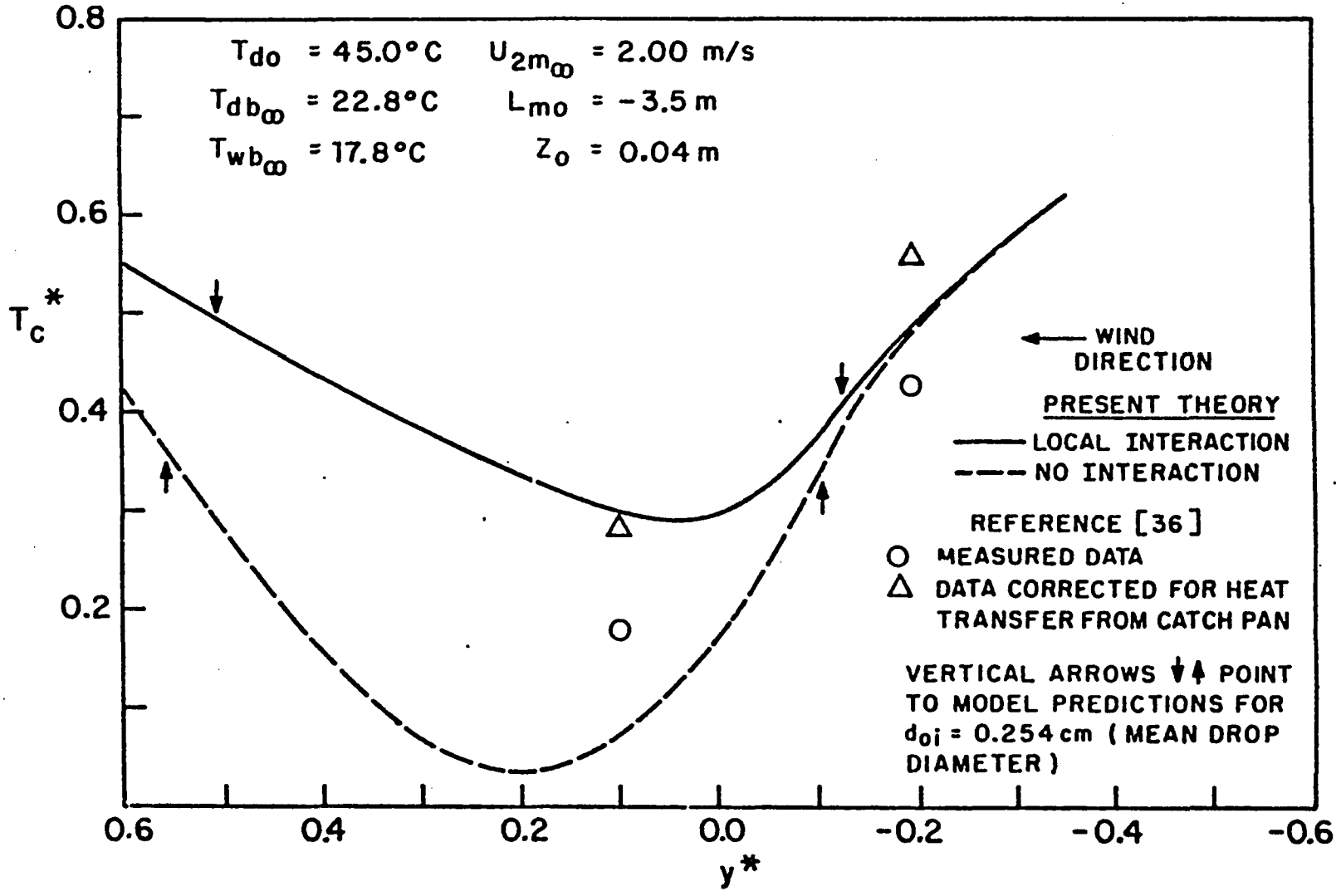

Figure 29. Centerline Droplet Return Temperature for Spraco 1751 ($U_{2m\infty}$ =2.00m/s)

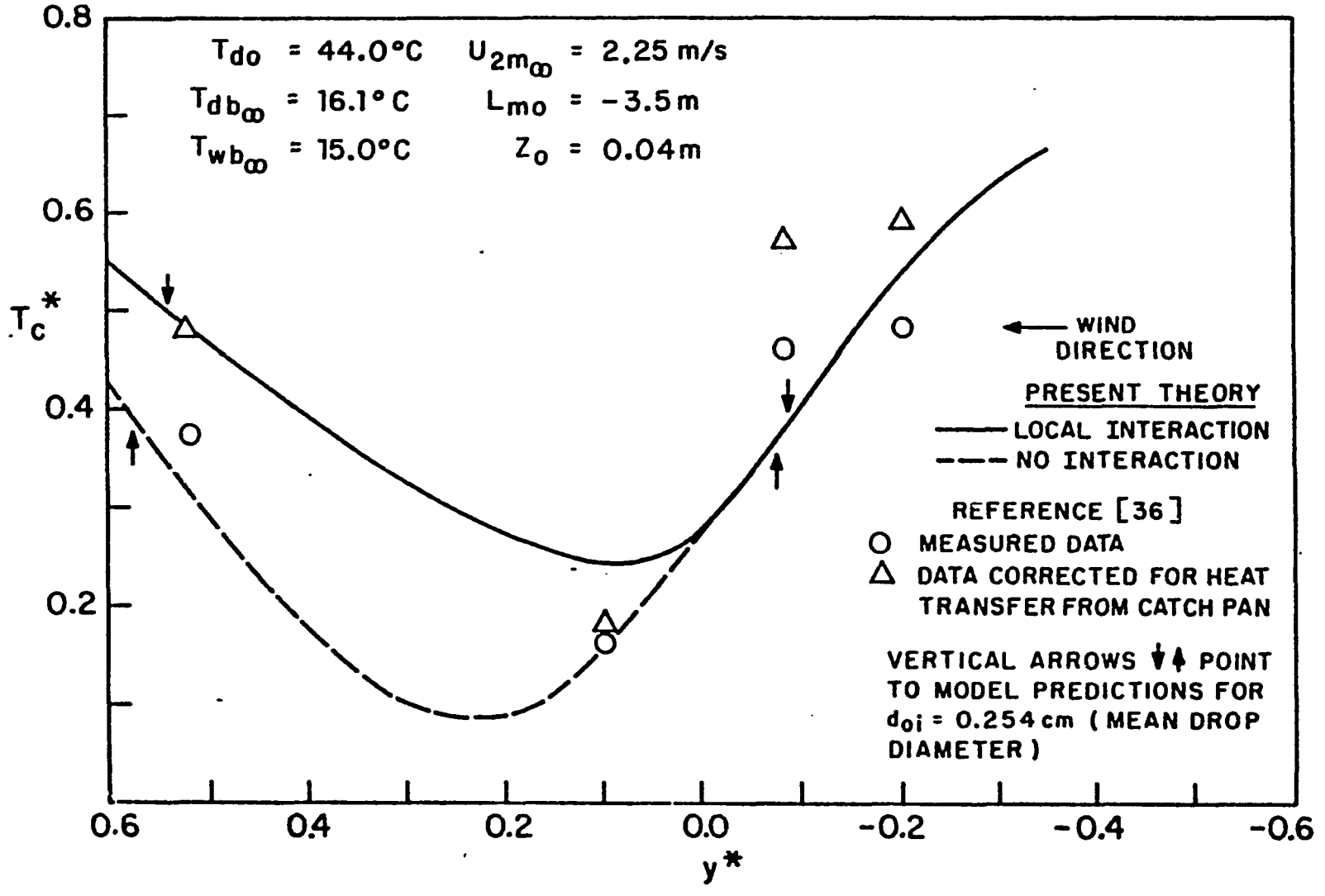

Figure 30. Centerline Droplet Return Temperature for Spraco 1751 (U_{2m_∞} =2.25m/s)

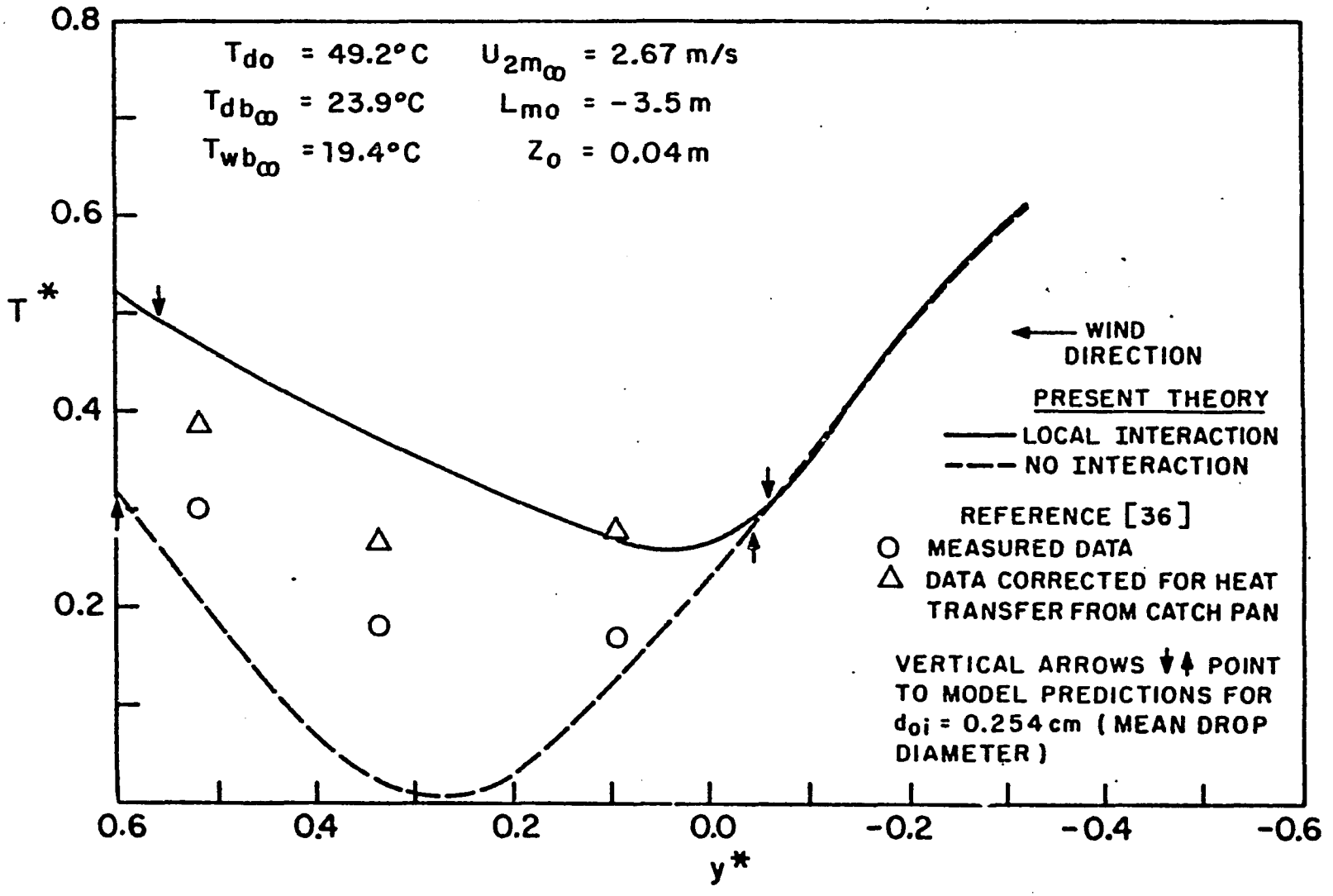

Figure 31. Centerline Droplet Return Temperature for Spraco 1751 (U_{2m_∞} =2.67m/s)

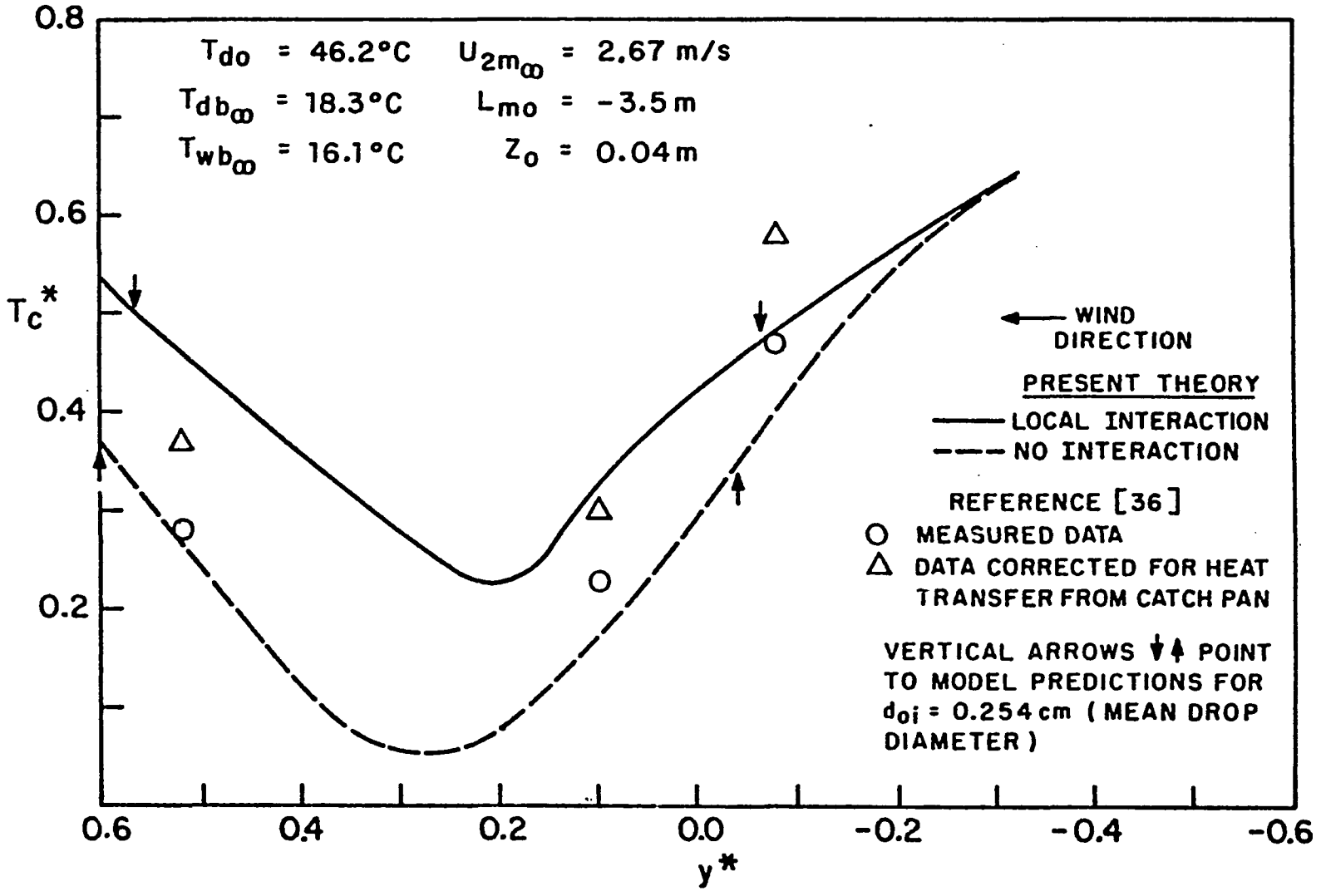

Figure 32. Centerline Droplet Return Temperature for Spraco 1751 ($U_{2m\infty}$ =2.67m/s)

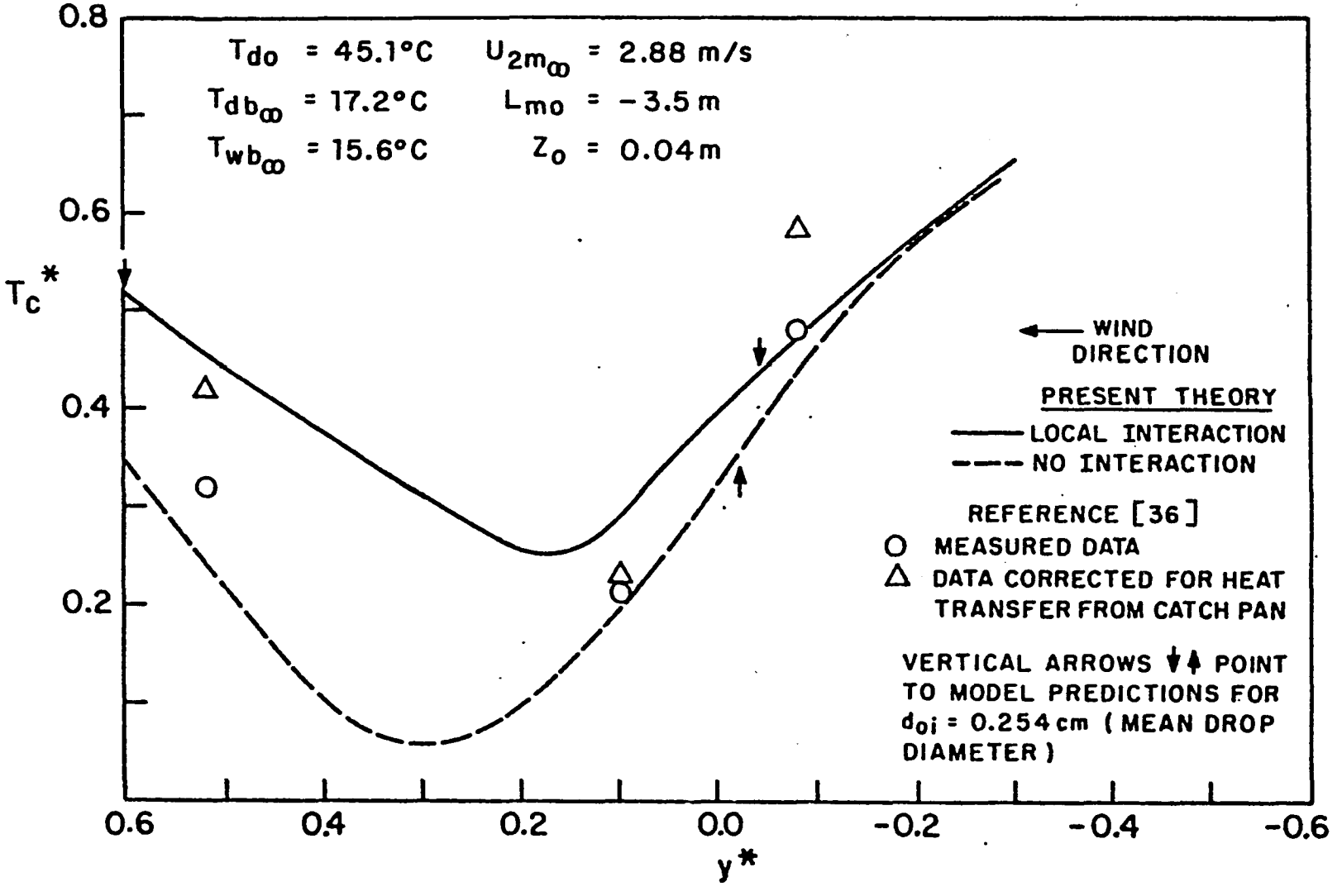

Figure 33. Centerline Droplet Return Temperature for Spraco 1751 (U_{2m_∞} =2.88m/s)

CHAPTER V

PARAMETRIC AND OPTIMIZATION STUDIES: DESIGN AND PERFORMANCE CHARTS

5. 1. The Governing Parameters

Formulation of the governing equations and boundary conditions for the present model in dimensionless form reveals the parameters which affect the performance of spray units. Since the present model contains no design dependent factors, optimization studies can be performed for design considerations.

Of primary interest in sprays is their cooling effectiveness within the constraints of power requirements and mass loss due to evaporation. The dimensionless dependent variable $\dot{Q}/\left(\dot{m}_o V_o^2/(2g_c)\right)$ represents the ratio of the heat removed from the spray to the theoretical power needed to operate it. Examination of the governing equations and boundary conditions shows that for the general case of a liquid spray in atmospheric air, this ratio depends on the sixteen parameters listed in Table 5. For the special case of water sprays in atmospheric air, the Prandtl number Pr, Schmidt number Sc, specific heat ratio $\tilde{C}_p$ and density ratio $\tilde{\rho}$ are approximately constant. In addition, the diffusivity turbulent number is equal to the momentum turbulent number times a constant given by equation (17a) or (17c), depending on atmospheric stability. These considerations reduce the number of governing parameters to eleven.

TABLE 5

GOVERNING PARAMETERS FOR LIQUID SPRAYS

B	Bowen ratio=ratio of convective to evaporative heat transfer $= C_{pa}\left(T_{do} - T_{wb\infty}\right) / \left[\omega_s(T_{do}) - \omega_\infty\right] L_o$
$\tilde{C}_p$	Specific heats ratio $= C_{pa}/C_{pd}$
Fr	Froude number $= v_o^2 / g d_o$
Gr	Grashof number=ratio of buoyancy to viscous forces $= c_o^3 \beta_T g d_o^3 \left(T_{do} - T_{wb\infty}\right) / \nu_a^2$
P_o	Power ratio=ratio of theoretical power input to spray to a reference power input= $\dfrac{\dot{m}_o V_o^2/(2g_c)}{E_{ref}}$
Pr	Prandtl number= $\mu_a C_{pa} / k_a$
Re_o	Reynolds number= $\rho_a v_o d_o / \mu_a$
Sc_o	Schmidt number= $\mu_a / \rho_a D_o$
Sf	Stefan number=latent to sensible heat $= L_o / \left[C_{pd}\left(T_{do} - T_{wb\infty}\right)\right]$
$Tu_{m\infty 2m}$	Momentum turbulent number=ratio of turbulent viscosity to kinematic viscosity= $K_{m\infty 2m} / \nu_a$
$Tu_{wv\infty 2m}$	Diffusivity turbulent number=ratio of turbulent thermal diffusivity to kinematic viscosity= $\dfrac{K_{wv\infty 2m}}{\nu_a}$
Ve	Velocity ratio= $U_{\infty 2m} / v_o$
α_s	Wind shear velocity ratio=ratio of friction velocity to wind velocity at (Z=2m)= $U_* / k' U_{\infty 2m}$
φ	Discharge angle
$\tilde{\rho}$	Density ratio= ρ_a / ρ_d
z_o^*	Turbulent length scale ratio= z_o / L_{mo}

Thus:

$$\dot{Q}^* = \frac{\dot{Q}}{\dot{m}_o V_o^2/(2g_c)} = f\Big(B, Fr, Gr, Po, Re_o, Sf, Tu_{m\infty 2m}, Ve, \alpha_s, \varphi, Z_o^*\Big) \qquad (60)$$

Of the eleven parameters given in equation (60), only five can be controlled by design considerations. These are: Fr, Po, Re_o, Ve and φ. The power ratio, Po, is the ratio of the theoretical power input to the spray to a specified reference power input. The reference power input used here (10.7kw) is the theoretical power required to operate a single spray of the PSM. Power ratio can be expressed as:

$$Po = \frac{\dot{m}_o V_o^2/(2g_c)}{E_{ref}} \qquad (60a)$$

where

E_{ref} = reference theoretical spray power input.

For a given discharge velocity, v_o, the power ratio distinguishes between sprays having different mass flow rates. The remaining six parameters in equation (60), B, Gr, Sf, $Tu_{m\infty 2m}$, α_s and Z_o* depend on meteorological conditions and water temperature. Therefore, for optimum design we have

$$\dot{Q}^* = f(Fr, Po, Re_o, Ve, \varphi) \qquad (61)$$

Parametric optimization studies of equation (61) define the optimum spray design. Although the number of parameters is large, such a study is nevertheless feasible due to the additional considerations detailed below.

The phenomenon of liquid jet breakup into droplets has been extensively studied. It has been shown by Gordon, et. al. [37] that the breakup length for jets of Newtonian fluids is a function of jet velocity and jet diameter. Correlations have been developed for the mean droplet diameter resulting from the breakup of jets issuing from nozzles, many of which are given by Masters [38] . Extensive work has been done in the development of empirical correlations for the mean droplet size formed by centrifugal spray nozzles [38] . It is generally known that the velocity head or pressure head exerts a major influence on the size of droplets produced by spray nozzles. Masters [38] suggests correlations of the form:

$$d_o = C_1 H^{C_2} \qquad (62)$$

where

C_1 and C_2 are constants and

H = velocity head of spray nozzle = $v_o^2/(2g)$

Soo [17] shows that for two "test" sprays, droplet diameter is affected by head. Little work has been done

to develop correlations for the mean drop size of sprays formed by cone impact diffusers (e.g. Powered Spray Module). For the purposes of the present optimization studies, the author developed reasonable correlations based on available information. Substituting the definition of velocity head H in equation (62) yields:

$$d_o = \frac{C_1}{(2g)^{C_2}} V_o^{2C_2} \qquad (63)$$

Equation (63) reveals the interrelationship between discharge velocity and mean droplet diameter. The dependence of d_o on v_o further reduces the number of independent parameters governing spray cooling efficiency. In particular, the Reynolds number and Froude number cannot be varied independently of each other, reducing the number of independent dimensionless parameters to four. Equation (61) can now be written:

$$\dot{Q}^* = f\left(P_o, Re_o, Ve, \varphi\right) \qquad (64)$$

7

5. 2. Parametric Studies

A theoretical study of equation (64) was carried out for summer design conditions. These conditions are:

T_{do}=51.7°C, $T_{db\infty}$=28.9°C, $T_{wb\infty}$=25.6°C, $U_{2m\infty}$=2.236 m/s (5mph), z_o=0.04m (atmospheric surface layer over 30 cm weeds), L_{mo}=-2.5m (strong daytime solar insolation: extremely unstable air).

Values of z_o and L_{mo} were obtained from [32] . The velocity ratio $V_e = U_{2m\infty}/v_o$ was not held constant in this study since the nozzle discharge velocity, v_o, varied with mean droplet diameter. The results, therefore, are valid only for the design wind speed. The correlation between d_o and v_o used in this study was found as described below.

If one assumes that the mean droplet diameter of a cone-diffuser spray is given by an expression of the form of equation (62), one can use the values of drop diameter and spray head given by Soo [17] to determine the constants c_1 and c_2. Solving the two simultaneous equations resulting from substitution of the test-spray data into equation (62) gives:

$$d_o = 2.44\, H^{-3.18} \text{ m} , \qquad (65)$$

where H is in meters.

Since the discharge velocity, spray flow rate and mean drop diameter are known for a unit of the Powered Spray Module (PSM), one can perform a check on the validity of the derived correlation equation (65). Calculating the value of d_o for the known head of the PSM one gets:

$$d_o = 2.44 \left[\frac{(11.64 \text{ m/s})^2}{2(9.8066 \text{ m/s}^2)} \right]^{-3.18} = 0.00523 \text{ m}$$

which is about one-third the mean drop diameter for the PSM. Assuming that d_o varies as the -3.18 power of the head, one can correct equation (65) to reflect designs similar to the PSM by basing c_1 on PSM data. The resulting correlation is:

$$d_o = 7.114H^{-3.18} \quad m. \tag{66}$$

where H is in meters.

To express the relationship between d_o and v_o, one can write equation (66) in the following form:

$$d_o = 9.17x10^{-4} \, v_o^{-6.36} \quad m. \tag{67}$$

where v_o is in meters per second.

Figure 34 shows the effect of mean droplet diameter (or Re_o), Power ratio (Po) and discharge angle (φ) on spray cooling efficiency. The reference theoretical power input (10.70kw) is of one unit of the PSM, representing a pump efficiency of 76.4%, where pump efficiency is the ratio of theoretical power input to the actual power input to the pump. The chart does not reveal a set of parameters giving optimum spray cooling efficiency (Q*). Cooling efficiency rises with increasing discharge angle and decreasing droplet size. Maximum efficiency occurs at a 90^o (vertical) discharge angle for any size of droplet. A droplet discharged vertically undergoes the largest temperature change due to maximum contact time with the air. Also, there is little buildup of local humidity or air dry-bulb temperature in the spray domain at large discharge

angles since there is insufficient time for humidity and thermal boundary layers to develop in the horizontally compressed spray field that is formed at these large discharge angles.

At a given mean droplet diameter, cooling efficiency increases with decreasing power ratio. Lower power ratios result in lower spray flow rates. At a given discharge angle, the lower the flow rate the fewer droplets there are in the spray domain and the lower the rise in local wet-bulb temperature. Lower power ratios exhibit improved efficiency due to local conditions that are closer to ambient conditions.

It is seen from Figure 34 that the curves for power ratios of 0.25 for a given droplet size are higher than the P_o=0.5 curves for the next smallest droplet size in the figure, over a certain range of φ. For example, the P_o=0.25 curve for d_o=1.524 cm is above the P_o=0.5 curve for d_o=1.27 cm and discharge angles of 45° to 64°. This indicates that even for sprays with large drops, there is a range of the governing parameters where such sprays are more effective dissipaters of heat than sprays having smaller drops. An additional consideration, however, is the cost of a spray system incorporating efficient sprays versus a second system incorporating less efficient sprays with a higher rate of heat dissipation. This aspect of the optimization problem can be analyzed with the help of Figures 34 and 35.

Using the example cited above, a spray unit with a discharge angle of 64°, a droplet diameter of 1.524 cm and

a power ratio of 0.25 has the identical cooling efficiency of a unit with the same discharge angle, a drop diameter of 1.27 cm and a power ratio of 0.5. Although having the same cooling efficiency, the second unit dissipates twice as much heat as the first unit. For any given spray system, half as many units of type 2 are necessary to dissipate a given amount of heat as of type 1, thus greatly reducing the length of the spray canal and the cost of the spray system. These conclusions, of course, are not based on an analysis of interactions among spray units in a system. The stated conclusions are valid for a system consisting of a single file of spray units down the length of the canal, with the wind perpendicular to the canal edge.

The dependence of total heat transfer from a spray unit on the governing parameters can be seen more clearly in Figure 35. For a given power ratio, total heat transfer increases with decreasing droplet size. The curve for P_o= 1.0 and d_o=1.524 cm is for the PSM. It can be seen that the performance curve for P_o=0.50 and d_o=0.762 cm crosses the PSM curve at $\varphi = 73^o$. Thus, the total cooling achieved by the PSM can be obtained with half the PSM's power input by a spray unit producing drops of diameter d_o=0.762 cm, which is half the droplet diameter of the PSM. This suggests that substantial savings in the power cost of operating a spray system can be realized by the use of this alternate spray unit design. It should be noted that the spray cooling efficiency of the PSM at a discharge

angle of 73° is Q*=105, whereas the efficiency of the alternate design is Q*=210, as is seen from Figure 34. This corroborates what was stated earlier: efficiency considerations alone cannot determine the most cost effective design of spray unit.

The alternate design would be unacceptable were it to produce excessive loss of water through evaporation. Figure 36 shows that at φ=73°, the PSM evaporation is 0.51% of the sprayed water whereas evaporation is 1.25% for the alternate design, which is well below the criteria given by Soo [17] of 2.5% evaporation for summer operation. The evaporative mass ratio $\dot{m}_e/\dot{m}_o$ for a spray unit is given by:

$$\frac{\dot{m}_e}{\dot{m}_o} = \frac{\pi f d}{6 \dot{m}_o} \sum_{j=1}^{T} \dot{n}_{dj} \left(d_j^3 - d_{cj}^3 \right) \qquad (68)$$

where $\dot{m}_e$ is the evaporation rate from the spray unit.

An additional observation on performance can be made by considering the curve for P_o=1.0, d_o=0.5in (1.27cm) in Figure 34. This curve suggests that greater cooling can be achieved for the PSM for the same power input by a change in pump design. A pump that produces a larger head will result in smaller droplets, at the expense of flow rate. A nozzle discharging 1.27 cm droplets will increase the PSM efficiency at φ =74° by about 28%. Performance curves are not shown for smaller values of d_o for P_o=1.0 because droplet number densities become so large at small drop sizes

and high spray flow rates that the air-vapor flow field cannot be described by the present Lagrangian formulation. A pronounced upwind influence exists that is evidenced by the crossing of the air-vapor streamlines. The streamlines cross when the average longitudinal air-vapor velocity in a streamtube becomes negative, resulting in a negative streamtube cross-sectional area. Large droplet number densities upwind of the nozzle can produce drag forces on the air in the negative y-direction of such a magnitude as to produce a negative y-component of the air-vapor velocity.

Figure 37 shows the capability of a spray to produce the maximum possible cooling under the specified summer design conditions. The parameter η is defined as:

$$\eta \equiv \dot{Q} / \dot{Q}_{max} \qquad (69)$$

where $\dot{Q}_{max}$ is the maximum possible rate of heat transfer from the spray. $\dot{Q}_{max}$ is given by:

$$\dot{Q}_{max} = \dot{m}_o C_{pd} \left(T_{do} - T_{wb\infty} \right) \qquad (70)$$

and states that the maximum rate of heat transfer is achieved when the sprayed water is cooled to the ambient wet-bulb temperature. One notices the poor performance of the PSM (lowest curve) compared with sprays producing smaller droplets. At a discharge angle of 74°, a spray of 0.762 cm drops having a power ratio of 0.25 performs 2.8 times better than the PSM.

A study was conducted to illustrate the effect of varying the discharge angle and the velocity ratio on the performance of the PSM. The results of the study are presented in Figure 38. It is seen that no optimum discharge angle exists for any given velocity ratio. Performance increases with both discharge angle and velocity ratio. Figure 38 also shows the effect of the rise in local wet-bulb temperature on cooling efficiency. At low velocity ratios, actual efficiency is considerably less than the maximum possible efficiency. The maximum efficiency is that obtained with no air-vapor-droplet interaction: no elevation of local wet-bulb temperature above the ambient value and no effect of the droplets on the ambient wind velocity profile. At low velocity ratios, the wind speed is insufficient to ventilate the spray and maintain ambient conditions in the spray domain. For example, at a velocity ratio of 0.2 and a discharge angle of 70^{o}, the local interaction theory gives a cooling efficiency 31% lower than the no-interaction theory. At higher velocity ratios, ventilation is more complete, resulting in improved performance. At discharge angles of 60^{o}, 70^{o}, and 80^{o}, the efficiency obtained from the local-interaction theory asymtotes to the no-interaction efficiency at high velocity ratios. At a 50^{o} discharge angle, spray ventilation is insufficient, even at high Ve, for the spray to perform at its maximum possible efficiency.

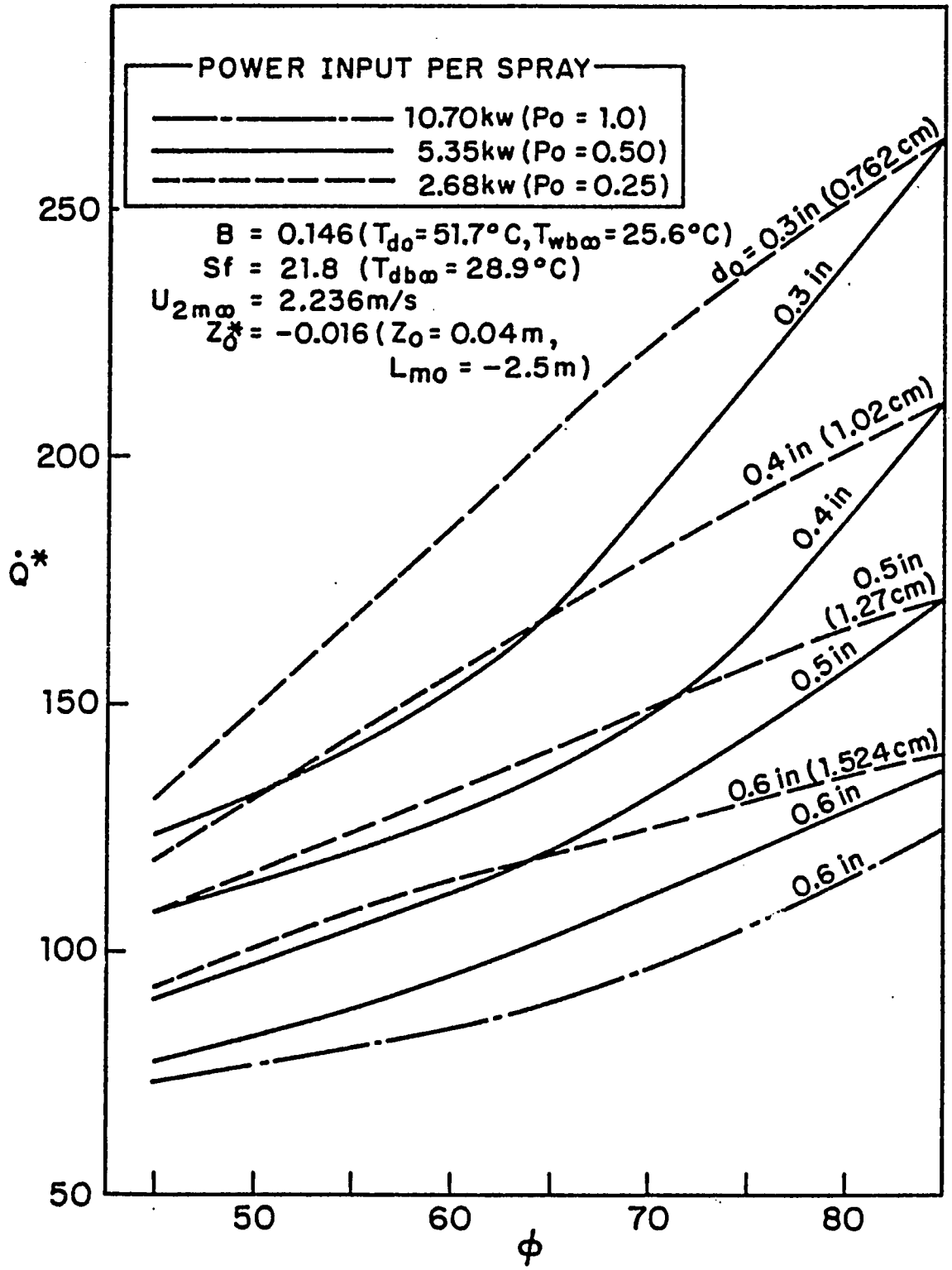

Figure 34. Cooling Efficiency for a Single Spray. Design Chart.

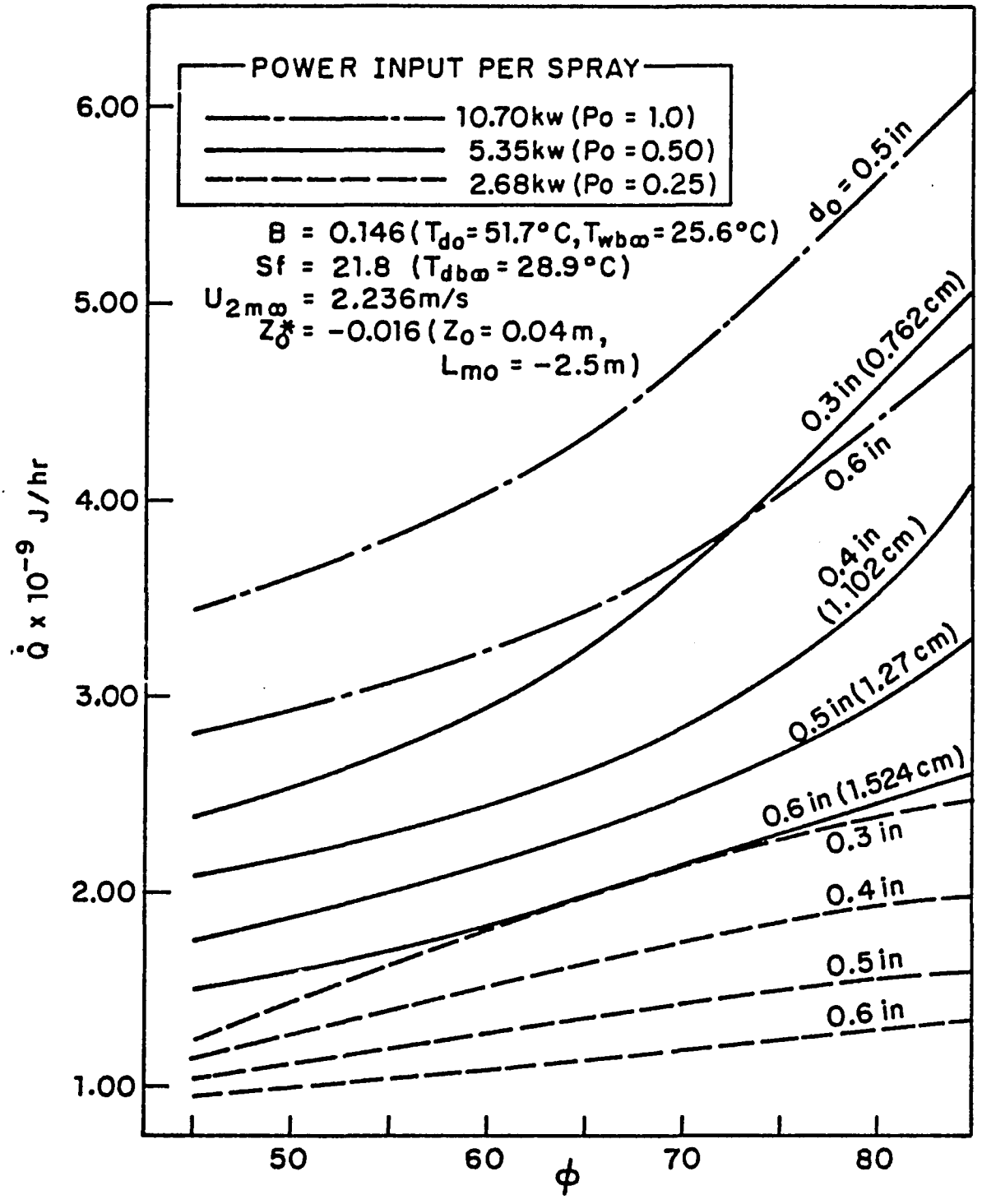

Figure 35. Total Heat Transfer for a Single Spray. Design Chart.

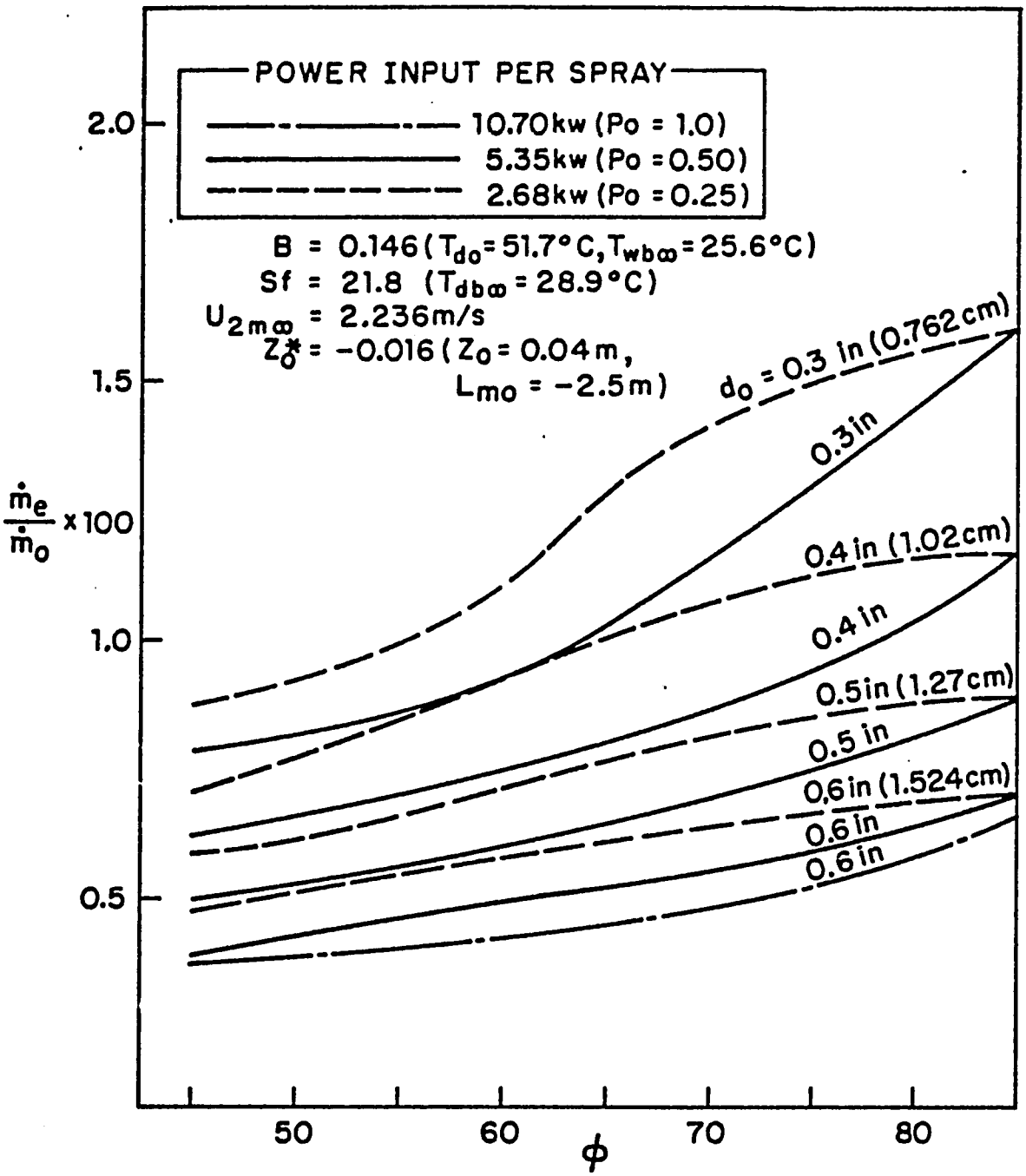

Figure 36. Evaporation as a Percentage of Spray Flow Rate for a Single Spray.

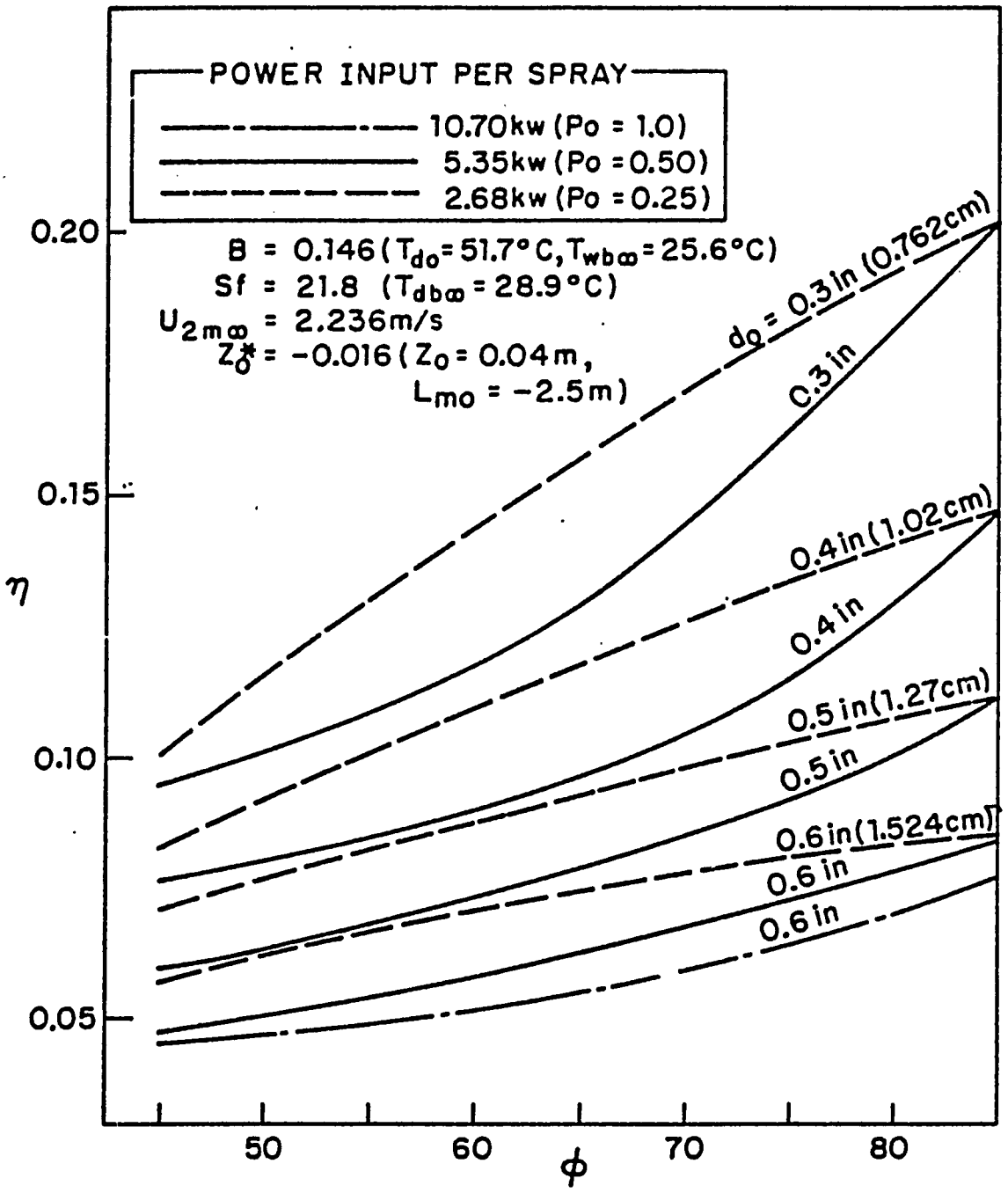

Figure 37. Cooling Effectiveness of a Single Spray. Design Chart.

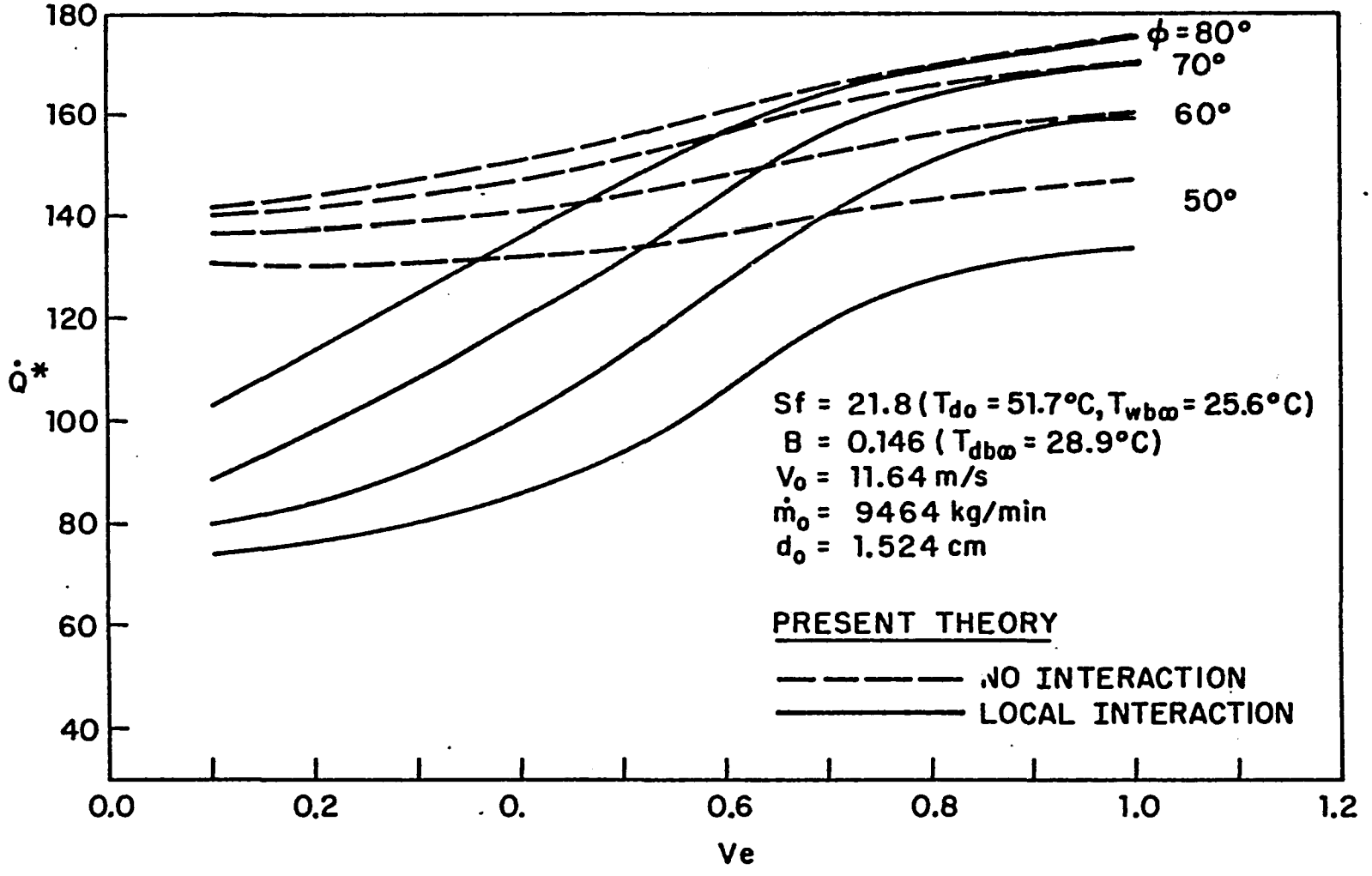

Figure 38. Effect of Discharge Angle and Wind Speed on PSM Single Spray Performance in Unstable Air.

5. 3. Performance Charts

For sprays of fixed design, the number of independent parameters is reduced to six: B, Sf, $T_{um\infty 2m}$, Ve, α_s, z_o*. The Grashof number is not an independent parameter since it is a constant multiple of the Stefan number for a fixed design. The turbulence parameters $T_{um\infty 2m}$, α_s and z_o* are determined by the stability of the atmosphere and the roughness of the earth's surface. Atmospheric stability depends on the amount of solar insolation and the wind speed. In the present study, the atmosphere was assumed to be unstable with strong solar insolation, and the earth's surface to be covered with 30 cm high weeds (z_o=0.04m). For these conditons, $T_{um\infty 2m}$, α_s and z_o* are determined by wind speed and are not independent of velocity ratio, Ve. Additional performance charts may be constructed for different amounts of solar insolation, different atmospheric stabilities and surface roughnesses. With the specification of atmospheric stability and surface roughness, the performance of a fixed design depends on Bowen ratio, Stefan number, and velocity ratio.

The fixed design analyzed in this study is one unit of the Powered Spray Module. In Figure 39 the spray cooling efficiency is plotted versus the Stefan number Sf for values of the velocity ratio Ve and the Bowen ratio B. The range of the Stefan number Sf, covers the normally encountered atmospheric conditions and condenser discharge

temperatures. Lower Stefan numbers reflect a greater potential for heat transfer due to a larger temperature difference between the initial droplet temperature and the ambient wet-bulb temperature. For a given Stefan number, the Bowen ratio B indicates the influence of evaporation on performance. Figure 39 shows that at a given velocity ratio, a low Bowen ratio (high percentage of evaporative heat transfer) is associated with improved spray efficiency over a high Bowen ratio. For a given Bowen ratio, efficiency improves with velocity ratio over the entire range of Stefan number. It is interesting to note, for example, that for a Bowen ratio of 0.4 and a velocity ratio of 0.1, spray performance is better than for a Bowen ratio of 0.7 and velocity ratios of 0.10 and 0.25. This shows that, contrary to the results obtained from both the NTU and SER models, spray efficiency is not solely a function of wind speed, but depends on the difference between the total enthalpy of the air and the enthalpy of saturated air at the droplet temperature. This consideration helps to explain the spread in NTU values in Figure 3 of [1] between the "best fit" curve of Porter and Chen and their summer data.

Figure 40 plots evaporation from the spray as a percentage of spray flow rate versus B, Sf and Ve for PSM operation in unstable air. It is seen that evaporation from the spray is below 1% even for summer conditions (B=0.15, Sf=20) at high velocity ratios.

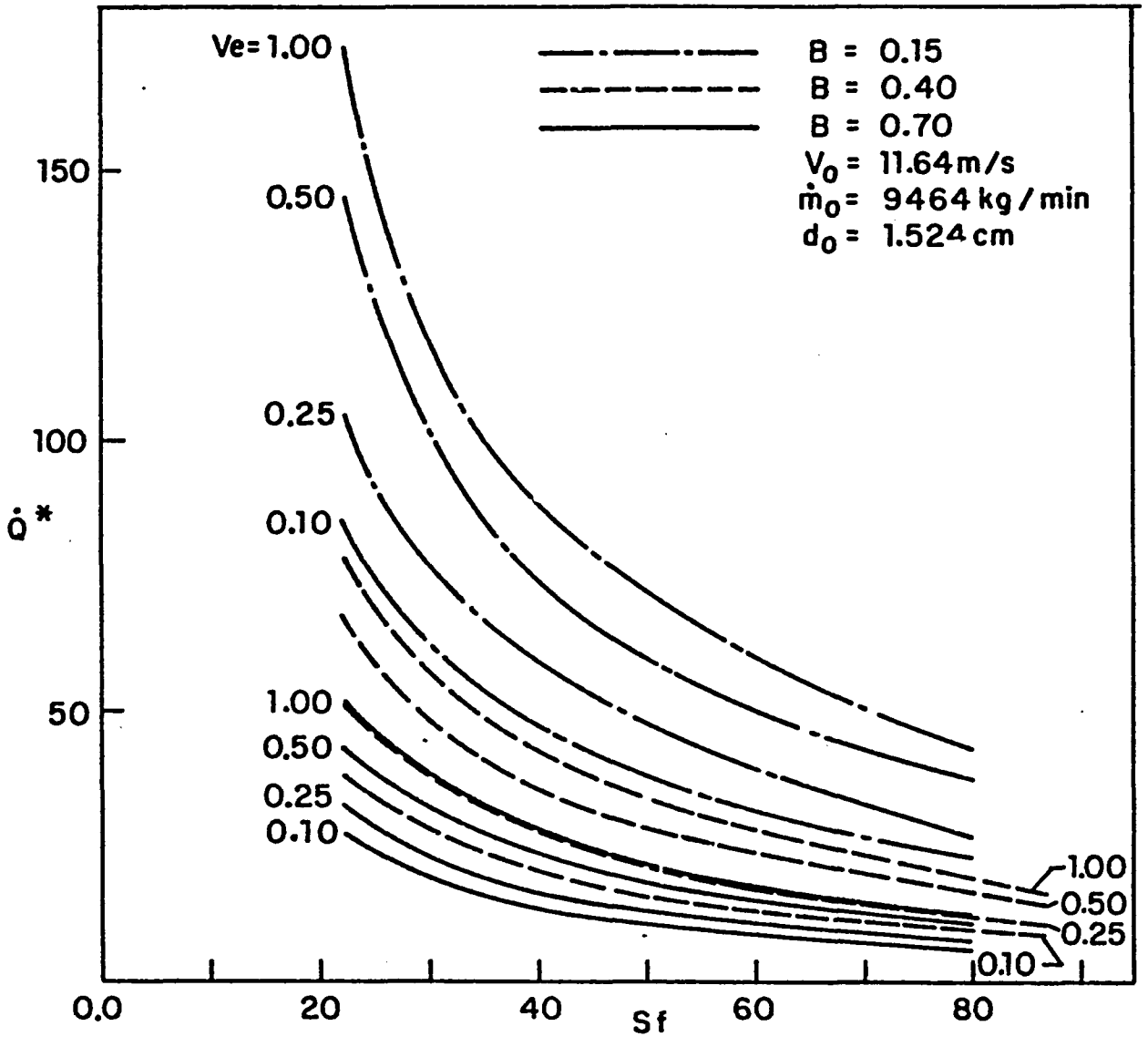

Figure 39. Performance Chart for PSM Single Spray in Unstable Air.

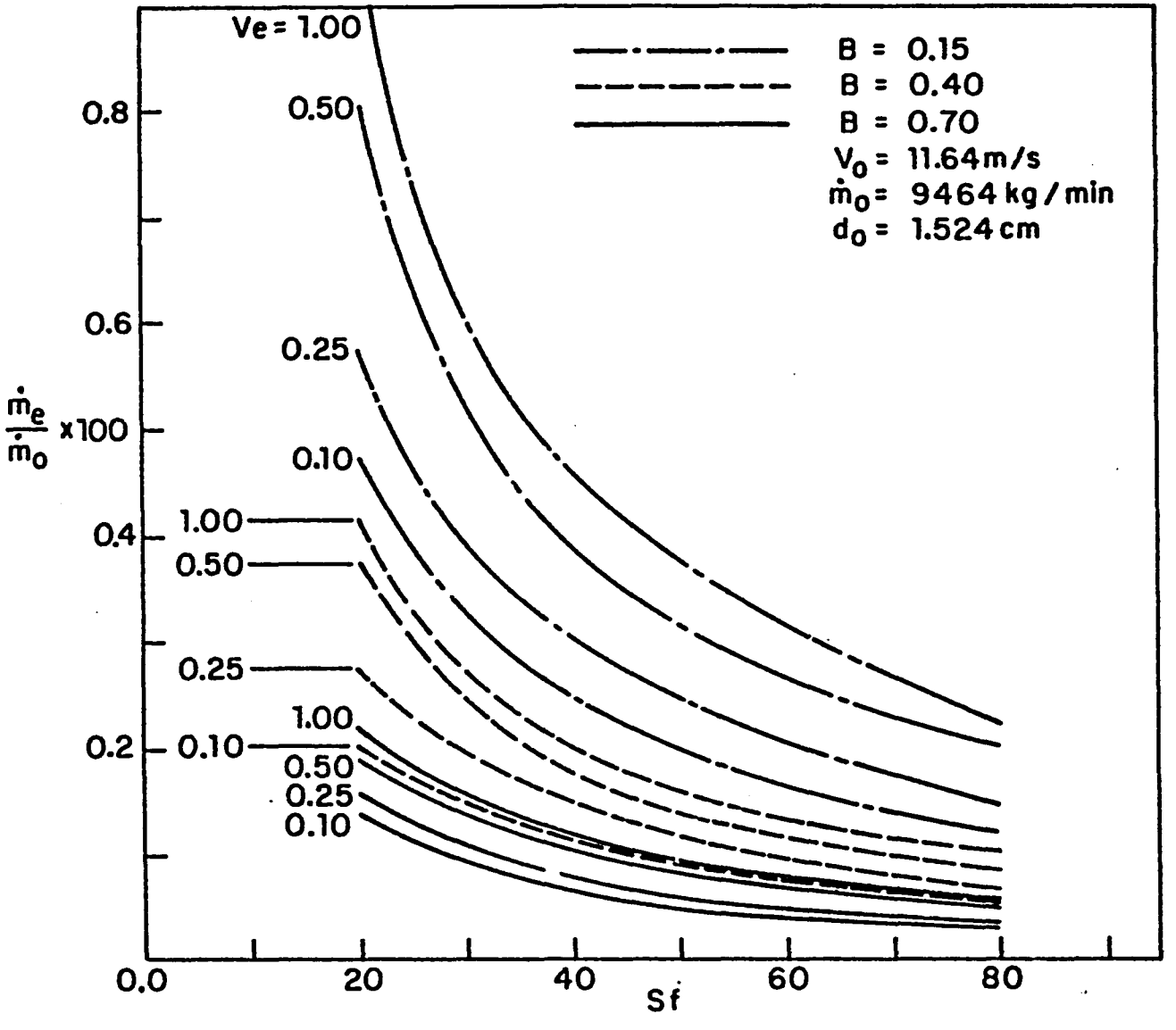

Figure 40. Evaporation as a Percentage of Spray Flow Rate for PSM Single Spray in Unstable Air.

CHAPTER VI

SUMMARY AND CONCLUSIONS

A three-dimensional model that examines the detailed two-phase flow field of a spray unit has been presented. The model is capable of predicting the local properties of both the air-vapor and the drops in the entire domain of the spray without recourse to design-dependent empirical factors.

The model was used to generate solutions for the spray characteristics of a single PSM spray. Comparisons of model predictions of droplet return temperature, downwind wet-bulb temperature and downwind air-velocity with data were made for the PSM and the Spraco 1751 nozzle. A parametric study was carried out to generate charts useful in designing more efficient spray units. As a part of this study, performance charts were constructed for a single spray of the PSM.

The following observations can be made concerning the results obtained with the model.

(1) The model reveals the dimensionless parameters governing the process of open-atmosphere spray cooling. The utility of these parameters is in designing efficient sprays for power plant cooling. It was shown in Chapter V that the cooling obtained from the PSM can be achieved by a more efficient spray unit design which uses half the power input required to operate the PSM.

(2) Theoretical predictions of the model compare favorably with experimental data. The model can be used to predict the heat transfer from current spray unit designs and more-efficient proposed designs.

(3) The performance of a fixed spray unit design was seen to depend upon three parameters (Bowen ratio, Stefan number and velocity ratio) for specified atmospheric stability and surface roughness. Cooling increases with decreasing Stefan number and increasing velocity ratio. Lower Bowen ratios, reflecting a higher percentage of evaporative heat transfer, generally result in improved cooling performance.

(4) The model fails to predict the two-phase flow field for sprays producing droplet number densities of sufficient magnitude to cause the average air-vapor velocity in a streamtube to become negative. A negative air-vapor velocity causes streamlines to cross, invalidating the Lagrangian description of the air-vapor flow field. This difficulty is not encountered with current designs of spray units.

(5) The model fails for cases of very low wind speed, for the reasons given in item (4) above. When very low velocity air tries to enter the spray umbrella, its motion is reversed by the drag of the upwind droplets, causing streamlines to cross.

(6) Since the model for a single spray can calculate the downwind profiles of air-velocity, dry-bulb

temperature and absolute humidity, it can predict the performance of other downwind spray units. This is possible upon extension of the single-unit model to handle a pass of sprays.

(7) The performance of sprays was seen to be markedly reduced at low velocity ratios due to the local buildup of humidity and the rise in the local dry-bulb temperature. Ventilation of the spray by the wind is not sufficient to purge the spray domain of accumulated heat and water vapor at low velocity ratios.

(8) High velocity ratios tend to keep local air near ambient conditions, providing for improved spray performance.

In all direct-contact atmospheric water cooling systems, the prediction of thermal performance depends to a large extent on a knowledge of the amount of air participating in the heat transfer process. The air flow rate in a forced draft cooling tower is known and controllable. For the case of an open-atmosphere spray, the amount of air participating in the heat and mass transfer with the droplets is subject to the transient nature of the ambient wind speed and direction which cannot be predicted. However, the present model is capable of determining the amount of air interacting with the droplets upon the specification of the ambient wind velocity. Previous models rely on design-dependent factors to account for the effect on performance of a finite air flow rate through the spray. If one assumes

the air to be an infinite sink of heat and water vapor, a detailed investigation of air-spray interaction is unnecessary. However, this assumption of the existence of ambient air in the entire domain of the spray results in gross overestimation of the amount of droplet cooling, as is shown in this work. The theoretical determination of the dynamics of the air participating in the spray cooling process, including the effects of spray-air momentum interaction, buoyancy and entrainment, removes the major stumbling block to the analytical design of efficient sprays.

The proposed alternate spray unit design that achieves the cooling obtained by the PSM at half the power cost, produces a mean size drop having half the diameter of that produced by the PSM. All sprays exhibit a size distribution and the production of a smaller mean size drop by a spray nozzle shifts the entire size distribution to smaller sizes. This effect could result in excessive loss of sprayed water at high wind speed due to drift. This loss increases make-up water requirements for a closed-cycle spray canal. This problem can be alleviated by decreasing the nozzle operating pressure during high wind conditions. The decreased pressure reduces the droplet exit velocity and increases the mean drop size. The larger drop diameter spray will exhibit less cooling for high wind conditions than the proposed alternate design. However, the need for large amounts of cooling is not critical at

high wind speed and it is possible to increase the mean drop size at high wind and still achieve the cooling obtained at low wind by a spray having a smaller mean drop size. A study should be carried out to predict the optimum droplet diameter necessary to achieve the cooling obtained at summer design conditions, without excessive drift, by a spray operating at various wind speeds. A study of this type would require the use of spray size distribution functions and a dynamical model to determine the trajectories of drift size ($d_o < 1000 \mu m.$) particles.

The present model shows that a fundamental approach to the prediction of spray cooling performance is practical and capable of extending the results of previous experimental studies to investigate new design concepts and suggest methods useful to industry to improve and economize on future designs of spray cooling devices. To obtain full benefit from the present model, additional research is necessary to delineate the effect of interaction among sprays in a canal. The modelling of spray unit behavior in a spray system requires the detailed knowledge of the air-vapor flow field which the present model provides.

APPENDIX

ORDER OF MAGNITUDE ANALYSIS OF THE DROPLET MOMENTUM EQUATION

The velocity of a droplet can be found by applying the law of conservation of momentum to a particle:

$$\rho_d \frac{\pi d^3}{6} \frac{d\bar{v}}{dt} = \rho_d \frac{\pi d^3}{6} \bar{g} - \rho_a \frac{\pi d^3}{6} \bar{g} - \frac{1}{2} C_D \rho_a \frac{\pi d^2}{4} |\bar{v}-\bar{u}| (\bar{v}-\bar{u})$$
$$- \frac{1}{2} \left(\frac{\pi d^3}{6}\right) \rho_a \frac{d}{dt}(\bar{v}-\bar{u})$$
$$- \frac{3}{2} d^2 \sqrt{\pi \rho_a \mu_a} \int_{t_0}^{t} \frac{d(\bar{v}-\bar{u})}{d\tau} \frac{d\tau}{\sqrt{t-\tau}}$$
$$+ 81.2 \mu_a (\bar{v}-\bar{u}) \left|\frac{d\bar{u}}{dz}\right|^{1/2} \frac{d^2}{4 V_a^{1/2}} \qquad (A-1)$$

The first term on the right-hand side of equation (A-1) is due to the gravitational force. The second term is due to buoyancy. Drag induced by the relative velocity between the drop and the air gives rise to the third term. The force necessary to accelerate the apparent or virtual mass of the droplet relative to the air is given by the fourth term. The Basset and Saffman forces are given by the fifth and sixth terms, respectively. The Basset force [39] is due to the viscous flow field that is established in the vicinity of a particle when the particle is accelerated relative to a surrounding fluid. The instantaneous flow

field is a function of the entire previous history of the particle motion. The Saffman force [39] is the transverse force acting on a particle by a viscous fluid in simple shear.

To determine which terms in equation (A-1) can be neglected, one can nondimensionalize the equation by defining the following dimensionless variables:

$$\tilde{\rho} = \frac{\rho_d}{\rho_a} \;,\quad t^* = \frac{t}{v_o/g} \;,\quad v^* = \frac{v}{v_o} \;,\quad u^* = \frac{u}{U_{2m\infty}} \quad \text{and}$$

$$V_e = U_{2m\infty} / v_o \;.$$

Substituting the above dimensionless variables into equation (A-1) and dividing the resulting equation by $(\tilde{\pi} d^3 \rho_d g)/6$ yields:

$$\frac{d\bar{v}^*}{dt^*} = -\bar{k} + \frac{\bar{k}}{\tilde{\rho}} - \frac{3 C_D v_o^2}{4 \tilde{\rho} d g} \left|\bar{v}^* - \bar{u}^* V_e\right| \left(\bar{v}^* - \bar{u}^* V_e\right)$$

$$- \frac{1}{2\tilde{\rho}} \frac{d}{dt^*} \left(\bar{v}^* - \bar{u}^* V_e\right)$$

$$- \frac{9}{\tilde{\rho} d} \sqrt{\frac{v_a v_o}{\tilde{\pi} g}} \int_{t_o^*}^{t^*} \frac{d\left(\bar{v}^* - \bar{u}^* V_e\right)}{d\tau^*} \frac{d\tau^*}{\sqrt{t^* - \tau^*}}$$

$$+ \frac{121.8}{\tilde{\pi} d \tilde{\rho}} \sqrt{\frac{v_a U_{2m\infty}}{g}} \left(\bar{v}^* - \bar{u}^* V_e\right) \left|\frac{d\bar{u}^*}{dz^*}\right|^{1/2} \qquad \text{(A-2)}$$

The magnitude of each term was calculated for the following conditions: air at 21.1°C (70°F); C_D = 0.44 (spherical particle, Re > 1000); a droplet temperature of 37.8°C (100.0°F); a typical droplet velocity of v_o = 9.0 m/s; the smallest droplet diameter used in this work (do = 0.1 cm); the design wind speed of $U_{2m\infty}$ =2.236 m/s. The magnitudes of the terms in equation (A-2) then are:

gravity	~ 1.0
buoyancy	$\sim 1.2 \times 10^{-3}$
drag	~ 3.3
virtual mass	$\sim 6.0 \times 10^{-4}$
Basset	$\sim 2.3 \times 10^{-2}$
Saffman	$\sim 8.7 \times 10^{-2}$

The forces due to gravity and drag are much larger than the other forces on the droplet, and are the only ones considered to be acting on the droplet in the present model.

For Reynolds numbers greater than 200, the droplet can no longer be considered spherical and the drag coefficient of the drop differs from values given by the drag curve for a solid sphere [40] . The shape of the droplet approaches that of a flat disc at very high Reynolds numbers. Deformation of a droplet results in an increase in form drag, giving higher values of the drag coefficient. The data of Gunn and Kinzer [41] indicate that the drag coefficient for a water drop deviates from that of a solid sphere by less than 5% for Reynolds numbers less than 1,000. For Reynolds numbers between 1,000 and 4,000, droplet drag

coefficients increase from a value of 0.46 to about 0.90. For distorted flat drops at higher Reynolds numbers, Levich [42] recommends a value of C_D equal to approximately 1.0. In the present work, the drag curve for a rigid sphere was used for Reynolds numbers less than 1,000, since this curve accurately predicts the droplet drag coefficient over most of its applicable range of Reynolds numbers. The equation representing this drag curve is given after equation (20b). Since the drag coefficient for a cluster of particles (as in a spray) is generally lower than that of a single particle at high Reynolds numbers [43] , the solid sphere drag coefficient ($C_D \simeq 0.44$) was used for Reynolds numbers greater than 1,000. A more quantitative analysis of the effect of the conglomeration of droplets in a power plant spray on the drag coefficient may be possible upon experimental determination of spray sheet thicknesses and void fractions in the spray domain. Knowledge of the distribution of void fraction in a spray can be used in conjunction with empirical drag correlations given in [43] to obtain estimates of the effect of drop-drop momentum interaction.

NOMENCLATURE

A	cross sectional area of streamtube
A_d	surface area of a representative droplet
B	Bowen ratio=ratio of convective to evaporative heat transfer= $c_{pa}(T_{do}-T_{wb\infty})/L_o(\omega_s(T_{do})-\omega_\infty)$
b_f	Constant= $dh/dT_d = b(T_f)$
C_{D_o}	drag coefficient for $Re > 1000$, $C_{D_o} = 0.44$
C_D	drag coefficient
C_p	constant pressure specific heat
$\tilde{C}_p$	specific heats ratio= C_{pa}/C_{pd}
C_s	specific heat of air-vapor mixture
D	diffusion coefficient
d	droplet diameter
E_{ref}	reference theoretical power input to a spray unit
f	wet-bulb temperature correction factor, defined by equation (5)
F_r	Froude number= v_o^2/gd_o
g	gravitational acceleration
g_c	dimensional constant= $1\ kg\text{-}m/nt\text{-}sec^2$
G_r	Grashof number=ratio of buoyancy to viscous forces= $\rho_o^3 \beta_T g d_o^3 (T_{do}-T_{wb\infty})/\nu_a^2$
H	velocity head of spray nozzle= $v_o^2/2g$
H_o	surface heat flux
h	droplet heat transfer coefficient
$h(T_d)$	total enthalpy of saturated air-vapor mixture at droplet temperature T_d
$h(T_c)$	total enthalpy of saturated air-vapor mixture at spray return temperature T_c

$h(T_H)$ total enthalpy of saturated air-vapor mixture at spray supply temperature T_H

$h(T_{wb})$ total enthalpy of air-vapor mixture at wet-bulb temperature T_{wb}

h_D droplet mass transfer coefficient

I total number of different droplet sizes in the air-vapor element

k thermal conductivity

k' von Karman's constant

$\bar{k}$ unit vector in the vertical direction

K_h turbulent thermal conductivity of air

K_m turbulent viscosity of air

K_{wv} turbulent thermal diffusivity of water vapor in air

ℓ lateral dimension of streamtube

L latent heat of vaporization of water

L_{mo} Monin-Obukhov length scale $= -\dfrac{\rho_a C_{pa} T_{db} U_*^3}{k' g H_o}$

M droplet mass

m number of canal rows, vertical dimension of streamtube

$\dot{m}_o$ mass flow rate of a spray unit

$\dot{m}_e$ evaporation rate from a spray unit

$\dot{N}_{d_i}$ number of drops of size d_i ejected from the nozzle per unit time

n number of droplets in an air-vapor element

$\dot{n}$ number of droplets ejected from a site per unit time

NTU number of transfer units

Nu Nusselt number= $h d / k_a$

P pressure

p number of passes in the canal

P_o Power ratio=ratio of theoretical power input to spray to a reference power input $= \dfrac{\dot{m}_o V_o^2/(2g_c)}{E_{ref}}$

Pr Prandtl number= $\mu_a C_{pa}/k_a$

$\dot{Q}$ rate of heat transfer from a spray unit

r fraction of canal flow rate which is pumped through each spray

Re Reynolds number= $\rho_a d|\bar{v}-\bar{u}|/\mu_a$

Re_o initial Reynolds number= $\rho_a V_o d_o/\mu_a$

s distance along a streamline or drop trajectory

Sc Schmidt number= $\mu_a/\rho_a D$

Sc_o initial Schmidt number= $\mu_a/\rho_a D_o$

Sf Stefan number=latent to sensible heat = $= L_o/[C_{pd}(T_{do}-T_{wb\infty})]$

Sh Sherwood number= $h_D d/D$

SER Spray Energy Release

T temperature, total number of trajectories

T_c spray cold water temperature at canal re-entry

T_f film temperature= $(T_H+\bar{T}_{wb})/2$

T_H, T_{do} spray supply temperature

T_{Hi} canal inlet temperature

T_{Ho} canal outlet temperature

$\bar{T}_{wb}$ average of the upwind and downwind wet-bulb temperatures

T_{wbf} downwind wet-bulb temperature

$Tu_{wv\infty 2m}$ diffusivity turbulent number=ratio of turbulent thermal diffusivity to kinematic viscosity= $\dfrac{K_{wv\infty 2m}}{\nu_a}$

$Tu_{m\infty 2m}$ momentum turbulent number=ratio of turbulent viscosity to kinematic viscosity= $K_{m\infty 2m}/\nu_a$

$\bar{U}_\infty$ wind velocity vector

$\bar{u}$ air velocity vector

u' induced air velocity (vector)

u_* friction velocity

V volume of a finite air-vapor element

$\bar{v}$ droplet velocity vector

v_o initial speed of the mean size drop

Ve velocity ratio= $U_{\infty 2m}/v_o$

x horizontal space coordinate perpendicular to the wind direction

x^* dimensionless space coordinate= $x/(v_o^2/g)$

y horizontal space coordinate in the wind direction

y^* dimensionless space coordinate= $y/(v_o^2/g)$

$z, \bar{z}$ vertical distance above canal surface

z^* dimensionless space coordinate= $\bar{z}/(v_o^2/g)$

z_o roughness height

Greek Letters:

α number of discharge sites around the circumference of of the nozzle

α_s wind shear velocity ratio= $u_*/k'U_{\infty 2m}$

β_T coefficient of thermal expansion of air

Γ_{ad} adiabatic lapse rate= 9.8 °C/km.

γ_i fraction of nozzle flow rate discharged as drops of size d_i

Δt^*_{ij} dimensionless time interval between droplets along a trajectory= $\dfrac{t_{fij}/(v_o/g)}{n_{dij}}$

$\Delta T_{wb2m\ell}$ change in local wet-bulb temperature of air passing through the spray

ϵ prescribed tolerance for convergence of spray heat transfer from successive iterations

η spray cooling effectiveness= $\dot{Q} / \dot{Q}_{max}$

θ droplet discharge angle in the horizontal plane (measured from the x-axis)

μ viscosity

ν kinematic viscosity

ξ wind angle to the canal

ρ density

$\tilde{\rho}$ density ratio= ρ_a/ρ_d

σ turbulent mixing parameter

φ spray discharge angle

ψ function defined by equations (13), (14), and (16)

ω absolute humidity

Superscript

$*$ dimensionless variable

Subscripts

o initial value at nozzle discharge

2m ambient value at a 2m height

∞ ambient value at any height

a air

d droplet

db dry bulb

i pass number, droplet size in size distribution

j row number, trajectory number

k iteration number

ℓ local value

max maximum value

min minimum value

s saturated air

wb wet bulb

x horizontal space coordinate perpendicular to the wind direction

y horizontal space coordinate in the wind direction

z vertical space coordinate

REFERENCES

1. Ryan, P.J. and Myers, D.M., "Spray Cooling: A Review of Thermal Performance Models, "Proceedings of the American Power Conference, Vol. 38, 1976, pp. 1473-1481.

2. Hoffman, D.P., "Spray Cooling for Power Plants," Proceedings of the American Power Conference, Vol. 35, 1973, p. 702-712.

3. Porter, R.W. and Chen, K.H., "Heat and Mass Transfer from Spray Canals, "ASME Journal of Heat Transfer, Vol. 96, No. 3, Aug. 1974, pp.286-291.

4. Porter, R.W., Yang, U.M., and Yanik, A., "Thermal Performance of Spray Cooling Systems, "Proceedings of the American Power Conference, Vol. 38, 1976, pp. 1458-1472.

5. Arndt, C.R., and Barry, R.E., "Simulation of Spray Canal Cooling for Power Plants - Performance and Environmental Effects, "ASME Paper 76-WA/HT-28, Dec. 1976.

6. Elgawhary, A.M., "Spray Pond Mathematical Model for Cooling Fresh Water and Brine," Ph.D. dissertation, Oklahoma State University, Stillwater, Aug. 1969.

7. Frediani, H.A., and Smith, N., "Mathematical Model for Spray Cooling Systems, "ASME Journal of Engineering for Power, Vol. 99, No. 2, April 1977, pp.279-283.

8. Ryan, P.J., "Heat Dissipation by Spray Cooling," Thermal Pollution Analysis Conference Proceedings, Virginia Water Resources Research Center, Virginia Polytechnic Institute and State University, 1974, pp. 18-22.

9. Ryan, P.J., "Spray Cooling," Engineering and Environmental Aspects of Heat Disposal from Power Generation, R.M. Parsons Laboratory for Water Resources and Hydrodynamics, Massachusetts Institute of Technology, Vol. II, 1975.

10. Migdal, D., and Agosta, V.D., "A Source Flow Model for Continuum Gas-Particle Flow," ASME Journal of Applied Mechanics, Vol. 34, No. 4, Dec. 1967, pp. 860-865.

11. Crowe, C.T., "A Computational Model for the Gas-Droplet Flow Field in the Vicinity of an Atomizer," Western States Section/The Combustion Institute, Paper No. 74-23, Oct. 1974.

12. Kliegel, J.R., "One-Dimensional Flow of Gas-Particle System," IAS Paper No. 60-55, 1960.

13. Hultberg, J.A., and Soo, S.L., "Two-Phase Flow Through a Nozzle," Astronautica Acta, Vol. 11, No. 3, May-June 1965, pp. 207-216.

14. Crowe, C.T., Sharma, M.P., and Stock, D.E., "The Particle Source in Cell (PSI-Cell) Model for Gas-Droplet Flows," ASME Paper No. 75-WA/HT-25, Dec. 1975.

15. Sharma, M.P., and Crowe, C.T., "A Novel Physio-Computational Model for Quasi One-Dimensional Gas Particle Flows," ASME Paper No. 76-WA/FE-36, Dec. 1976.

16. Sharma, M.P., and Crowe, C.T., "A Computer Mathematical Model for Gas-Particle Two-Phase Flows," Presented at the Second Multi-Phase Flow and Heat Transfer Symposium-Workshop, Miami Beach, Florida, April 1979.

17. Soo, S.L., "Power Spray Cooling-Unit and System Performance," ASME Paper No. 75-WA/Pwr-8, Nov. 1975.

18. Chen, K.H., and Trezek, G.J., "Spray Energy Release (SER) Approach to Analyzing Spray System Performance," Proceedings of the American Power Conference, Vol. 38, 1976, pp. 1435-1448.

19. Berger, M.H., and Taylor, R.E., "An Atmospheric Spray Cooling Model," Environmental Effects of Atmospheric Heat/Moisture Releases, The Second AIAA/ASME Thermophysics and Heat Transfer Conference, Palo Alto, California, May 1978, pp. 59-64.

20. Porter, R.W., "Analytical Solution for Spray-Canal Heat and Mass Transfer," Joint AIAA Paper 74-764, ASME Paper 74-HT-58, July 1974.

21. Chaturvedi, Sushil, and Porter, R.W., "Air-Vapor Dynamics in Large Scale Atmospheric Spray Cooling Systems," ASME Journal of Fluids Engineering, Vol. 100, No. 1, March 1978, pp. 65-72.

22. Weinstein, H., Porter, R.W., Chaturvedi, S., Kulik, R.A., and Paganessi, J.E., "Dispersion of Heat and Humidity from Atmospheric Spray-Cooling Systems," Proceedings of the Waste Heat Management and Utilization Conference, University of Miami, Coral Gables Vol. 2, May 1977, pp. 1107-1147.

23. Haltiner, G.J., and Martin, F.L., Dynamical and Physical Meteorology, McGraw Hill, New York, 1957.

24. Sutton, O.G., Micrometeorology, McGraw Hill, New York, 1953.

25. Panofsky, H.A., "The Atmospheric Boundary Layer Below 150 Meters," Annual Review of Fluid Mechanics, Vol. 6, 1974, pp. 147-177.

26. Winnikow, S., and Chao, B.T., "Droplet Motion in Purified Systems," Physics of Fluids, Vol. 9, No. 1, January 1966, pp. 50-61.

27. Chao, B.T., "Transient Heat and Mass Transfer to a Translating Droplet," ASME Journal of Heat Transfer, Vol. 91, No. 2, May 1969, pp. 273-281.

28. Ranz, W.D., and Marshall, W.R., Jr., "Evaporation from Drops," Chemical Engineering Progress, Vol. 48, No. 3, Feb. 1952, pp. 141-146, 173-180.

29. Dorsey, N.E., Properties of Ordinary Water Substance, Reinhold Publishing Corporation, New York, 1940.

30. Wallis, G.B., One-Dimensional Two-Phase Flow, McGraw Hill, New York, 1969.

31. Chou, J.C.S., and Rowe, A.M., Jr., "Enthalpies of Aqueous Sodium Chloride Solutions from 32 deg. F," Desalination, Vol. 6, 1969, pp. 105-115.

32. Hoffert, M.I., "Atmospheric Transport, Dispersion, and Chemical Reactions in Air Pollution: A Review," AIAA Journal, Vol. 10, No. 4, April 1972, pp. 377-387.

33. Carrier, W.H., "Rational Psychrometric Formulae," ASME Transactions, Vol. 33, 1911, pp. 1005-1053.

34. Wilson, D.C., "Thermal Performance of Powered Spray Modules," Master's Thesis, University of Illinois, Urbana-Champaign, 1972.

35. Yang, U.M. and Porter, R.W., "Thermal Performance of Spray Cooling Systems - Theoretical and Experimental Aspects," Waste Energy Management Technical Report TR-76-1, Illinois Institute of Technology, December, 1976.

36. Chen, K., "Heat and Mass Transfer from Power Plant Spray Cooling Ponds," Doctoral Dissertation, University of California, Berkeley, 1975.

37. Gordon, M., Yerushalmi, J., and Shinnar, R., "Instability of Non-Newtonian Jets," Transactions of the Society of Rheology, Vol. 17, No. 2, 1973, pp. 303-324.

38. Masters, K., Spray Drying, Leonard Hill, London, 1972.

39. McCormack, P.D. and Crane, Lawrence, Physical Fluid Dynamics, Academic Press, New York, 1973.

40. Beard, K.V. and Pruppacher, H.R., "A Determination of the Terminal Velocity and Drag of Small Water Drops by Means of a Wind Tunnel," Journal of the Atmospheric Sciences, Vol. 24, No. 5, Sept. 1969, pp. 1066-1072.

41. Gunn, R., and Kinzer, G.D., "The Terminal Velocity of Fall for Water Droplets in Stagnant Air," Journal of Meteorology, Vol. 6, August 1949, p. 243.

42. Levich, V.G., Physicochemical Hydrodynamics, Prentice Hall, Englewood Cliffs, New Jersey, 1962.

43. Soo, S.L., Fluid Dynamics of Multiphase Systems, Blaisdell Publishing, Waltham, Mass., 1967.